

Investigations of Hydrogen-Deficient Stars and Related Objects

A thesis
submitted for the degree of
DOCTOR OF PHILOSOPHY

In
The Faculty of Science
Bangalore University, Bangalore

By
Gajendra Pandey



Indian Institute of Astrophysics
Bangalore - 560034
India

September 1999

Declaration

I hereby declare that this thesis is the result of the investigations carried out by me at the Indian Institute of Astrophysics, Bangalore under the supervision of Prof. N. Kameswara Rao. This thesis has not been submitted for the award of any degree, diploma, associateship, fellowship, etc. of any university or institute.

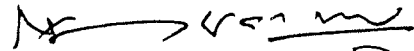


Gajendra Pandey
(Candidate)

Bangalore 560034
1999

Certificate

This is to certify that the thesis entitled "Investigation of hydrogen deficient stars and related objects" submitted to the Bangalore University by Mr. Gajendra Pandey for the award of the degree of Doctor of Philosophy in the faculty of Science, is the result of the investigations carried out by him under my supervision and guidance, at the Indian Institute of Astrophysics. This thesis has not been submitted for the award of any degree, diploma, associate-ship, fellowship, etc. of any university or institute.



Prof. N. Kameswara. Rao
(Supervisor)

Bangalore 560034
1999

Acknowledgements

I am indebted to Prof. N. Kameswara Rao for suggesting the topic, his guidance and constant encouragement throughout the course of the project. I am extremely grateful to him for introducing me to Observational Astronomy and Stellar Spectroscopy.

The high quality data, without which it would have been impossible to address some of the important and interesting aspects about hydrogen-deficient stars in this work, were kindly provided by Prof. David L. Lambert and Prof. N. Kameswara Rao.

My special thanks go to Prof. David L. Lambert for patiently going through the chapters. His to-the-point suggestions and comments have helped me considerably in understanding many of the finer points involved in abundance calculations. I am grateful to Dr Simon Jeffery and Dr Martin Asplund for kindly making available the hydrogen-deficient stellar atmosphere models and the relevant synthesis codes. I thank them for promptly replying to my queries and clarifying all my doubts.

I sincerely thank Prof. D. C. V. Mallik for patiently going through the thesis, and his valuable suggestions and comments which considerably improved the presentation of the thesis. The discussions with him and Prof. H. C. Bhatt on stellar evolution and surface chemical composition were very fruitful.

I am extremely thankful to Dr Sunetra Giridhar, Dr A. V. Raveendran and Dr M. V. Mekkaden for patiently going through the thesis. Their suggestions and comments have helped me to give a final shape to the thesis. It is a great pleasure to thank Mr Baba Varghese and all the other friends at I.I.A. for their help at various stages in the preparation of the thesis.

I thank Prof. Ramanath Cowsik, Director of Indian Institute of Astrophysics, for providing all the facilities needed to complete the thesis.

I take this opportunity to thank all the former Chairmen, Prof. A. R. Hanumanthappa, and the faculty of the Bangalore University for their help during registration, conduction of the pre-PhD examination and other formalities.

I am grateful to all the staff members of VBO, Kavalur for their help and co-operation. I thank the computer personnel, Mr A. V. Ananth, Mr J. S. Nathan and Mr K. N. Kutty, for helping me whenever I had any problems while handling the software packages. I thank the I.I.A. library staff for making available all the required books and journals, and Mr Kanakaraj and Mr Thyagaraja for preparing the bound copies of the thesis.

Finally I wish to express my immense gratitude to my uncle, aunt, mother, father, brother and sisters for their constant encouragements.

Summary

Hydrogen-deficient stars are divided mainly into three groups based on their carbon abundance – the carbon normal group, the carbon rich group, and the carbon strong group. The carbon rich group, which shows C/He $\sim 1\%$ by number, is further sub-divided into hydrogen-deficient carbon stars, R CrB stars, extreme helium stars, and helium sub-dwarf O⁺ stars. The position of these stars in the log g -log T_{eff} plane indicates that their progenitors are probably of low and intermediate masses. The evolutionary link within this group is not yet well-established. In this thesis we study the chemical composition of the atmospheres of these stars with a view to exploring the possible evolutionary link between R CrB stars, cool extreme helium stars, and hot extreme helium stars and their kinship with other post-AGB stars.

The thesis consists of seven chapters, each with several sections and subsections. In the first chapter we give a general description of the various groups of hydrogen-deficient stars, and discuss the evolutionary sequence of low and intermediate mass stars as these are probably the progenitors of hydrogen-deficient stars. We also discuss briefly the nucleosynthesis taking place in the star, and the various stages during which the processed material is brought to the surface during the course of its evolution. The two scenarios – final helium shell flash and merging of two white dwarfs – which are proposed to explain the formation of hydrogen-deficient stars and their observed chemical composition are then reviewed. We describe the observations, the data reduction procedure, and the details followed in the spectral line identification in Chapter 2. A brief description of the model atmospheres of normal and hydrogen-deficient stars, and an overview of the construction of hydrogen-deficient model atmospheres used in our abundance analysis are presented in Chapter 3. The abundance analysis procedure followed in the present work is discussed in detail in Chapter 4. In Chapter 5, we present an investigation of the emission line spectra of MV Sgr, and discuss the results. In the following chapter we make a comparison of the derived elemental abundances of R CrB, and cool and hot extreme helium stars, and present an interpretation of the derived elemental abundances and their implications in the context of nucleosynthesis and evolutionary scenarios. Finally, the conclusions are summarized in Chapter 7.

Contents

1	Introduction	4
1.1	The hydrogen-deficient star groups	4
1.1.1	R CrB stars and cool hydrogen-deficient carbon stars	5
1.1.2	Extreme helium stars and hydrogen-deficient binaries	6
1.1.3	Hydrogen-deficient subdwarf O and B stars	7
1.1.4	Non DA-white dwarfs	7
1.1.5	Intermediate helium stars	8
1.1.6	Wolf-Rayet stars	8
1.2	Carbon abundance in hydrogen-deficient stars	9
1.3	Evolution of low and intermediate mass stars	10
1.4	Photospheric chemical evolution	13
1.5	Models of the hydrogen-deficient stars	14
1.5.1	The Double Degenerate scenario (DD scenario)	14
1.5.2	The Final helium-shell Flash scenario (FF scenario)	15
1.6	Aim of the thesis	17
2	Observations, data reductions and spectral line identification	21
2.1	The sample	21
2.1.1	FQ Aqr	22
2.1.2	LS IV -14° 109	22
2.1.3	BD -1° 3438	22
2.1.4	LS IV -1° 002	23
2.1.5	MV Sgr	23
2.2	Observations	24
2.3	Data reductions	25

2.3.1	Basic steps in the reduction	25
2.3.2	Extraction of spectrum	26
2.3.3	Wavelength calibration	26
2.3.4	Spectral line identification	27
2.3.5	Measurement of equivalent widths	27
3	Model stellar atmospheres	29
3.1	Atmospheres of normal stars	29
3.2	Atmospheres of hydrogen-deficient stars	30
3.2.1	Construction of model atmospheres	31
3.2.2	Models for $T_{eff} \leq 9,500$ K	32
3.2.3	Models for $T_{eff} \geq 10,000$ K	32
3.2.4	Continuous opacities	33
4	Abundance analysis of EHe stars	34
4.1	Normalization of abundances	34
4.2	Dominant sources of continuous opacity	36
4.3	Carbon to helium ratio	38
4.4	Abundance analysis	46
4.4.1	Atomic data	55
4.4.2	T_{eff} , $\log g$, ξ and C/He	55
4.5	Abundances	79
4.6	Error Analysis	81
5	Emission–line spectrum of MV Sgr	119
5.1	Description of the spectrum	119
5.2	Radial velocities	120
5.3	Emission lines	123
5.3.1	Forbidden lines	124
5.3.2	Fe I and Fe II lines	129
5.3.3	Li I emission at 6707 Å	132
5.3.4	H α , He I and C II profiles	133
5.3.5	Variation of the emission width with excitation potential	134

6	Results and discussion	136
6.1	EHe stars	136
6.1.1	Elemental abundances	136
6.1.2	Comparison with R CrB stars and hot EHe stars	141
6.1.3	Metallicity	147
6.1.4	The “carbon problem”	148
6.1.5	Evolutionary aspects	150
6.2	MV Sgr	152
7	Conclusions and future prospects	154
7.1	Cool EHe stars	154
7.2	MV Sgr	157
7.3	Future prospects	159
	Bibliography	161

Chapter 1

Introduction

1.1 The hydrogen-deficient star groups

All stars begin their lives converting hydrogen to helium inside the core and settle on the main sequence, where they spend a substantial fraction of their life-times. During their subsequent evolution, which proceeds at a much rapid rate, heavier elements, synthesized deep inside the cores through various processes, are dredged-up and mixed with the original hydrogen-rich photospheric material at varying degrees. Almost all stars have hydrogen as the major constituent of the photosphere through out their lives. However, there exists a small group of fascinating objects which do not conform to these norms, the hydrogen-deficient group.

Hydrogen-deficient stars consist mainly of helium; the other elements, which are referred to as trace elements, are present only in small quantities. The carbon content in these stars is more, when compared to solar type stars. Their photospheres show little or no evidence of the presence of hydrogen; hydrogen is underabundant by a factor of 10^6 or more in their photospheres. In the hydrogen dominated universe, it is of great interest to determine the stellar physics that governs these objects and the sequence of evolution that lead to their formation.

The discovery of the group of hydrogen-deficient stars may be traced back to May 1795, more than two centuries ago when Edward Pigott (Pigott 1797) discovered the variability of the R Coronae Borealis (R CrB). He noticed the disappearance and subsequent re-appearance of a star, later named R CrB, in the constellation Northern Crown (Latin:

Corona Borealis).

Ludendorff (1906) was the first to notice that the Balmer line $H\gamma$ is weak in R CrB. Berman's (1935) pioneering analysis of R CrB showed that carbon is overabundant (69%) and hydrogen is deficient (27%) in R CrB. The first hydrogen-deficient, helium star HD 124448 was discovered by Popper (1942). He reported the absence of hydrogen lines and the presence of sharp and strong helium lines, along with lines of C II and O II in its spectrum.

Presently, several distinct groups of stars that exhibit hydrogen-deficiency are recognized (Drilling 1996): cool hydrogen-deficient carbon stars, R CrB stars, extreme helium stars, hydrogen-deficient subdwarf O and B stars, non DA-white dwarfs, hydrogen-deficient binaries, intermediate helium stars, Wolf-Rayet stars and Type I supernovae.

1.1.1 R CrB stars and cool hydrogen-deficient carbon stars

The R CrB stars are variables which undergo declines in light by as much as eight magnitudes in a few weeks at irregular intervals. The relatively rapid decrease is followed by a slower return to maximum light, where the star spends most of its time. The characteristic deep declines are thought to be due to random episodes of dust formation in the stellar envelope (Loreta 1934; O'Keefe 1939; Woitke et al. 1996). As the dust cloud is pushed far from the star by radiation pressure, it obscures the photosphere and also induces changes in the observed spectrum. These stars at maximum light show F-G Ib type spectra with strong carbon features except the CH bands, and weak or absent Balmer lines. Lambert and Rao (1994) have presented a list of 32 R CrB stars, which is essentially a revised version of that given by Drilling and Hill (1986). In addition to several R CrB stars, the list of Drilling and Hill (1986) also contains five cool hydrogen-deficient carbon stars (HdC), which are spectroscopically similar to R CrB stars (Warner 1967; Schönberner 1975; Cottrell and Lambert 1982; Lambert 1986). In these stars large declines in brightness have never been observed; Kilkenny, Marang and Menzies (1988) have, however, observed small amplitude light variations similar to those shown by some R CrB stars at maximum light. There are three stars, V348 Sgr, MV Sgr and DY Cen, which have been observed to undergo R CrB-type light declines; these stars, however, show absorption spectra similar to those of the extreme helium stars rather than R CrB stars, and are classified as "hot R CrB" stars.

1.1.2 Extreme helium stars and hydrogen-deficient binaries

The extreme helium stars (EHe) are characterized by strong lines of He I, and weak or absent Balmer lines (Hunger 1975). The spectra of EHe stars also show lines of C II, C III, N II, O II, Al II, Al III, Si II, Si III, S II, S III, etc.

The catalog of *Luminous Stars in the Southern Milky Way* (LSS) by Stephenson and Sanduleak (1971) was the result of Case-Hamburg OB star surveys. The catalog lists 5132 OB stars and supergiants of spectral types B6–G2, identified on Kodak IIA-O photographic plates taken with the Curtis Schmidt Telescope and UV-transmitting objective prism at the Cerro Tololo Inter-American Observatory. The instrumental setup yielded a resolution of about 4 Å at H γ , which allowed rough MK types to be assigned to supergiants of spectral types B6–G2. The OB stars, which show nearly continuous spectra, were classified as OB⁺, OB and OB[−], in the order of increasing Balmer absorption-line strength. The six earlier catalogs of *Luminous Stars in the Northern Milky Way* (LSI – LSVI) were based on similar objective-prism plates taken with the large Schmidt telescopes at the Hamburg Observatory (Drilling and Bergeron 1995). Altogether these surveys cover the entire disc of the Milky Way down to photographic magnitude 12 (galactic latitudes $\pm 10^\circ$ for $l = \pm 60^\circ$, except in the case of LSIV, where the coverage in galactic latitude was extended to $\pm 30^\circ$). At the resolution ($\approx 4\text{Å}$) employed in the Case-Hamburg OB star surveys, the spectra of EHe stars have nearly featureless appearances, and hence are classified as OB⁺. It has thus been possible to obtain a complete sample of EHe stars down to photographic magnitude 12 by observing all of the OB⁺ stars in the Case-Hamburg-LSU surveys, which cover the entire galactic disc, and their extension to $b = \pm 30^\circ$ for $l = \pm 60^\circ$ at a resolution of 2 Å or better (Drilling 1987; Drilling and Bergeron 1995). Eleven new EHe stars were discovered as a result of this survey. Before this survey, only six “classical” EHe stars were known. MacConnell et al. (1970, 1972) discovered two more EHe stars during an objective-prism survey. Altogether there are 19 EHe stars listed in Jeffery et al. (1996) excluding subdwarf O stars (sdO) and hydrogen-deficient binaries (HdB).

The four hydrogen-deficient binaries, *v* Sgr, KS Per, HDE 320156 and CPD 58° 2721, have spectroscopic characteristics extremely similar to EHe stars. These systems have orbital periods between 30 and 360 days and show late-B type spectra. These are single-lined spectroscopic binaries and according to Drilling (1986), they differ from single EHe stars in the following ways:

1. considerably high, photospheric abundance ratios of nitrogen-to-carbon,

2. strong H α emission in their spectra,
3. a large infrared excess,
4. radial velocities very close to those expected for circular orbits about the galactic center, and
5. the distances from the galactic plane less than 200 pc.

1.1.3 Hydrogen-deficient subdwarf O and B stars

The number of known helium rich subdwarf O (sdO) and hydrogen-deficient subdwarf B (sdB) stars has increased as a result of various surveys. The sdO and sdB stars are classified into different subgroups based on two parameters: the strengths of the He II lines relative to that of He I lines and the strengths of the He lines with respect to that of H lines.

1. *sdB stars*: These objects are characterized by small He II/He I. Sargent and Searle (1968) originally defined a sdB star as “a star which has colours corresponding to those of a B star and in which the Balmer lines are abnormally broad for the colour, as compared to Population I main-sequence stars. Some, but not all, sdB stars have He I lines that are weak for their colour.” Green et al. (1986) have sub-divided the classical sdB’s into three subclasses and added a fourth subclass. Since these four classes of sdB stars differ in the strengths of the He I lines relative to H, Drilling (1996) proposed that they be called sdB1, sdB2, sdB3 and sdB4 in the order of increasing He I/H.

2. *sdOB stars*: These objects have intermediate He II/He I. Two classes have been identified sdOB1 and sdOB2 based on the strength of hydrogen Balmer absorptions.

3. *sdO stars*: Objects belonging to this subgroup display large He II/He I. Two classes have been identified, sdO1 and sdO2, based on the strengths of the Balmer absorption lines. A number of sdO stars are known to be central stars of planetary nebulae.

1.1.4 Non DA-white dwarfs

White dwarfs can be classified into two distinct spectroscopic sequences. The majority are hydrogen rich (type DA) and can be found starting with effective temperatures $T_{eff} > 100,000$ K all the way down the white dwarf cooling sequence. The rest are hydrogen-

deficient (type non DA). Non DA-white dwarfs are helium rich and comprise DO ($T_{eff} > 45,000$ K), DB ($11,000 < T_{eff} < 30,000$ K) and DC ($T_{eff} < 11,000$ K) white dwarfs (Liebert 1986). The spectral appearance of the helium rich white dwarfs is determined by the ionization balance of the helium plasma depending on the effective temperature of the star. The DO's display a pure He II line spectrum at the hot end and a mixed He I/He II spectrum at the cool end, while DB's are characterized by a pure He I line spectrum. An effective temperature below $\approx 11,000$ K is too low to excite He I lines, making the DC's featureless white dwarfs. Those DO's with detectable traces of metals are denoted by DOZ. At the highest effective temperatures the DO's are connected to the helium-, carbon- and oxygen-rich PG 1159 stars (also denoted as DOZ by Wasemael et al. 1985), which are the proposed precursors of the DO white dwarfs.

1.1.5 Intermediate helium stars

The spectra of intermediate helium stars are similar to those of normal stars of MK spectral type B2V, but show abnormally high He I/II line intensity ratios ranging between those of normal stars and unity (Walborn 1983; Hunger 1986). Walborn (1983) concludes that the intermediate helium stars are primarily young, massive stars of Population I.

1.1.6 Wolf-Rayet stars

Wolf-Rayet (W-R) stars were first detected by Wolf and Rayet (1867) due to the presence of strong emission lines in their spectra. These are massive stars that have evolved very fast with extensive mass loss. They have blown away most of their outer H-rich envelope exposing the matter that has either experienced complete hydrogen burning, or partial helium burning. The unusual line ratios in W-R spectra indicate that the atmospheres of these stars have compositions far different from solar (Smith 1973; Conti et al. 1983; Crowther et al. 1995abc; Koesterke and Hamann 1995; Hamann et al. 1995). Many of the W-R stars have no detectable hydrogen emission; those that do, have a H/He ratio less than the solar value by a factor of two or more. The W-R stars fall into three classes:

1. *WN stars*: The spectra of these stars are dominated by the emission lines of He and N. Carbon emission is also seen, while emission or absorption features due to hydrogen are readily detected in some stars. In the Galaxy approximately half of the W-R stars

within 2.5 kpc of the Sun are of this type, but in the LMC they comprise approximately 80% of the W-R stars known (Massey and Armandroff 1991). In these stars we are seeing the products of the CNO cycle at the surface. Thus the stars are deficient in H, C and O and rich in He and N. The N/He and C/N ratios deduced are consistent with those expected from CNO burning (Crowther et al. 1995b). It is believed that the progenitors of WN stars are less massive than those of WC stars.

2. *WC stars*: The spectra of the stars belonging to this group are dominated by emission lines due to He, C, and O. No hydrogen emission has been detected. They constitute roughly 50% of the W-R stars known in our galaxy. In these stars we are seeing the products of helium burning at the surface. The C/He mass fraction in these stars is typically greater than 0.1, and may approach unity (Hillier 1989; Koesterke and Hamann 1995).

3. *WO stars*: Only 5 of these stars are known (Kingsburgh et al. 1995). The sequence is distinguished from WC stars by the presence of strong O VI $\lambda\lambda$ 3811, 3834 emission.

The W-R stars discussed above are high mass stars and belong to Population I. Among the central stars of planetary nebulae (CSPN), which are low mass, Population II objects, there are two groups: hydrogen-rich and hydrogen-deficient (Mendez 1991). The difference in the surface abundances is because the hydrogen envelope is present in the former group while it is virtually lost in the latter group. The hydrogen-deficient CSPN show Wolf-Rayet type spectra, identical to type WC, and are designated as [WC].

1.2 Carbon abundance in hydrogen-deficient stars

The number of hydrogen-deficient stars studied has tremendously increased in the last 12 years, thereby a need arose to group these stars into different categories and to study the evolutionary aspects. Hydrogen is depleted in these stars; the hydrogen abundance may vary by several orders of magnitude from star to star, which makes it difficult to group these stars based on their hydrogen abundance. If the grouping of low-mass hydrogen-deficient stars is done based on the carbon content, three distinct groups emerge (Jeffery 1994):

(i) *The carbon-normal group:* This group consists of stars of different types, like the HdB and the helium-rich sdB stars, and does not appear to have carbon enrichment.

(ii) *The carbon-rich group:* This group comprises R CrB stars including the hot R CrB stars, Hydrogen-deficient carbon stars (HdC), Extreme Helium stars (EHe) and helium sub-dwarfs O⁺ (He-sdO⁺) stars. The carbon-to-helium ratios by mass cluster around 1%, (except for MV Sgr which shows C/He of $\approx 0.1\%$), and all other heavier elements, including nitrogen and oxygen, are present only in traces.

(iii) *The carbon-strong group:* The carbon-strong group includes Wolf-Rayet central stars of planetary nebulae, PG 1159 stars and O(C) stars. PG 1159 stars, which are pulsating white dwarfs (McGraw et al. 1979), are also sometimes associated with PN (eg. NGC 246). O(C) stars are spectroscopically very similar to PG 1159 (Leuenhagen et al. 1994). The carbon-to-helium ratio by mass is $\geq 10\%$, and also oxygen can be quite strong, O/He ≈ 0.1 . The evolutionary sequence within this group, most likely, is from cool to hot (Schönberner 1996).

1.3 Evolution of low and intermediate mass stars

The positions of hydrogen-deficient stars in the $\log g$ - $\log T_{eff}$ plane indicate that the progenitors of these stars are probably of low and intermediate masses. Hence, before discussing the formation of hydrogen-deficient stars, we will present a brief outline of the evolution of low and intermediate mass stars. One of the major issues in the study of hydrogen-deficient stars is this: at what stage during the course of evolution does the hydrogen-deficiency occur (if at all)?

All single stars spend most of their life burning hydrogen in their cores ($\approx 10^{10}$ years for a $1M_{\odot}$ star, $\approx 10^8$ years for a $5M_{\odot}$ star; Bowers 1984). Once hydrogen is exhausted in the core, the star leaves the main sequence, crosses the Hertzsprung gap and ascends the Red Giant Branch (RGB) with hydrogen burning in the shell (see Fig. 1.1). At the tip of the RGB the star ignites the helium in the core. The ignition happens under degenerate conditions for stars less massive than $2.3M_{\odot}$, while for more massive stars the core simply reaches a temperature sufficient for helium burning by the triple-alpha process.

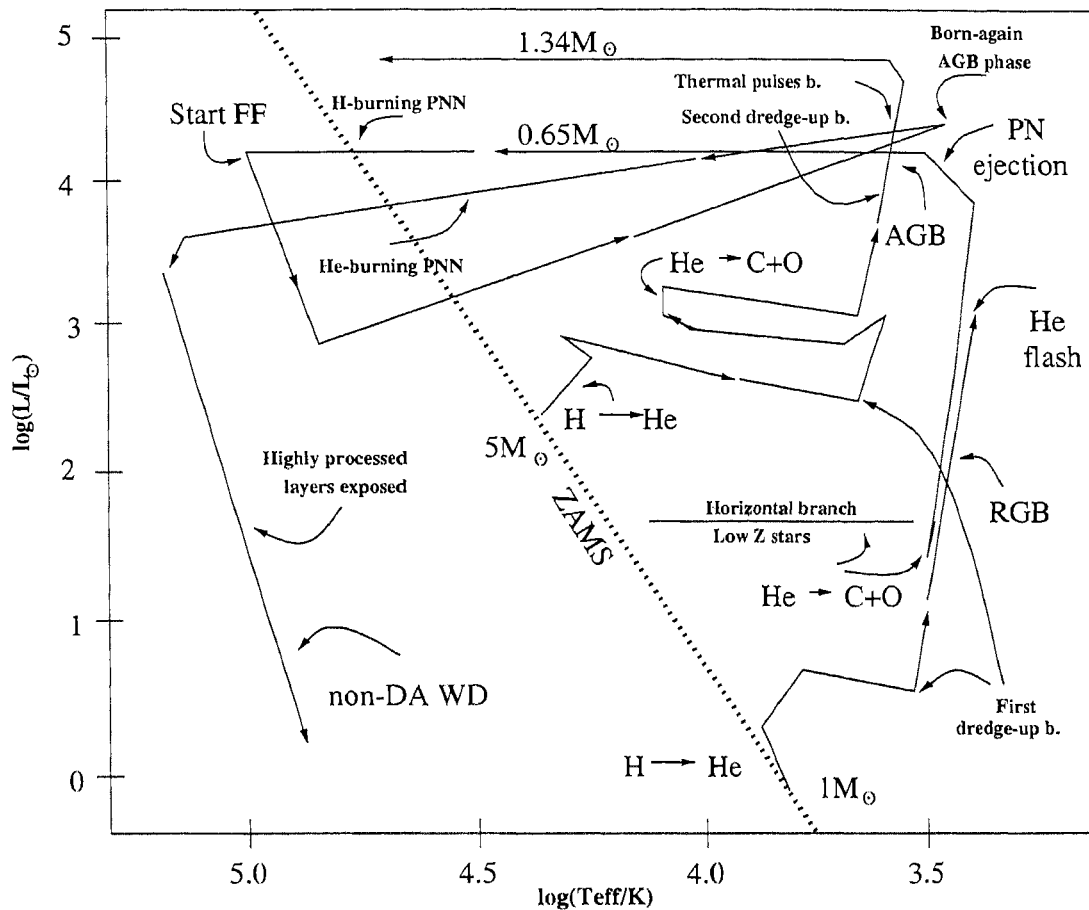


Figure 1.1: Evolutionary tracks for $1M_{\odot}$ and $5M_{\odot}$ stars plotted on the $\log(T_{eff})$ - $\log(L/L_{\odot})$ plane (reproduced from Iben 1984, 1985). The dotted line represents the Zero Age Main Sequence labelled as ZAMS. A 'b.' means 'begins'. 'PNN' stands for 'Planetary Nebula Nucleus', while 'FF' stands for 'Final Flash'. The Central Stars of Planetary Nebulae (CSPN) of $1.34M_{\odot}$ might continue to become a white dwarf or might undergo a FF event. For $0.65M_{\odot}$, we have traced the *born-again* evolution although not all remnants of that mass become *born-again* (see text).

The helium-burning in the core produces carbon and oxygen. Once the helium in the core is exhausted, the carbon-oxygen core contracts increasing the pressure and temperature of the overlaying layers. Now helium ignites in a shell near the core while hydrogen shell is pushed out and extinguished. The star at this stage has a carbon-oxygen degenerate core, which is not burning, a helium shell source, and a hydrogen shell which is not ignited. These layers are protected by a large hydrogen-rich envelope into which

the products of the previous nucleosynthesis have been mixed by the first and/or second dredge-ups (Becker and Iben 1979; Iben and Renzini 1983). The star at this stage is near the base of the Asymptotic Giant Branch (AGB; $L \approx 10\text{-}2000L_{\odot}$, $T_{eff} \approx 4000\text{ K}$), the Early-Asymptotic Giant phase (E-AGB). As the helium shell source dumps its ashes on to the helium-exhausted core, its mass increases (Paczynski 1971) causing an increase in luminosity at virtually constant temperature. The star simultaneously expands and acquires a giant structure for the second time.

When hydrogen shell is re-ignited the star enters the double shell (helium and hydrogen) source phase, called the thermally pulsating AGB phase (TP-AGB). During this phase, near the tip of the AGB, the star experiences a series of thermal pulses due to the helium shell undergoing sudden thermonuclear runaway episodes. The number and frequency of these episodes depend on the mass of the star, although it is not clear exactly what relationship ties these quantities (Iben 1975). Nor is it clear just how much mass is lost during the AGB (Reimers 1975; Iben and Rood 1970; Knapp et al. 1982). AGB stars are optically obscured by the dust shells, which are formed by the enormous amounts of material that is lost by these fairly cool objects. Based on the properties of circumstellar dust, an estimation of the amount of mass lost during the AGB phase is possible.

The mass loss rate continues to increase towards the end of the AGB phase. During this phase the H-rich outer envelope is essentially lost. The large mass loss, which is via a powerful stellar wind (Bowen and Willson 1991), prevents the core from reaching the Chandrasekhar limit ($1.4M_{\odot}$) before carbon ignites under degeneracy conditions. When the envelope mass is the order of $10^{-2}M_{\odot}$, the AGB phase is terminated (Hayashi limit), and the star (stellar core) evolves along a constant luminosity track across the H-R diagram. Simultaneously the velocity of the stellar wind, which imparts momentum to the dust particles in the envelope, increases, and the circumstellar material ejected previously is swept up. Soon the stellar temperature is sufficiently high enough to excite the surrounding gas to produce a planetary nebula (PN).

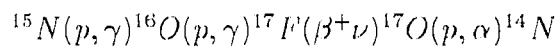
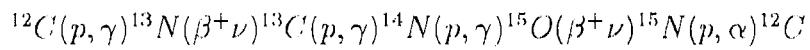
Eventually all nuclear burning ceases and the remnant continues to contract and cool. As the core mass does not exceed the Chandrasekhar limit for low and intermediate mass stars, the stellar relic ends up as a degenerate star. This is the beginning of the evolution of a white dwarf (WD) shining only dimly due to the heat radiating out. The star has reached its final fate when ultimately not even this energy source provides any luminosity.

1.4 Photospheric chemical evolution

One of the most important tracers of stellar evolution is the photospheric chemical content of the star. The nucleosynthesis takes place alternately in the core and in the shells surrounding the core, during the course of its evolution. There are mainly three stages, called the dredge-up phases, during which the products of core and shell-burning are brought to the surface of the star by convective mixing. Thus the study of the chemical content of the photosphere, the only region accessible for observations, will give us information about the location and evolutionary status of these stars in the H-R diagram.

We limit our description to the chemical evolution of low to intermediate mass stars, or in other words, those objects which are thought to end their lives as cooling white dwarfs.

First dredge up: During the ascent on the red-giant branch, the convective envelope brings material, which was subjected to hydrogen shell burning via the CNO-cycles, to the photosphere:



The $^{14}\text{N}(p, \gamma)^{15}\text{O}$ reaction has the lowest cross-section, which implies a net increase in ^{14}N at the cost of C and O. The total sum of CNO nuclei remains constant. Also an increase in $^{13}\text{C}/^{12}\text{C}$ ratio occurs in the hydrogen burning layers. ^{13}C ion also serves as a neutron source via $^{13}\text{C}(\alpha, n)^{16}\text{O}$ during a later stellar evolutionary phase of He burning. The outcome of first dredge up is an increase in N at the expense of C, while He and O remain unchanged. This is rather well established by theory and observations (Iben, 1991 and references therein).

Second dredge up: This phase of mixing happens during the ascent from the horizontal branch towards the AGB. Again the material from the hydrogen burning shell is brought to the surface of the star yielding basically the same enhancement as during the first dredge up and also an enhancement in the helium abundance (Becker and Iben, 1979).

Third dredge up: The main nucleosynthetic process and energy source during a thermal pulse is the 3α -process, $3\alpha \rightarrow ^{12}\text{C}$. As the ensuing reaction $^{12}\text{C}(\alpha, \gamma)^{16}\text{O}$ is slower, the

final $^{12}\text{C}/^{16}\text{O}$ ratio by mass becomes about 2 (Iben and Renzini, 1983). Subsequent α -captures on ^{12}C may also generate α -elements like Ne, Mg, Si and S. The rate of this reaction is not well determined and is responsible for one of the most important uncertainties in nuclear astrophysics. The abundances of medium mass elements and $^{12}\text{C}/^{16}\text{O}$ ratio depend critically on its determination (Weaver and Woosley 1993; Wallerstein et al. 1997). The other important nucleosynthetic processes happening in the He burning episodes of an AGB star involve neutron production. The two main neutron sources are the $^{22}\text{Ne}(\alpha, n)^{25}\text{Mg}$ and the $^{13}\text{C}(\alpha, n)^{16}\text{O}$ reactions. ^{22}Ne is the result of successive α -captures on ^{14}N , while ^{13}C is synthesised by hydrogen CNO burning. $^{22}\text{Ne}(\alpha, n)^{25}\text{Mg}$ reaction is thought to be the main source of neutrons in more massive AGB stars, while $^{13}\text{C}(\alpha, n)^{16}\text{O}$ is more important in low mass objects (Iben and Renzini 1983; Gallino et al. 1989). The ^{22}Ne and ^{13}C ions are mixed to the helium burning layer during a thermal pulse and the free neutron can be captured by Fe seed nuclei, resulting in s-process isotopes. The produce of a thermal pulse can become visible only when the material subjected to helium burning and neutron capture process is brought to the surface during the third dredge up. A net increase in He, an increase in C, N and O, an enhancement of s-process elements and probably an increase in α -isotopes are expected.

1.5 Models of the hydrogen-deficient stars

Two scenarios are put forward to explain the formation of HdC, R CrB and EHe stars: (i) merging of two white dwarfs, also known as the Double Degenerate scenario, and (ii) final helium-shell flash in a single Post-AGB star which bloats the star to giant dimensions, also known as the born-again scenario.

1.5.1 The Double Degenerate scenario (DD scenario)

The DD scenario tries to explain, in particular, the formation of R CrB and EHe stars. From the knowledge of binary star evolution it is expected that a small fraction of binary systems evolve finally into a pair of degenerate white dwarfs, consisting of either two helium white dwarfs or one carbon-oxygen white dwarf, surrounded by helium and hydrogen layers, and one helium white dwarf, which is less massive than the carbon-oxygen white dwarf. Angular momentum losses via gravitational wave radiations reduce the separation of both components, resulting in the shrinking of the orbit. The merging is expected to

take place until the lower mass component fills its Roche lobe and transfers material to the heavier mass component and in the process gets totally disrupted and engulfed by the companion. Subsequently, the merged star undergoes helium shell burning that might result in an expansion of its envelope to red giant dimensions, which might last up to $\sim 10^5$ years. These ideas were put forward by Webbink (1984), Iben and Tutukov (1985). In addition the condition that the core mass of the merged system is less than $1.4M_{\odot}$ has to be maintained. The calculations of such a merging process by Iben (1990) also show that the resulting helium shell burning supergiants of low mass and high luminosity could last for a considerable length of time ($10^4 - 10^5$ years). In this scenario, the coexistence of high abundances of C and N at the surface of R CrB stars is explained by invoking some mixing between the C-O WD which contains C but no N, and the He WD which contains N but no C. The mixing takes place possibly at the time of merging (Iben and Tutukov 1985). In the above mentioned scheme, it is not clear whether a surface $C/O > 1$ would result. The advantages of this scenario are the generation of low mass helium supergiants with rather long lifetimes, and the ability to account for the absence of ^{13}C , since such an isotope is virtually absent in both merging WDs. But, it is hard in this scenario to account for the surface abundance of H and Li, and perhaps also C observed in R CrB stars.

The DD scenario implicitly assumes the existence of sufficient number of C-O + He WD pairs close enough to merge in a time less than the Hubble time. Survey by Bragaglia et al. (1990) indicate that perhaps 10% of WDs are DD systems, but their relatively long periods make them to take many Hubble times to merge.

1.5.2 The Final helium-shell Flash scenario (FF scenario)

Instead of continuing its evolution towards white dwarf, a post-AGB star may move towards AGB again due to a Final Helium-Shell Flash, occurring on the white dwarf track (Fujimoto 1977; Schönberner 1979). In this model about 10% of all the post-AGB stars are predicted to experience a final helium shell flash, after the hydrogen shell has extinguished, and while the star is moving towards WD stage. During this phase, the convective shell generated by the FF may ingest the residual surface hydrogen of the post-AGB star. The hydrogen ingestion provides enough energy to expand the upper half of the convective shell to a giant (R CrB) size (Iben and Renzini 1983 and the references therein). The duration of the bright post-ingestion phase is about 10% of the typical

bright post-AGB phase. Perhaps, during 10% of this time (post-ingestion phase) the star is large enough to be called a giant, while during the rest of the time it is a hot helium star or a hot Post-AGB star with WR spectral characteristics; this suggests that 1 out of every 1000 post-AGB stars might exhibit R CrB characteristics.

In the above scenario, the R CrB-surface composition is expected to result in the following way. Along with hydrogen, some ^3He will also be ingested in the convective shell, as this isotope is expected to be present in nearly one part in thousand by mass in the envelope of low mass evolved stars. The reaction $^3\text{He}(\alpha, \gamma)^7\text{Be}(e^+ \nu)^7\text{Li}$ will soon convert ^3He to ^7Li via electron capture, a process commonly known as Cameron-Fowler process (Cameron and Fowler 1971). The ability to account for the presence of lithium in some R CrB stars is one of the attractive features of FF scenario. The precise proportion of ^{13}C and ^{14}N produced by the reaction chain $^{12}\text{C}(p, \gamma)^{13}\text{N}(e^+ \nu)^{13}\text{C}(p, \gamma)^{14}\text{N}$ operating at the base of the outer convective shell will depend on the actual C/H ratio, which is around unity. A large abundance of ^{13}C is expected, with the $^{12}\text{C}/^{13}\text{C}$ ratio not too far from the equilibrium value, ≈ 3.5 . This does not, however, explain the reported absence of isotopic Swan bands in R CrB stars. Recent studies of Sakurai's object, which is believed to have experienced the final He-shell flash, show isotopic bands of the Swan system, $^{12}\text{C}/^{13}\text{C} \sim 5$ (Lambert et al. 1999). The absence of ^{13}C in R CrB stars may be due to the operations of the reaction $^{13}\text{C}(\alpha, n)^{16}\text{O}$. Calculation by Iben and McDonald (1995) shows that once all the hydrogen is virtually burned (ingested) in the upper shell (hydrogen shell source), the two convective shells (hydrogen shell source and helium shell source as described in section 1.3) reconnect. The products of hydrogen burning (^{13}C and ^{14}N) are convected to the hot, still helium burning base of the reconnected shell. Once the ^{13}C -rich material has reached a temperature $\approx 1.5 \times 10^8$ K, the reaction $^{13}\text{C}(\alpha, n)^{16}\text{O}$ operates, liberating again a lot of energy, and a second shell splitting episode could take place. Now ^{13}C might burn at the base of the upper shell, while helium continues to burn at the base of the lower shell. In this way ^{13}C can be efficiently removed from the upper shell. The reaction $^{13}\text{C}(\alpha, n)^{16}\text{O}$ operates at a lower temperature compared to the α -capture reaction on ^{14}N , which saves the ^{14}N from being destroyed at the cost of ^{13}C . Eventually the flash dies out, the lower convective shell disappears, and the surface is left rich in ^4He , ^{12}C , ^{14}N , possibly with residual traces of unburned hydrogen and ^7Li , similar to the composition we observe in R CrB stars. The neutrons produced by the α -capture reaction on ^{13}C , could be captured by ^{14}N . Those neutrons which escape nitrogen-capture will produce

enrichment of s-process elements, as observed in R CrB stars (Rao and Lambert 1996).

The FF scenario still faces the challenge to explain successfully: (i) the expansion of the carbon-rich intershell region to $50\text{-}100R_{\odot}$, (ii) duration of the R CrB phase, once red giant dimensions have been achieved, and (iii) the very special surface composition of R CrB stars.

It is encouraging to find three objects that substantiate FF scenario; these are the famous old PNe A30 and A78, and the false-nova V605 Aql. Recent observations of two more objects, FG Sge (Gonzalez et al. 1998) and Sakurai object (Asplund et al. 1997), also support the FF conjecture.

The two scenarios described above have theoretical and observational flaws and need a more comprehensive study. The study by Rao and Lambert (1996) indicates that R CrB stars can be grouped into two classes—minority and majority, based on the abundance ratios Si/Fe and S/Fe, which are non-solar. The majority class R CrB stars shows lower Si/Fe and S/Fe ratios, as compared to the minority class. The two classes may be the outcome of the two scenarios suggested for the formation of R CrB stars. Lambert and Rao (1994) earlier speculated that large S/Fe and Si/Fe ratios could result from rp-process due to the merger of two white dwarfs. In all probabilities, both evolutionary scenarios might be responsible for the formation of hydrogen-deficient stars.

1.6 Aim of the thesis

The observed surface composition offers a unique opportunity to study the nucleosynthesis that had occurred deep inside the stars in the past and to test our understanding of the energy-providing reactions. Fine analysis of the spectra using appropriate model atmospheres enables one to obtain reliable surface abundances, surface gravities and effective temperatures. Earlier abundance analyses of hydrogen-deficient stars were mainly based on coarse-analysis or curve-of-growth method. The first self-consistent spectroscopic analyses using hydrogen-deficient model atmospheres for the classical B-type, EHe star HD 124448 (Popper's star) and for three R CrB stars were performed by Schönberner and Wolf (1974) and Schönberner (1975), respectively. The above analyses provided quanti-

tative estimates of hydrogen-deficiency and overabundance of helium and carbon in these stars.

EHe stars can be roughly grouped into two sequences, one with $\log(L/M) \sim 4.5$ and the other with $\log(L/M) \sim 3.7$, when plotted in the $\log g$ - $\log T_{eff}$ plane. Their surface temperature ranges from 8000 K to 30,000 K. Some of the EHe stars show low amplitude photometric and radial velocity variations with periods ranging from a few hours to a few days. EHe stars have the following abundances: $n_{He} = 0.99$, $n_C = 0.01$ and $n_H \leq 0.001$; nitrogen is enriched relative to iron, when compared with the solar abundance, $0.4 < [N/Fe] < 1.2$; oxygen abundance relative to iron lies in the range, $[O/Fe] = -0.6$ to 0.8 ; the mean silicon and sulphur abundances relative to iron are $[Si/Fe] \sim [S/Fe] \approx 0.4$ (Jeffery 1996).

R CrB stars also lie along a line which represents the locus of constant $\log(L/M)$ in the range 3.5 to 4.5, when plotted in the $\log g$ - $\log T_{eff}$ plane. Most of the R CrB stars lie in the temperature range 5000 K to 8000 K, and show radial pulsations with periods ≈ 40 days. The pulsation amplitudes are larger compared to EHe stars. R CrB stars exhibit a range in hydrogen deficiency ($n_H \leq 0.001$), and possibly have $C/He \approx 1\%$. The iron abundance is a very important indicator of the different populations, and hence of age. The minority class and majority class R CrB stars show a linear relation in $Si/Fe \sim S/Fe$ ratios. The majority class R CrB stars have lower $[Si/Fe] \sim [S/Fe] \approx 0.6$ ratios when compared to the minority class. $[N/Fe] \approx 1.6$ for the majority R CrB stars. The s-process elements relative to iron are overabundant in R CrB stars with respect to solar abundance (Lambert et al. 1999).

Hydrogen deficiency, luminosity-to-mass ratio, C/He , and abundance pattern suggest a possible link between the two sub-groups, R CrB and EHe stars.

In a tentative evolutionary chain ($HdC \rightarrow R\ CrB \rightarrow EHe \rightarrow He\text{-}sdO^+ \rightarrow$ non DA-white dwarfs), HdC/R CrB stars are seen as precursors of hot R CrB /EHe stars; these then evolve to the He- sdO^+ stars and then to non DA-white dwarfs (Jeffery 1994; Schönberner 1996 and references therein), if one goes by their location in the $\log g$ - $\log T_{eff}$ plane and the assumption that they evolve towards hotter temperatures. The evolutionary chain mentioned above within the carbon-rich group, proposed by Jeffery (1994), is not well established. In the carbon-rich group a few sub-groups exist, and the interconnections between these sub-groups are yet to be established.

A group of four hydrogen-deficient stars classified as EHe stars of intermediate temper-

ature (8000 K – 13,000 K) are available in the list provided by Jeffery et al. (1996). These stars overlap with R CrBs in temperature, but do not undergo the light decline which is typical of R CrBs. They possibly represent an intermediate stage in the evolutionary sequence, R CrB – hot EHe stars. These stars, however, show low amplitude photometric and radial velocity variations with periods which are larger than that of hot EHe stars, but smaller than that of R CrB stars (Lawson et al. 1993). Two of these intermediate group stars (FQ Aqr and LS IV -14° 109) that have been analyzed spectroscopically were found to be similar to R CrB stars in their photospheric abundances and L/M (Rao et al. 1996; Lambert et al. 1999). These two stars fall on the line of constant L/M, along with R CrB stars and hot EHe stars when plotted in the $\log g$ - $\log T_{eff}$ plane, which is equivalent to the H-R diagram. Lines of constant L/M in the $\log g$ and $\log T_{eff}$ plane are representative of the evolutionary tracks of giants contracting towards the white dwarf sequence. The location of these stars across the H-R diagram implies that these are giants expanding towards or contracting away from the red limit, which occurs at constant luminosity (Jeffery 1996 and the references therein).

Since it is likely that the intermediate temperature EHe stars are evolutionarily linked to the R CrB and hot EHe stars, it is quite possible that they are transition objects evolving either to hot EHe stars or to R CrB stars. The main objective of the present work was to carry out an extensive abundance analysis of these intermediate temperature stars and to explore whether they exhibit abundance characteristics that lie in between those of R CrB and hot EHe stars. Fine analyses of the spectra of these stars with appropriate model atmospheres give us estimates of T_{eff} , $\log g$, and photospheric elemental abundances that may provide continuity and connections with properties of R CrB and EHe stars and thus might suggest evolutionary connections. Most of the R CrB stars show enhancement of light s-process elements, like Y and Zr, over the heavy s-process elements, like Ba and La, when compared with the solar abundance. This suggests neutron exposures to stellar material with composition different from that of solar (Rao and Lambert 1996). The photospheric elemental abundances of the intermediate temperature EHe stars, in particular, the s-process elemental abundances, are not explored so far. The abundance ratios S/Fe and Si/Fe when combined with the s-process elemental abundances provide additional clues to examine the possible evolutionary links between these objects, hot EHe stars and R CrB variables. The abundances of s-process elements might also provide us with additional clues to establish the kinship with other post-AGB stars.

MV Sgr, one of the three stars classified as hot R CrB stars, is known to show several prominent emission lines, including forbidden lines. With a view to investigating the distribution of the emitting gas and the atmospheric mass flows in MV Sgr, we also planned to carry out a high resolution study of its emission line spectra.

Chapter 2

Observations, data reductions and spectral line identification

2.1 The sample

Jeffery et al. (1996) have compiled a list of hydrogen-deficient stars, which includes both R CrB stars and EHe stars. The EHe stars with temperatures greater than 13,000 K have been the objects of several spectroscopic investigations (Jeffery 1996 and references therein), while the EHe stars in the temperature range 8,000 – 13,000 K have received comparatively less attention spectroscopically, especially at high resolution. We selected four stars in the above temperature range from the list of Jeffery et al. (1996) – FQ Aqr (BD +1° 4381), LS IV -14° 109, BD -1° 3438 and LS IV -1° 002 – for a detailed elemental abundance analysis using high resolution, high S/N spectra. These stars are cooler among the extreme helium stars, and overlap in temperature with the hotter end of R CrB stars.

In addition to these objects we have carried out an extensive study of the emission line spectra of MV Sgr (Pandey et al. 1996), which is classified as a hot R CrB with an effective temperature of 16000 K and similar to EHe stars.

2.1.1 FQ Aqr

FQ Aqr (BD +1° 4381) was discovered to be a hydrogen-deficient star by Drilling (1979). He concluded that it has an effective temperature similar to that of the hydrogen-deficient binary v Sgr ($T_{eff} = 13000$ K), and a comparatively lower hydrogen abundance. Drilling et al. (1984) have estimated an effective temperature of 9500 ± 400 K, using the ultraviolet flux distribution obtained with the International Ultraviolet Explorer (IUE) and broad-band photometry. Drilling et al. (1984) and Heber and Schönberner (1981) have estimated the E_{B-V} values as 0.1 and 0.23, respectively. The recent abundance analysis of FQ Aqr by Lambert et al. (1999) have yielded a T_{eff} of 8500 K and a $\log g$ of 1.5. The reported apparent visual magnitude m_V is 9.6 (Jeffery et al. 1996). FQ Aqr is suspected to be a low amplitude, photometric and radial velocity variable (Lawson and Cottrell 1997).

2.1.2 LS IV -14° 109

This star was discovered to be an extreme helium star by Drilling (1979) who determined its effective temperature to be slightly lower than that of the HdB v Sgr. Later, Drilling et al. (1984) revised the effective temperature of the star to be 8400 ± 500 K, using ultraviolet flux distribution obtained with the IUE and broad-band photometry. Drilling et al. (1984), and Heber and Schönberner (1981) derived the reddening towards LS IV -14° 109 as $E_{B-V} = 0.2$ and $E_{B-V} = 0.43$, respectively. The recent abundance analysis of LS IV -14° 109 by Lambert et al. (1999) have shown that the $T_{eff} \approx 9000$ K and $\log g \approx 1.0$. The apparent visual magnitude of the star is 11.2 (Jeffery et al. 1996). Most likely, LS IV -14° 109 is a low amplitude, photometric and radial velocity variable (Lawson and Cottrell 1997).

2.1.3 BD -1° 3438

This is one of the eight stars described by Hunger (1975) as extreme helium stars. This star was found on IIA-O objective prism plates taken with the University of Michigan's Curtis Schmidt-type telescope situated at Cerro Tololo, Chile. The spectrum of BD -1° 3438 was found to be very similar to those of the known hydrogen-deficient B stars HD124448, HD168476, and BD +10° 2179, which were also observed on IIA-O plates (MacConnell et al. 1972). Drilling et al. (1984) have estimated an effective temperature of 10900 ± 600 K for this star, using the ultraviolet flux distribution obtained with the

IUE and broad-band photometry. The reddening estimates are $E_{B-V} = 0.4$ and $E_{B-V} = 0.55$, by Drilling et al. (1984), and Heber and Schönberner (1981), respectively. The preliminary result of a fine analysis is $T_{eff} = 12500 \pm 1000$ K (Schönberner 1978). The reported m_V is 10.3 (Jeffery et al. 1996). The observations by Lawson and Cottrell (1997) showed that BD $-1^\circ 3438$ is a low amplitude, photometric and radial velocity variable, like FQ Aqr and LS IV $-14^\circ 109$.

2.1.4 LS IV $-1^\circ 002$

LS IV $-1^\circ 002$ was discovered to be a hydrogen-deficient star by Drilling (1980). He found that the spectrum of this object is nearly identical to that of the extreme helium star HD168476, for which Schönberner & Wolf (1974) had found $T_{eff} = 13500$ K. From the strengths of Si II and Mg II lines, which appear a little stronger in LS IV $-1^\circ 002$, he predicted that the effective temperature might be slightly lower. The effective temperature that is estimated using ultraviolet flux distribution and broad-band photometry is 11900 ± 400 K (Drilling et al. 1984). Drilling et al. (1984), and Heber and Schönberner (1981) found the E_{B-V} values to be 0.45 and 0.52, respectively. The reported m_V is 11.0 (Jeffery et al. 1996). LS IV $-1^\circ 002$ is also a low amplitude, photometric and radial velocity variable, like the rest of the cool EHe stars mentioned above (Lawson and Cottrell 1997). Most of the cool EHe stars exhibit a velocity amplitude of about 2.0 km s^{-1} and a light amplitude of about 0.03 mag. On the contrary R CrB stars have, typically, velocity amplitudes of 10 to 20 km s^{-1} and light amplitudes of 0.2 to 0.3 mag (Lawson and Cottrell 1997).

2.1.5 MV Sgr

MV Sgr, with DY Cen and V348 Sgr, is one of the select trio of hot R Coronae Borealis stars. Its identification as a R CrB variable was made by Hoffleit (1958). The spectrum of MV Sgr at maximum light has been described by Herbig (1964, 1975a) as that of a hydrogen deficient B-type star with several emission lines prominent in the red and attributable to $H\alpha$, Fe II, He I, Si II, Ni, Ca II and O I. He suggested that the excitation temperature of the Fe II emission region is substantially lower than the colour temperature of the star. Rao and Nandy (1982) noticed low excitation lines of Fe II, Si II, Cl I, O I, Al II in absorption in the ultraviolet and showed that they varied in strength whereas

higher excitation absorption lines (e.g. C II, Al III) did not. From the dereddened flux distribution from the visual to the ultraviolet, Drilling et al. (1984) estimated the star's T_{eff} as 15400 ± 400 K.

Based on high resolution spectra obtained in the blue, Jeffery et al. (1988) analyzed the photospheric (absorption) spectrum at maximum light and concluded from the hydrogen and helium lines that the star is hydrogen deficient to the same degree as the hot helium star HD 124448 ($H/He < 1 \times 10^{-4}$), but nitrogen and silicon are underabundant by about a factor of ten and carbon is down by a factor of about 100 relative to it. They also remarked that all Fe II emission lines present in their spectrum are split with a peak separation of 68 km s^{-1} . It was argued that the emitting region was optically thick in the Fe II lines. Other emission lines were attributed to Mg II, Ca II, Ti II and Si I. Rao et al. (1990) identified forbidden [S II] lines in the blue.

An infrared excess was observed by Feast and Glass (1977), Kilkenny and Whittet (1984), and Walker (1986). The infrared spectrum appears to be a composite of two black bodies, one at 1600 K and a second at 230-550 K. The distribution of the dust around the star is unknown but one presumes the 1600 K dust is closer to the star than the 250 K dust.

2.2 Observations

The high resolution optical spectra of EHe stars were obtained on 25 July 1996 at the W. J. McDonald Observatory 2.7-m telescope with the coude cross-dispersed echelle spectrograph (Tull et al. 1995). The spectrograph setup gives a 2-pixel resolving power ($R = \lambda/\Delta\lambda$) of 60,000. The detector was a Tektronix 2048×2048 CCD. The recorded spectrum covered a wavelength range from 3800 \AA to 10000 \AA , but the spectral coverage was incomplete longward of about 5500 \AA . A Th-Ar hollow cathode lamp was observed either just prior to or just after exposures of the programme stars to provide wavelength calibration. In order to remove the pixel-to-pixel variation in the sensitivity of the CCD flat-field exposures are needed; these were obtained by observing a lamp providing a continuous spectrum. Typical exposure times of our programme stars were 30 minutes, and two exposures were co-added as it was necessary to improve the signal-to-noise ratio of the final spectrum, and to identify and eliminate cosmic rays. There was no wavelength overlap in the red orders. To compensate for the missing wavelength regions, observations

were made at a slightly different grating setting on 26 July 1996, to get full wavelength coverage for two of the programme stars, FQ Aqr and BD -1° 3438. The FWHM of the Th-Ar comparison lines and the atmospheric lines present in the spectra corresponds to 6.0 km s^{-1}

The spectra of MV Sgr were obtained with the 4-m telescope at the Cerro Tololo Inter-American Observatory, equipped with a Cassegrain echelle spectrometer and CCD detector. The observations were obtained on the night of 22/23 May 1992. The spectrum covers the wavelength range $5480 \text{ \AA} - 6980 \text{ \AA}$. The FWHM of the terrestrial [O I] line at 5577 \AA in the final co-added spectrum corresponds to 9.0 km s^{-1} , or a resolution of 33,000. This resolution is confirmed by the widths of the Th lines in exposures of a Th-Ar hollow cathode lamp taken immediately following the stellar exposures. The signal-to-noise ratio in the continuum at the peak of the echelle blaze runs from about 80 at 5500 \AA to 85 at 6800 \AA .

2.3 Data reductions

We have used the Image Reduction and Analysis Facility (IRAF) software packages for reducing the spectra of extreme helium stars. IRAF is developed and distributed by the National Optical Astronomy Observatories and operates under the UNIX environment. The spectra of MV Sgr were reduced using RESPECT and IRAF software packages. RESPECT is an interactive software package that was developed at Vainu Bappu Observatory in 1985 for the reduction of astronomical spectroscopic data. RESPECT operates on the VAX VMS platform and a description of the software can be found in Prabhu et al. (1987). For MV Sgr most of the basic reductions and wavelength calibrations were done using RESPECT while the equivalent width measurements were done using IRAF.

2.3.1 Basic steps in the reduction

The bias and dark frames are first subtracted from the object spectra and then the flat field correction is applied on the object CCD images to correct for pixel-to-pixel variation in response; these are the preliminary steps involved in the reduction of the spectra. The bias frames taken on each night are averaged using the IRAF task *zerocombine*, and the resultant master bias is subtracted from the object frames and the flat field frames of that particular night. The task *ccdproc* in the CCDRED package is used for the above. The

bias subtracted flat-fields are then combined using the median option in the *flatcombine* task. The flat-fields are then normalized using the *apnorm* task in the SPECRED package in IRAF. The bias subtracted object frames are divided by the normalized master flat images, to remove the wavelength dependent pixel-to-pixel variations across the CCD chip. The dark current is also subtracted from the object frames using CCDPROC. Now the one dimensional spectrum can be extracted from the object frames which are bias-subtracted, flat-fielded and corrected for dark current.

2.3.2 Extraction of spectrum

The extraction of one-dimensional spectrum involves specifying the location of the object on the slit, and the aperture, which is determined by the spatial extent of the object, and then tracing the curvature of the object spectrum along the dispersion axis. It is necessary to assign appropriate aperture to each order because the width of the spectrum changes from order to order. In some cases, where the background is high, either due to long exposures or due to contamination by moonlight, the background subtraction from adjacent pixels within the slit is required and the sample regions for estimating the sky background should be provided. The signal within the defined apertures (normally 6–10 pixels) is then summed and the background is removed. The task *apall* in SPECRED (ECHELLE) package allows one to perform all the above mentioned operations for extracting the one-dimensional spectrum from the object frame. This task also provides an option to remove cosmic ray hits from the spectrum. The resulting output from running the task *apall* is the extracted one-dimensional star spectrum (echelle orders) in the form of counts versus pixel numbers and is free of cosmic ray hits.

2.3.3 Wavelength calibration

Wavelength calibration of the star spectrum requires similarly extracted spectra of the comparison source (Thorium–Argon). The emission lines in the spectrum of the thorium–argon comparison source are identified using the atlas of thorium–argon laboratory spectra by D’Odorico et al. (1987). The dispersion correction is determined from the wavelength calibrated spectrum of the comparison source by fitting a legendre polynomial of order 2 or 3. The above procedure is carried out by using the task *identify* in SPECRED or the *ecidentify* task in the ECHELLE package. Finally, the object spectrum is wavelength

calibrated using the task *dispcor* with the corresponding comparison source spectrum as the reference. Now we have the stellar spectrum in counts versus wavelength. The stellar spectrum is then normalized to the continuum, by fitting a slowly varying function such as cubic spline to the continuum. The continuum is estimated visually, using the average of the highest points in the spectrum, from regions free of emission and absorption features.

2.3.4 Spectral line identification

Spectral lines of cool EHe stars were identified using Revised Multiplet Table, RMT (Moore 1972), the selected Tables of Atomic Spectra (Moore 1970), Kurucz and Peytremann (1975), and also from the investigations of Hill (1964, 1965) and Heber (1983). For confirmation we have checked for different lines and their intensities within a multiplet. A number of C I, C II and He I lines were identified. No lines of He II were found. With the notable exception of hydrogen, lines of all elements, which would be expected and observed in early B-type normal stars, have been found. A large number of lines of the ionized metals of the iron group are identified. These lines are much stronger when compared with those observed in early B-type normal stars, a notable feature of the spectra of cool EHe stars, and can be attributed to the relatively low opacity in the atmosphere due to hydrogen deficiency. Our large spectral coverage (3780–11000Å) enabled us to identify all important elements in one or two stages of ionization.

2.3.5 Measurement of equivalent widths

The equivalent width (W_λ) is the ultimate measurement that is made in order to proceed with the determination of elemental abundances in stellar photospheres. Equivalent width is a measure of line strength. The equivalent widths have been measured in two ways using the *splot* task in IRAF:

- 1) by fitting a gaussian profile to the absorption line and
- 2) by measuring the total area under the line.

If the line is symmetric, full width at half maximum of the intensity is taken to fit a gaussian profile. But if the line is not symmetric and has only the left or right wing of the profile as a gaussian form then preference is given to that wing and the left half-widths or right half-widths are used to define the gaussian. The uncertainties in equivalent width measures may be due to the incorrect placement of the continuum between each

measurement and (or) to the fact that the spectral lines are not perfectly gaussian. Slightly blended lines are de-blended using the routines available in the *splot* package. Gaussians were fit to the individual absorption lines and equivalent widths were measured. Severely blended lines were not used in the abundance analysis.

The estimated error involved in the equivalent width measurement, which is due to the inaccuracy in the placement of continuum, is about 10%.

Chapter 3

Model stellar atmospheres

3.1 Atmospheres of normal stars

The physical conditions in the atmospheres of stars must be known in order to account for the observed low and high excitation lines, and the different ionization states of an element. The curve of growth technique, which assumes that the ratio of line to continuous absorption is constant in the atmosphere, is not adequate for comparing the relative behaviour of neutral, singly ionized, and doubly ionized lines of an element. Hence, we need to use a model which allows the variations of the physical parameters with depth.

The atmospheres of normal stars have hydrogen as the major constituent. The continuous absorption (continuum opacity), which determines the shape of the spectral energy distribution, in these stars is mainly due to hydrogen, directly or indirectly, and is listed below:

- (i) In cool stars (spectral types K and M), which occupy the temperature range 4000 K – 5000 K, the continuum absorption is mainly due to H^- , H_2^- and OH^- .
- (ii) In F and G type stars of intermediate temperature (approximately 5000 K to 7500 K), H^- , neutral hydrogen and metallic continua in ultraviolet are the major sources of continuum opacity.
- (iii) In intermediate hot stars (B2 to A0), which lie in the temperature range 10,000 K – 20,000 K, neutral hydrogen controls the continuum opacity. In the case of giants electron scattering also becomes important.
- (iv) In stars of spectral types O to B0, which are hotter than 25,000 K, H I, He I, He II,

and electron scattering are major contributors to continuum opacity.

The abundance of an element in normal stars is conventionally represented relative to hydrogen because of its dominant contribution to continuum opacity.

3.2 Atmospheres of hydrogen-deficient stars

The cool extreme helium stars, like R CrB stars, are hydrogen poor, but overabundant in carbon and nitrogen. However, helium is still the most abundant element. For R CrB stars the continuum opacity is mainly determined by carbon through its bound-free and free-free absorption in the line forming regions. A superposition of the spectra of R CrB stars of F-G type temperature range shows that all C I lines have essentially the same strength in all the stars in spite of differences in the stellar parameters (T_{eff} , surface gravity and microturbulence), while lines from other elements vary greatly (Rao and Lambert 1996).

The continuum opacity in the line-forming regions is completely dominated by the photoionization of C I, and hence the C I line strength is independent of the carbon abundance. Assuming the C I line to be weak and hence on the linear part of the curve-of-growth, we have

$$W_\lambda \sim l_\nu / \kappa_c \propto N_{CI} / N_{CI} = \text{a constant},$$

for the case of C I lines. Here, W_λ , l_ν , κ_c and N_{CI} denote the equivalent width, the line opacity, the continuum opacity and the number density of neutral carbon atoms, respectively. The same is the case for the hydrogen line strength in normal stars, which is insensitive to the number density of hydrogen atoms, because hydrogen (H^- or H) is the major source of continuous opacity. Furthermore, in the case of R CrB stars, carbon is the most important electron donor, and hence indirectly affects the contribution from two other important continuum opacity sources: He^- (mainly in infrared) and electron scattering (Asplund 1997a).

The C I lines observed in the R CrB stars have a minor dependence on T_{eff} because the lower excitation potential of these lines is only slightly smaller than the energy needed for the photoionization of C I. Since the same ionization stage provides the continuous opacity, the C I lines are also insensitive to the adopted surface gravity of the star.

Analysis of the spectra of hydrogen-deficient stars requires model atmospheres with appropriate chemical composition. The chemical composition of these stars gives an

idea of the major sources of continuous opacity, which helps in constructing the model atmospheres. In this section we discuss the construction of hydrogen-deficient model atmospheres for different temperatures and list the important sources of continuum opacity taken into account while computing these model atmospheres.

3.2.1 Construction of model atmospheres

In constructing the hydrogen-deficient model atmospheres, the following issues are to be considered:

- (i) Helium is the most abundant element, but the opacity is made up by other elements, in most cases by the photoionization of neutral carbon.
- (ii) Due to the rather low opacity, the observed lines of many elements are quite strong and cause important blanketing effects.
- (iii) The existing theory of broadening of lines of helium, especially that of ionized helium, need to be considerably improved. The stark broadening of highly ionized carbon or oxygen is still uncertain.
- (iv) Most objects are either quite hot and/or quite extended and demand a full non-LTE treatment and in some cases plane parallel approximation may not be valid.
- (v) The CSPN with Wolf-Rayet spectra have expanding envelopes and need a special treatment incorporating expansion velocity.

Our sample stars have a range in effective temperature ($T_{eff} = 8,000$ K to 13,000 K). For the abundance analysis of stars with $T_{eff} \leq 9,500$ K, we used the new line-blanketed models described by Asplund et al. (1997a), kindly made available by Dr. Martin Asplund. For stars with $T_{eff} \geq 10,000$ K, model atmospheres computed by Jeffery and Heber (1992) were kindly made available by Dr. Simon Jeffery.

The model atmospheres have been computed with the usual assumptions that (1) the energy flux is constant, and (2) the atmospheres consist of plane-parallel layers in hydrostatic and local thermodynamic equilibrium (LTE). Local thermodynamic equilibrium essentially means that the populations of the atoms and ions in different energy levels obey the Saha-Boltzmann statistics.

The LTE assumption is relatively a poor description of the outer atmospheric layers of these stars, and hence some of the very strong lines do require non-LTE treatments. Nevertheless, the LTE approach is used, and care has been taken to avoid strong lines. LTE is an adequate approximation to weak lines formed in deep atmosphere.

Unfortunately, the temperature ranges considered by Asplund et al. and Jeffery et al. (private communications) in the construction of model atmospheres do not overlap.

3.2.2 Models for $T_{eff} \leq 9,500$ K

The important features of this model are the inclusion of the effects of line-blanketing, and new values for continuum opacities. The term line-blanketing describes the influence of thousands to millions of spectral lines on the shape of the continuum. The above grid of models are calculated for temperatures in the range $5000 \text{ K} \leq T_{eff} \leq 9500 \text{ K}$ and gravities in the range $-0.5 \leq \log g \leq 2.0$ [cgs]. The microturbulence is adopted to be $\xi_{turb} = 5 \text{ km s}^{-1}$. The abundances used for the standard grid are mainly taken from Lambert and Rao (1994), and are normalized to $\log \sum \mu_i n_i = 12.15$, where μ_i is the atomic weight of an element i , and n_i its number density. The numerical code solves the radiative transfer equation under the condition of hydrostatic equilibrium with appropriate opacity sampling. The program is an extension of the original MARCS-code (Gustafsson et al. 1975). As already mentioned, in hydrogen-poor stars the opacity is mainly determined by carbon through its bound-free and free-free absorption in the line-forming regions. Also, carbon is the most important electron donor and therefore its abundance affects the contributions from the other major opacity sources, like He^- and electron scattering. All these opacity sources and their effects on the emergent spectra have been included in the model, along with the effects of electron scattering and Rayleigh scattering. In addition to these, the effects of some of the important molecular line opacities are also included in the calculations.

3.2.3 Models for $T_{eff} \geq 10,000$ K

Jeffery and Heber (1992) computed a grid of models for hydrogen-deficient stars using the LTE stellar atmosphere code described by Wolf (1973) and by Schönberner and Wolf (1974). The opacity calculations were made after taking into account the effects of line-blanketing using the tables of opacity distribution functions for helium- and carbon-rich material. The line formation calculations were carried out with the Belfast LTE line-formation code (Dufton, Lennon and Conlon 1989, unpublished) which was extended to operate with hydrogen-deficient mixtures and opacities appropriate to the model atmospheres. The low densities and the scattering dominated continuous opacities encountered

in the atmospheres of hydrogen-deficient supergiants demanded two major modifications to the Belfast code. These are the use of better partition functions in the Saha equation and the inclusion of scattering terms in the radiative transfer equations.

3.2.4 Continuous opacities

It is essential that all important sources of continuous opacities are identified and included in the model atmosphere calculations for a meaningful elemental abundance analysis. Bound-free absorption of H, He, C, N, O, Mg, Al, Si, Ca and Fe, both for neutral and singly ionized species, are included in the models. Free-free opacity of the negative ions of helium, carbon, nitrogen and oxygen are also taken into account. While considering the radiative transfer in the stellar atmospheres, electron scattering and Rayleigh scattering (against H, He and C) are included in the source function $S_\nu = (\kappa_\nu B_\nu + \sigma_\nu J_\nu)/(\kappa_\nu + \sigma_\nu)$, where the first term represents thermal emission and the second the scattering contribution. Atomic and molecular line opacities are also included. Models with temperatures ≤ 9500 K use continuum opacities from Opacity project (Seaton et al. 1994 and references therein), while models with temperatures ≥ 10000 K use opacities from Kurucz (1970) and Peach (1970). Free-free opacity of He I, C I and C II (Peach 1970) have been incorporated together with those for H and H⁻. These are found to be important only in the infrared and in the deeper regions of the atmosphere where temperature is very high.

Using the above described model atmospheres, the line strength is numerically calculated for each line and compared with its observed strength. The details of fine analysis and abundance determination of individual stars is described in the next chapter.

Chapter 4

Abundance analysis of EHe stars

4.1 Normalization of abundances

In the case of normal stars, we calculate the abundance of any element X with respect to hydrogen. The abundance of any element X is given by N_X/N_H , which is its fractional abundance relative to hydrogen, where N_X and N_H are the number of X atoms and number of hydrogen atoms per cubic centimeter, respectively. For normal stars in the temperature domain of R CrB stars and cool EHe stars the continuous opacity is governed by hydrogen. Therefore, in the case of normal stars, for a particular species X, the line strength $\approx l_\nu/\kappa_c \propto N_X/N_H$. This implies that in normal stars the line strength of a particular species is a direct measure of its fractional abundance relative to hydrogen. Similarly, in the context of R CrB stars and cool EHe stars, we take the line strength of a particular species as a measure of its abundance. Since these stars are hydrogen-poor, the continuum opacity is not controlled by hydrogen, but by the photoionization of neutral carbon (Searle 1961; Schönberner 1975). Helium, though the most abundant element in these stars, is a minor source of continuum opacity, unless the C/He is very small; however, it provides the gas pressure. Therefore, in the case of R CrB stars, for a particular element X, the observed line strength $S(X)$ is given by $N_X/N_{CI} = N_X/N_C$.

The mass fraction $Z(X)$, which is a measure of the fractional abundance of a particular element X, is given by

$$Z(X) = \frac{\mu_X N_X}{\mu_H N_H + \mu_{He} N_{He} + \mu_C N_C + \dots} = \frac{\mu_X N_X}{(\sum \mu_i N_i)}, \dots\dots(1)$$

where, μ_i is the atomic mass of element i and the summation in the denominator is conserved through all stages of nuclear burning. The derived abundances are normalized to $\log \sum \mu_i N_i = 12.15$. To convert the observed line strength $S(X) = N_X/N_C$ (only if carbon is the source of continuum opacity) to the more fundamental quantity, the mass fraction $Z(X)$, it is necessary to determine or to assume the carbon to helium ratio ($N_C/N_{He} = C/He$), since He is likely to be the most abundant element. Hence equation (1) may be written in terms of the observable quantity $S(X)$ and C/He ($\ll 1$) to give,

$$Z(X) = \frac{\mu_X}{\mu_{He}} \frac{C}{He} S(X) \dots\dots(2).$$

For cool EHe stars it is necessary to estimate to what extent carbon relative to helium contributes to the continuous opacity so as to find which of the two species is the leading contributor. Thus, the carbon abundance and hence C/He is an important parameter to be determined.

The role of the C/He largely disappears while considering the abundance ratios involving elements other than carbon and helium,

$$\frac{Z(X_1)}{Z(X_2)} = \frac{\mu_{X_1}}{\mu_{X_2}} \frac{S(X_1)}{S(X_2)} \dots\dots(3).$$

The above described abundance representation is followed for the EHe stars which fall at the cool end (see section 4.3) and are similar to F-G type R CrB stars.

For the EHe stars which fall at the hot end (see section 4.3), He I is the major source of continuum opacity (see section 4.2). Since helium is also the most abundant species in these stars, the line strength of any species is a direct measure of its fractional abundance, X/He . The abundances finally derived for these stars are also normalized to $\log \sum \mu_i N_i = 12.15$.

In EHe stars which fall at the cool end, a large number of He I lines are available in their spectra. The line strength of He I is a direct measure of He/C as C I controls the continuum opacity at this end. Therefore, a direct spectroscopic estimate of C/He is possible for the stars which lie at the cooler end using He I lines. Similarly, in the case of EHe stars which fall at the hot end, C I and C II lines provide us a direct spectroscopic estimate of C/He , since it is He I that controls the continuum opacity at the hot end.

4.2 Dominant sources of continuous opacity

We have calculated the individual contributions of important sources to the continuous opacity as a function of optical depth (Warner 1967). The continuous opacity calculations were made for the following model atmospheres:

- (i) $T_{eff} = 9500$ K, $\log g = 1.0$ and $C/He = 1\%$,
- (ii) $T_{eff} = 11000$ K, $\log g = 1.0$ and $C/He = 1\%$, and
- (iii) $T_{eff} = 13000$ K, $\log g = 2.0$ and $C/He = 1\%$.

The above model atmospheres were chosen because they cover the range of T_{eff} and $\log g$ shown by the programme stars (see section 4.4.2). Figures 4.1, 4.2 and 4.3 show the variation of continuous opacity as a function of optical depth due to the major contributors for the above model atmospheres at 5000 \AA .

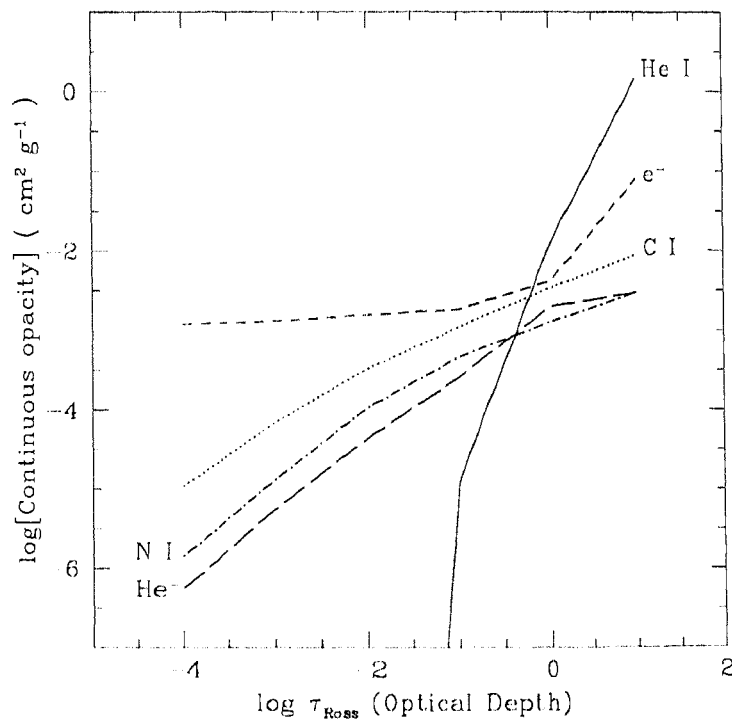


Figure 4.1: Dominant sources of continuous opacity as a function of depth for the model atmosphere: $T_{eff} = 9500$ K, $\log g = 1.0$ and $C/He = 1\%$.

Figure 4.1 shows that e^- and C I are the major sources of continuous opacity in the

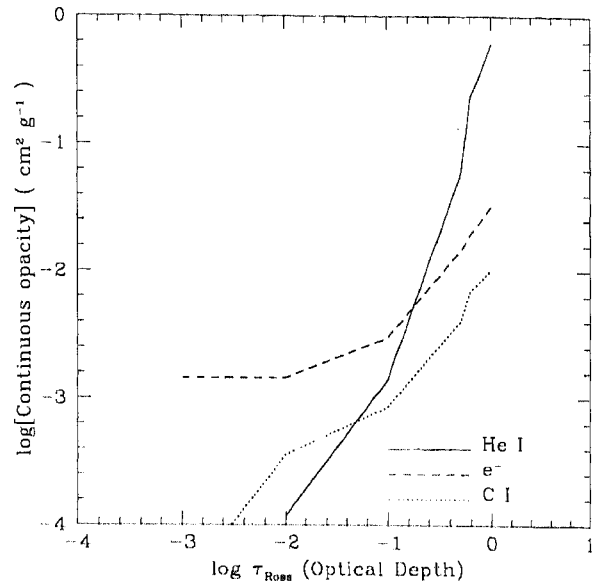


Figure 4.2: Dominant sources of continuous opacity as a function of depth for the model atmosphere: $T_{eff} = 11000$ K, $\log g = 1.0$ and $C/He = 1\%$.

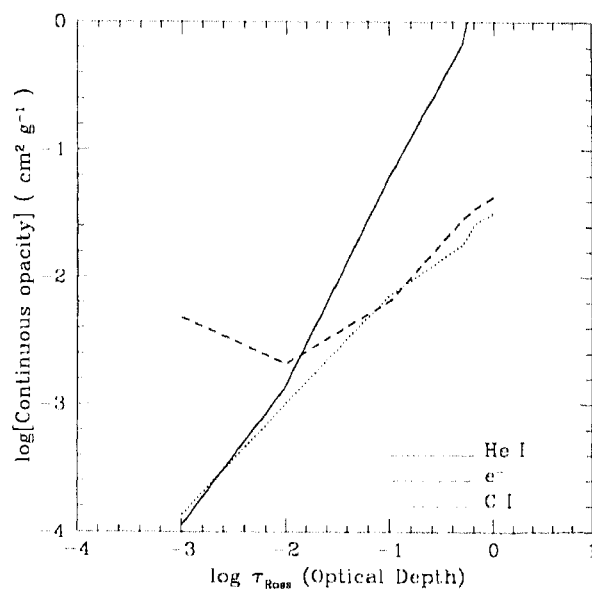


Figure 4.3: Dominant sources of continuous opacity as a function of depth for the model atmosphere: $T_{eff} = 13000$ K, $\log g = 1.0$ and $C/He = 1\%$.

line forming regions ($\log \tau = -2$ to $\log \tau = 0$), and the electron scattering dominates over photoionization of C I. Most of the carbon is in singly ionized state and contributes 50% of the total free electrons.

He I starts dominating as a source of continuous opacity for depths corresponding to $\log \tau$ greater than -0.5 . At $\log \tau = -0.25$, C I and He I contribute to the continuous opacity equally. He I lines, which are expected to form between $\log \tau = -1$ and 0, are direct indicators of He/C in the case of FQ Aqr and LS IV $-14^\circ 109$. On the other hand, for the hotter stars, namely BD $-1^\circ 3438$ and LS IV $-1^\circ 002$, it is evident from Figures 4.2 and 4.3 that He I controls the continuum opacity, and hence C I and C II lines are expected to provide a direct estimate of C/He.

4.3 Carbon to helium ratio

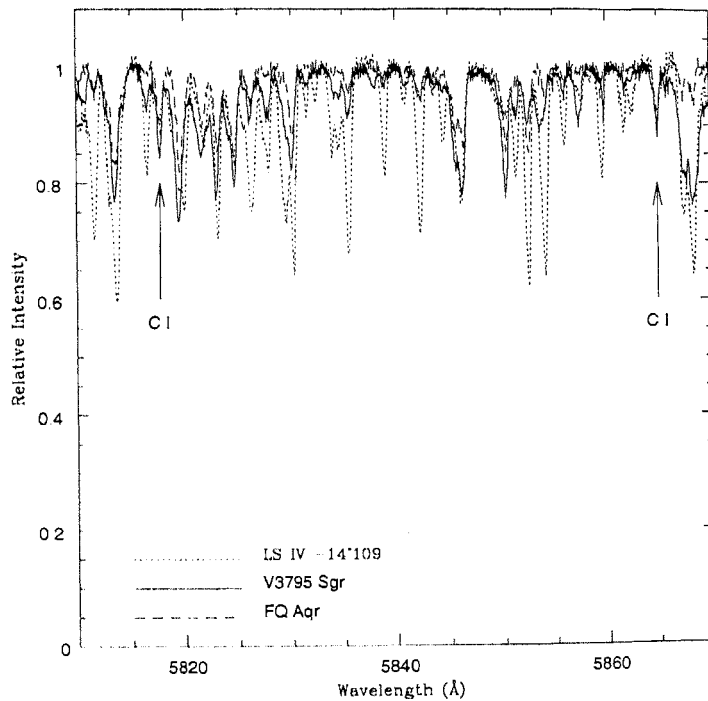


Figure 4.4: Spectra of V3795 Sgr (R CrB type star), FQ Aqr and LS IV $-14^\circ 109$ superposed one on another. Note that weak C I lines have approximately the same strength in all these stars.

We superpose the spectra of V3795 Sgr (R CrB-type, $T_{eff} = 8000$ K), FQ Aqr and LS IV -14° 109 in Figure 4.4, where we find that the C I lines ($\lambda\lambda$ 5817.7, 5864.95 Å) have approximately the same strength in all these stars. This implies that the continuous opacity in the line-forming regions of the two cool EHe stars is also dominated by photoionization of C I, and hence the C I line strength is not sensitive to carbon abundance. For estimating the major sources of continuum opacity in cool EHe stars, the carbon to helium ratio must be known a priori. A spectroscopic determination of carbon to helium ratio for cool EHe stars is also essential (i) in the context of their evolutionary status, and (ii) in estimating the contribution to the continuum opacity due to C I and He I, separately.

The carbon to helium ratio can be guessed if a similarity of EHe stars with the *hot* R CrB stars, where the ratio is determined from C II, C III and He I lines, is assumed.

In the spectra of R CrB stars, which occupy the temperature range from 6000 K to 8000 K, one observes many C I lines. The feature at 5876 Å observed in their spectra is the only evidence for the presence of He I, and the estimation of carbon to helium ratio for R CrB stars is based entirely on the strength of this feature. Unfortunately, this feature is not a good indicator of C/He for the following reasons (Lambert et al. 1999):

- (i) In the temperature domain of R CrB stars, the 5876 Å feature is a blend of C I lines; C I contributes appreciably to the strength of this feature for the cooler R CrB stars.
- (ii) The carbon to helium ratio derived from this feature is very sensitive to the adopted T_{eff} and $\log g$. For $T_{eff} \approx 7000$ K, the equivalent width of the 5876 Å feature computed for C/He = 1% agrees well with that computed for C/He = 3%, if T_{eff} is raised by about 500 K, resulting in large uncertainties.
- (iii) He I 5876 Å line with its high excitation potential forms in the deepest layers of the photosphere, and hence is highly saturated, even if it appears weak.

Since it is thought that hot EHe stars might be related to R CrB stars, Rao and Lambert (1996) and Lambert et al. (1999) assumed that they possibly have the same carbon to helium ratio. The C/He is directly estimated in hot EHe stars from C II and He I lines, and it is approximately 1% (Jeffery 1996).

As already mentioned, our programme stars are of intermediate temperatures which lie in between the cool R CrB stars and hot EHe stars. These stars show C I, C II and He I lines in their spectra. In principle, estimating C/He would be possible from the above lines. The feature at 5876 Å has negligible contribution from C I lines in the temperature domain of these stars, and hence will be a good indicator of C/He, provided

carbon controls the continuum opacity of these stars.

One of the most important issues that we have attempted to address in the present work is the determination of C/He in cool EHe stars. The C/He can be fixed if we observe lines of C I, C II, C III, etc. and helium in their spectrum. Before we calculate the abundance using a particular species of an element, it is necessary to confirm that this species is not a major source of continuum opacity. For example, to calculate the carbon abundance from C I lines one must ensure that C I should not be the major source of continuum opacity. Alternatively, if we want to calculate carbon abundance from C II lines, then neither C II nor C I should be the dominant contributor to the continuous opacity. This is because the C II lines are essentially the result of photoionization of C I. The same argument is valid in the determination of helium abundance using He I lines. In the case of hot EHe stars He I controls the continuum opacity, and hence the carbon lines (mostly C II) give us the direct estimate of C/He. Similarly, in the cases where C I controls the continuum opacity, He I lines will provide an estimate of He/C.

We have observed C I, C II and He I lines in the spectra of the programme stars. In the temperature domain of these stars (8000 K to 14000 K) we have computed the equivalent widths (see section 4.4.1 for the atomic data used) of some of the C I, C II and He I lines which are observed in these stars across a grid of $\log g$ and T_{eff} for different values of C/He. The aim is to study how the strengths of these lines vary across the grid. The lines that have been considered are:

(i) C I ($\lambda\lambda$ 4770, 5380, 6010, 6076, 6335, 7476 Å)

(ii) C II ($\lambda\lambda$ 3918.97, 3920.68, 6578.05, 6582.85 Å)

(iii) He I ($\lambda\lambda$ 5016, 5048, 5876, 6678 Å)

The predicted equivalent widths of these lines are plotted against T_{eff} for different values of C/He (0.3%, 1.0% and 3.0%) and $\log g$ (1.0, 1.5 and 2.0) in Figures 4.5, 4.6, 4.8 and 4.9. From the Figures 4.5 and 4.6, we find that the equivalent widths of C I lines are essentially the same for C/He values of 1.0% and 3.0% at the cooler end ($T_{eff} = 8000$ K to 10000 K) for $\log g$ 1.5 and 2.0. But for lower gravities, say $\log g = 1.0$, the equivalent widths of C I lines start to show a dependence on C/He as the temperature

increases. The changes in the equivalent widths in fact depend on the C/He itself, in the sense that the larger the changes the smaller the C/He. The equivalent widths of C I lines corresponding to C/He = 0.3% are very different from those corresponding to C/He = 1.0% and C/He = 3.0%. This is due to the fact that for C/He \geq 1%, C I is the major source of continuum opacity and for C/He < 1%, the contribution to the continuous opacity due to C I reduces considerably with decreasing C/He. For C/He \leq 0.3%, electron scattering starts dominating the continuum opacity.

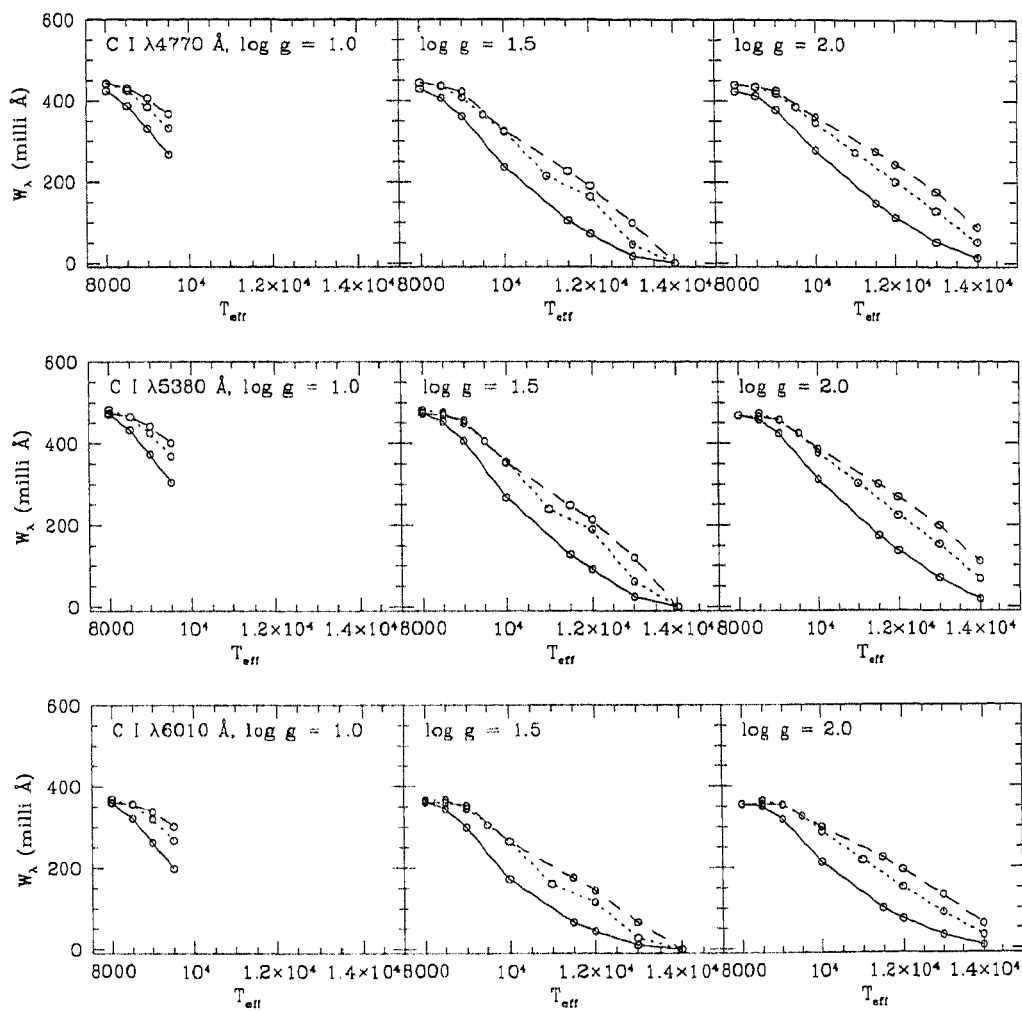


Figure 4.5: Predicted equivalent widths of C I lines plotted against T_{eff} for $\log g$ values of 1.0, 1.5 and 2.0. The solid, dotted and dashed lines represent models with C/He of 0.3%, 1.0% and 3.0%, respectively.

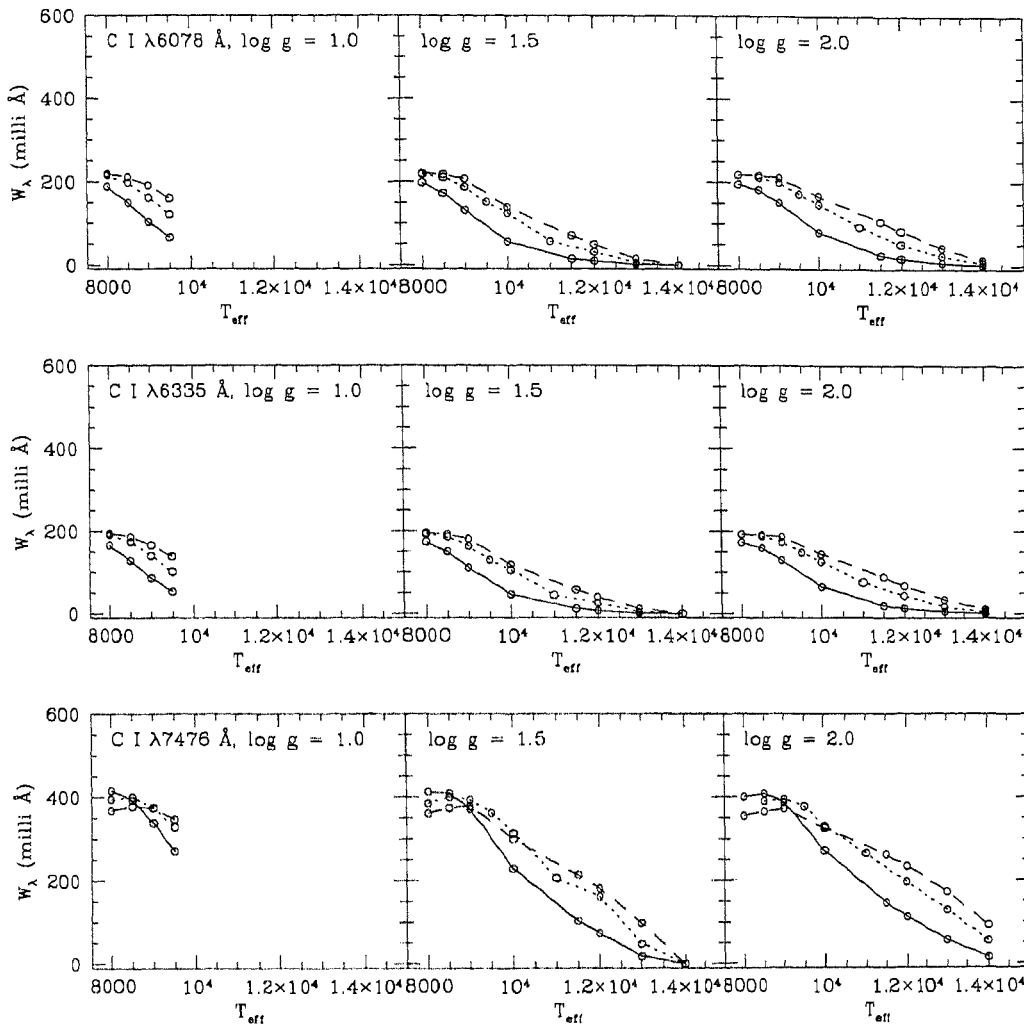


Figure 4.6: see Figure 4.5 for caption

In principle one could estimate C/He of BHe stars at the cool end from the equivalent widths of C I lines, if they have C/He < 1% (see Figures 4.5 and 4.6). For stars in the same temperature range with C/He \geq 1%, it is not possible to estimate the C/He precisely from the equivalent widths of C I lines because the line strengths do not show appreciable changes with increase in C/He. The variations in the predicted equivalent widths of C I lines in the temperature range 8500 – 10000 K with the changes in the input C/He, as evident from an inspection of Figures 4.5 and 4.6, are graphically represented in Figure 4.7. Instead of plotting the equivalent widths themselves, the C/He that one would derive

from them are shown along the y-axis. It is clear from Figure 4.7 that in the temperature range 8500 – 10000 K, the C/He estimated from the equivalent widths of C I lines would be always 1% irrespective of the actual surface C/He if it is greater than 1% because the strengths of C I lines get saturated above this value.

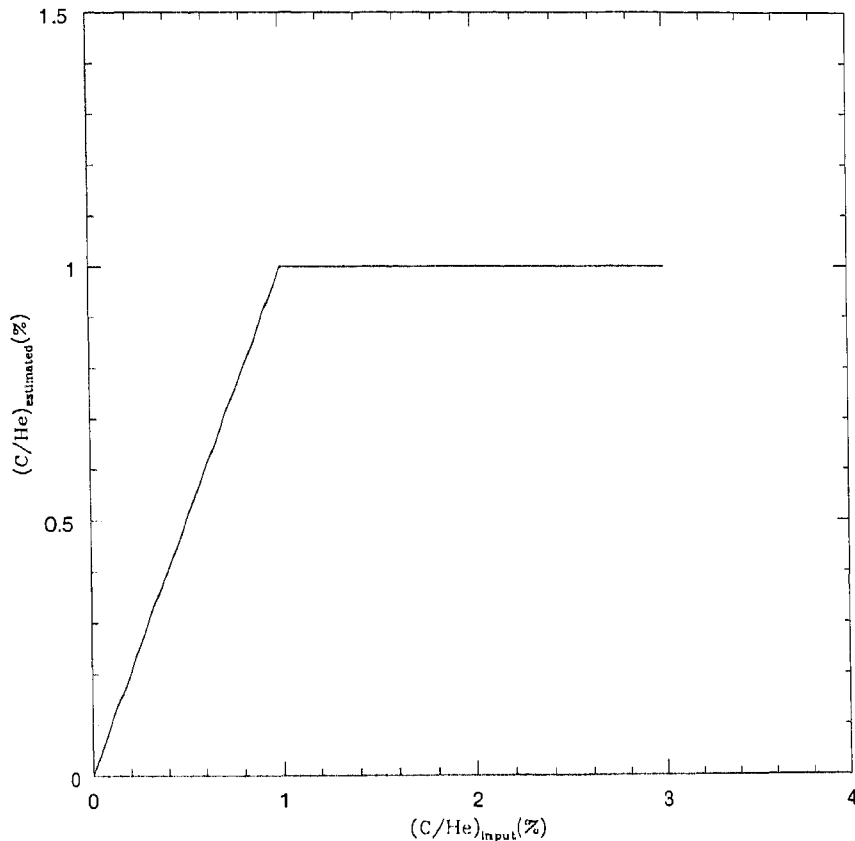


Figure 4.7: C/He that would be estimated from the C I line equivalent widths $(C/He)_{estimated}$, plotted against the actual C/He $(C/He)_{input}$, for stars in the temperature range 8500 – 10000 K.

At higher temperatures (10000 K to 14000 K) most of the carbon is in the form of C II resulting in a decrease in the equivalent widths of C I lines with an increase in the temperature (Figures 4.5 and 4.6). The equivalent widths of C I and C II lines are sensitive to the adopted C/He in this temperature range and hence provide a direct estimate of C/He.

For hydrogen-deficient stars which are cooler than 8500 K, like R CrB stars, C/He

cannot be estimated from the equivalent widths of C I lines as these are independent of the C/He.

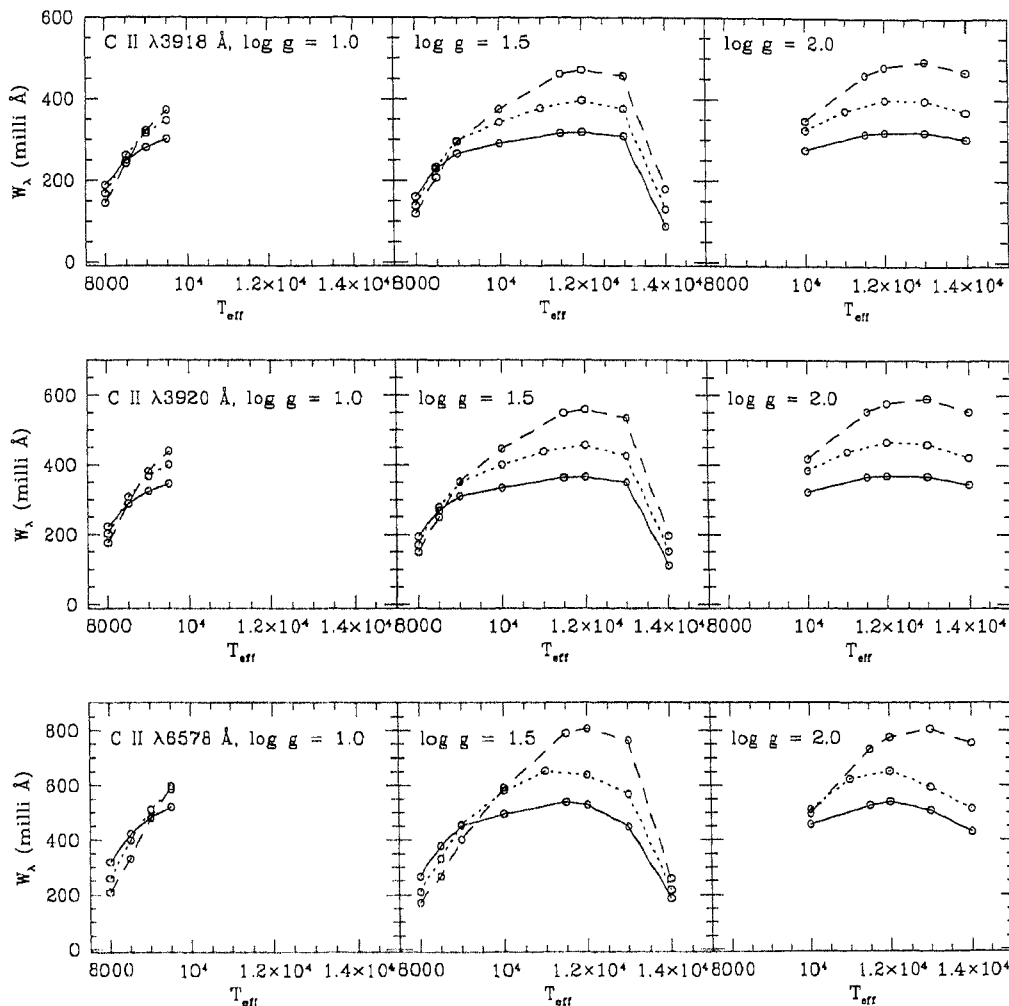


Figure 4.8: Predicted equivalent widths of C II lines plotted against T_{eff} for $\log g$ values of 1.0, 1.5 and 2.0. The solid, dotted and dashed lines represent models with C/He of 0.3%, 1.0% and 3.0%, respectively.

The equivalent widths of C II lines are also insensitive to the adopted C/He (0.3%, 1.0% and 3.0%) at the cool end, as discussed for C I lines (see Figure 4.8).

On the contrary, the equivalent widths of He I lines becomes insensitive to the adopted C/He (0.3%, 1.0% and 3.0%) in the temperature range 11500 K to 14000 K. The equivalent

widths of He I lines are very sensitive to the adopted C/He (0.3%, 1.0% and 3.0%) in the temperature range 8000 – 12000 K (see Figure 4.9). The equivalent widths of He I lines decreases for temperatures ≥ 13000 K due to the ionization of He I.

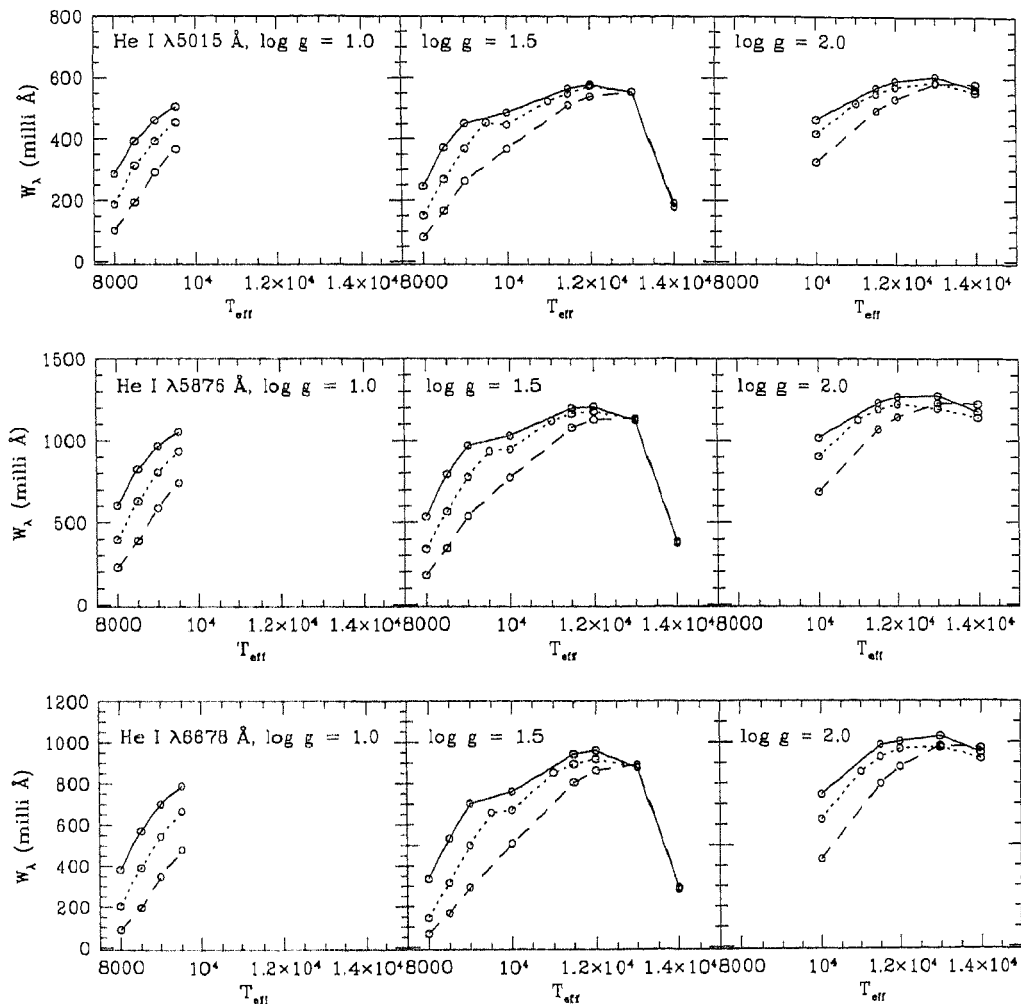


Figure 4.9: Predicted equivalent widths of He I lines plotted against T_{eff} for $\log g$ values of 1.0, 1.5 and 2.0. The solid, dotted and dashed lines represent models with C/He of 0.3%, 1.0% and 3.0%, respectively.

It is clear from the above results that the C/He can be estimated using C I and C II lines for the programme stars which lie in the hot end, and He I lines can be used to determine C/He for those which lie in the cool end.

4.4 Abundance analysis

In our abundance analysis we have used new line-blanketed model atmospheres constructed by Asplund et al. (1997a) for stars with temperatures ≤ 9500 K. For higher temperatures, model atmospheres were provided by Jeffery (Jeffery and Heber 1992). The line strengths were calculated using ‘Eqwrun’ and ‘Spectrum’ radiative transfer codes. The Eqwrun and Spectrum codes use the model stellar atmospheres of Asplund (1997a) for temperatures ≤ 9500 K and of Jeffery and Heber (1992) for temperatures ≥ 10000 K, respectively. In our analysis C/He of 0.3%, 1.0% and 3.0% models have been used (see section 4.4.2 for C/He determination).

The fine analysis of the stellar spectra involves the determination of T_{eff} , surface gravity ($\log g$), microturbulence (ξ) and photospheric elemental abundances of the star using model atmospheres and atomic data in the following way:

(1) The microturbulence is derived by requiring that lines of all strengths for a particular species give the same value of abundance. The derived ξ is found to be independent of T_{eff} , $\log g$ and C/He, adopted for the model atmosphere (see Figures 4.10 to 4.19).

(2) T_{exc} is estimated by requiring that the lines of a particular species of differing excitation potentials should predict the same elemental abundance. The estimated T_{exc} is found to be independent of the adopted $\log g$ and C/He for the model atmosphere (see Figures 4.20 to 4.25).

(3) The surface gravity is estimated such that the model atmosphere gives the same predicted abundances for neutral, singly, and doubly ionized lines of a given element. In our analysis of FQ Aqr and BD $-1^\circ 3438$, we find that the ionization equilibria are independent of the adopted C/He for the model atmosphere.

The abundance analysis is done with the new line-blanketed model atmospheres described in Chapter 3.

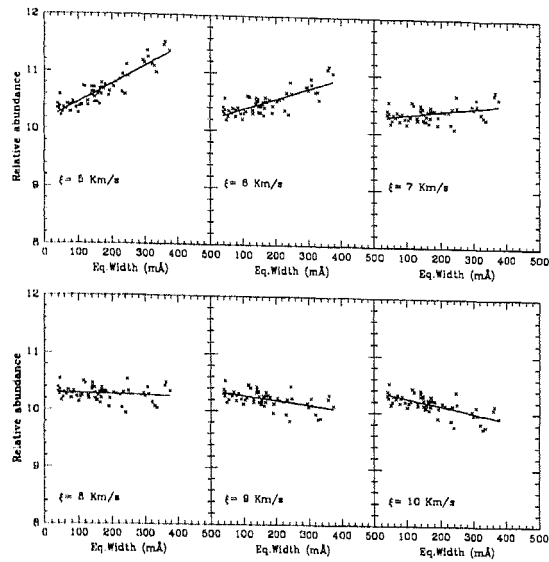


Figure 4.10: Relative abundances from Fe II lines for FQ Aqr, plotted against their Eq.Widths for different values of ξ , showing the estimated ξ is independent of the C/He used. The model used is $T_{eff}=8500$ K, $\log g=0.5$ and C/He=3%.

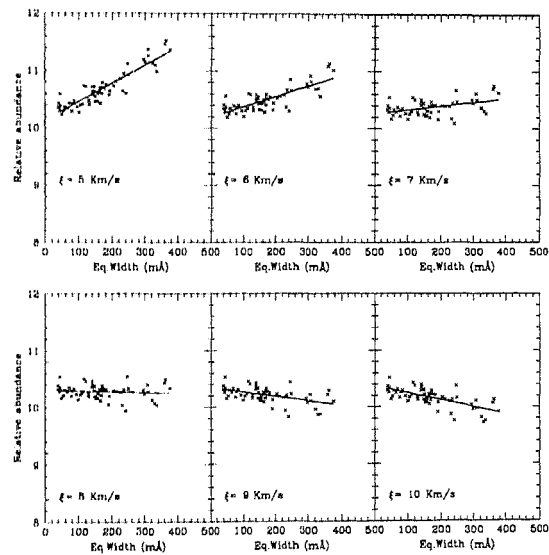


Figure 4.11: Relative abundances from Fe II lines for FQ Aqr, plotted against their Eq.Widths for different values of ξ , showing the estimated ξ is independent of the C/He used. The model used is $T_{eff}=8500$ K, $\log g=0.5$ and C/He=0.3%.

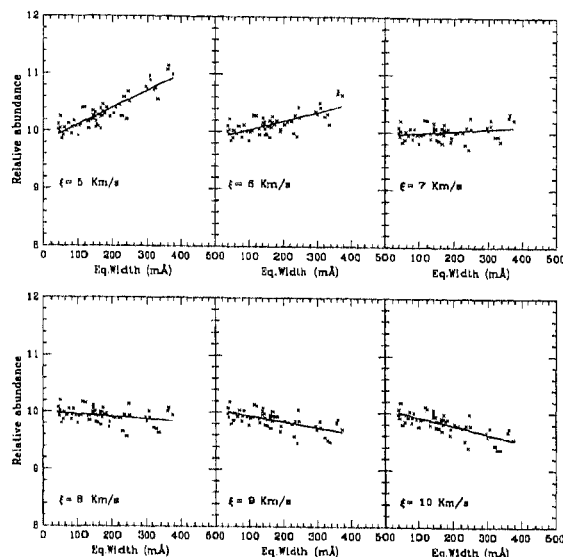


Figure 4.12: Relative abundances from Fe II lines for FQ Aqr, plotted against their Eq.Widths for different values of ξ , showing the estimated ξ is independent of the C/He used. The model used is $T_{eff}=8500$ K, $\log g=0.5$ and C/He=1%.

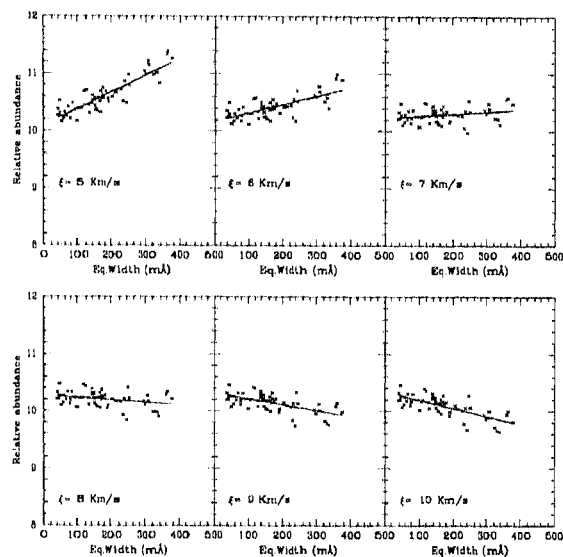


Figure 4.13: Relative abundances from Fe II lines for FQ Aqr, plotted against their Eq.Widths for different values of ξ , showing the estimated ξ is independent of the C/He used. The model used is $T_{eff}=8500$ K, $\log g=1.5$ and C/He=1%.

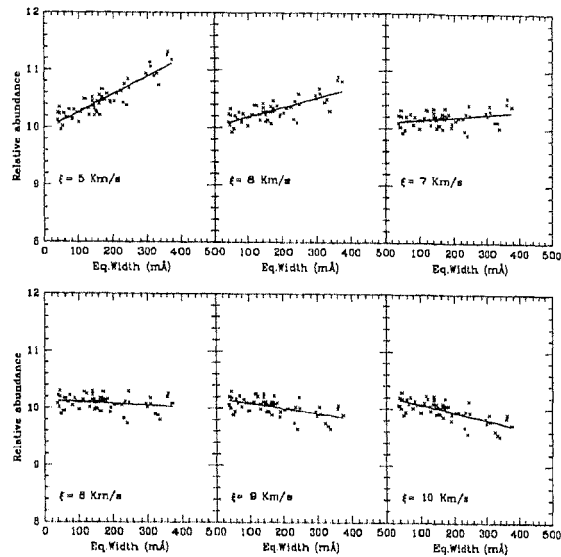


Figure 4.14: Relative abundances from Fe II lines for FQ Aqr, plotted against their Eq.Widths for different values of ξ , showing the estimated ξ is independent of the C/He used. The model used is $T_{eff}=9000$ K, $\log g=1.0$ and C/He=1%.

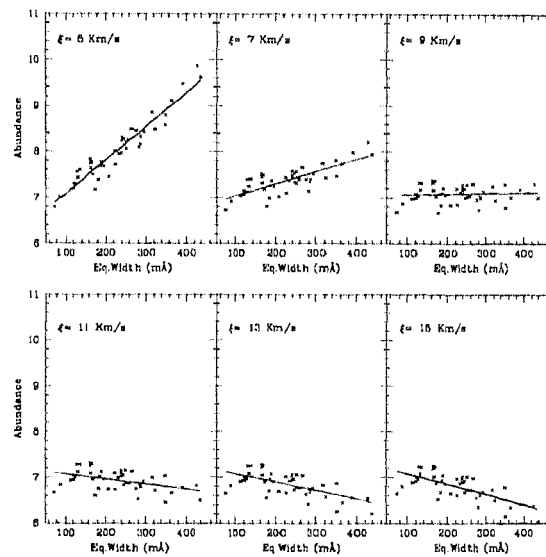


Figure 4.15: Abundances from Fe II lines for BD -1° 3438, plotted against their Eq.Widths for different values of ξ , showing the estimated ξ is independent of the C/He used. The model used is $T_{eff}=11500$ K, $\log g=2.0$ and C/He=3%.

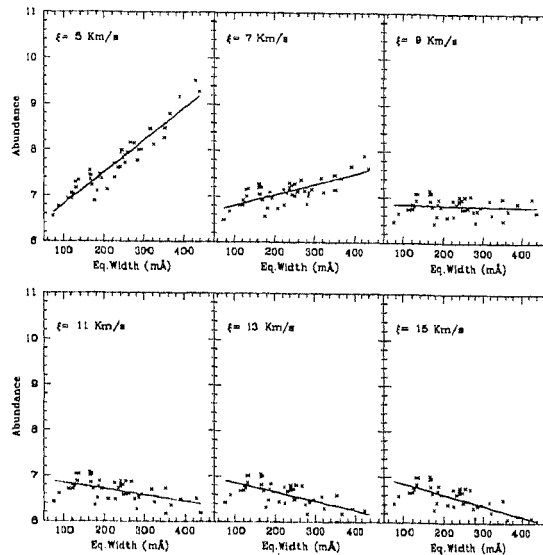


Figure 4.16: Abundances from Fe II lines for BD -1° 3438, plotted against their Eq.Widths for different values of ξ , showing the estimated ξ is independent of the C/He used. The model used is $T_{eff}=11500$ K, $\log g=2.0$ and C/He=0.3%.

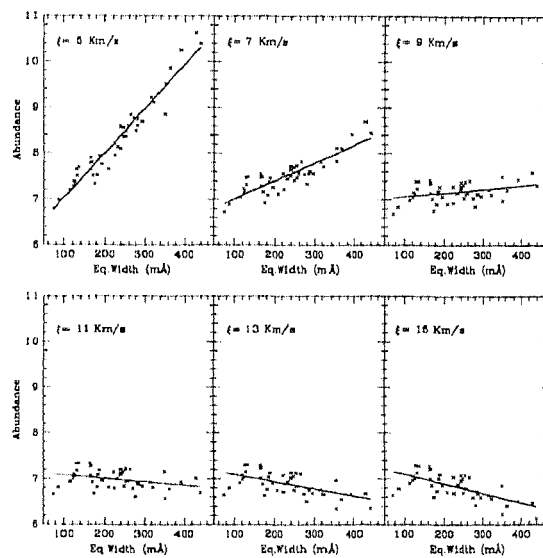


Figure 4.17: Abundances from Fe II lines for BD -1° 3438, plotted against their Eq.Widths for different values of ξ , showing the estimated ξ is independent of the C/He used. The model used is $T_{eff}=12000$ K, $\log g=2.0$ and C/He=1%.

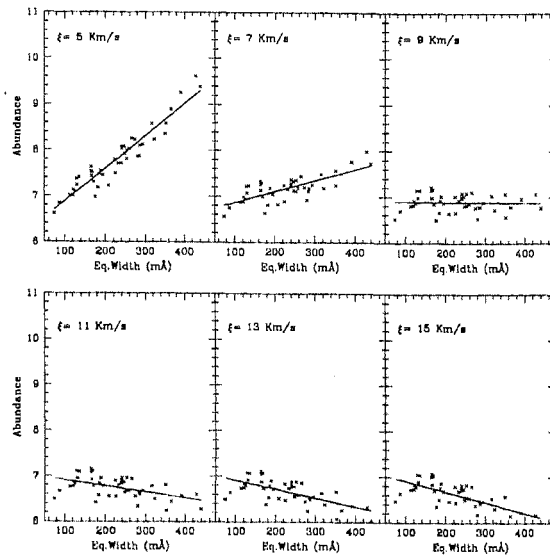


Figure 4.18: Abundances from Fe II lines for BD -1° 3438, plotted against their Eq.Widths for different values of ξ , showing the estimated ξ is independent of the C/He used. The model used is $T_{eff}=11500$ K, $\log g=2.0$ and C/He=1%.

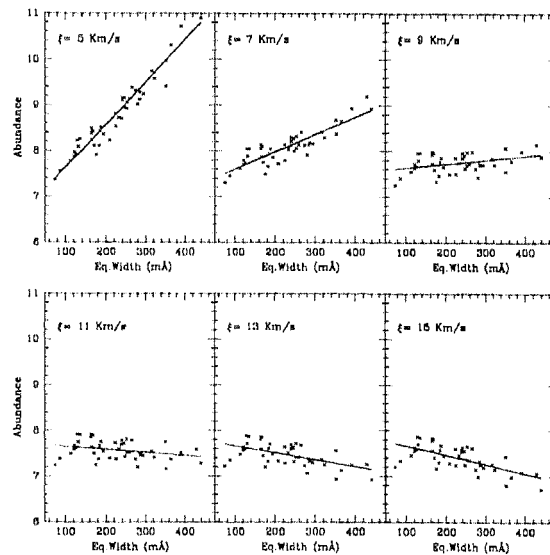


Figure 4.19: Abundances from Fe II lines for BD -1° 3438, plotted against their Eq.Widths for different values of ξ , showing the estimated ξ is independent of the C/He used. The model used is $T_{eff}=11500$ K, $\log g=1.0$ and C/He=1%.

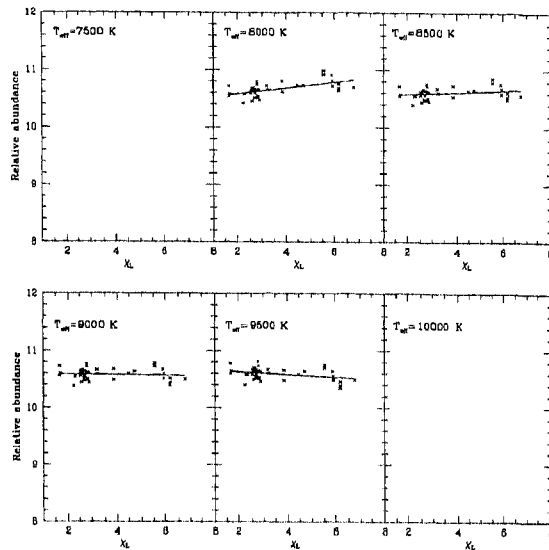


Figure 4.20: Relative abundances from Fe II lines for Fq Aqr, plotted against their χ_L for different values of T_{eff} , showing the estimated T_{exc} is independent of the adopted $\log g$ and C/He. The adopted $\log g$ and C/He are 1.5 and 3%, respectively.

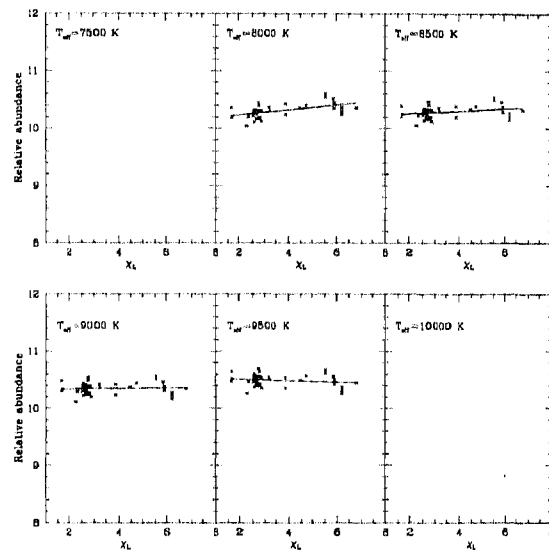


Figure 4.21: Relative abundances from Fe II lines for Fq Aqr, plotted against their χ_L for different values of T_{eff} , showing the estimated T_{exc} is independent of the adopted $\log g$ and C/He. The adopted $\log g$ and C/He are 0.5 and 3%, respectively.

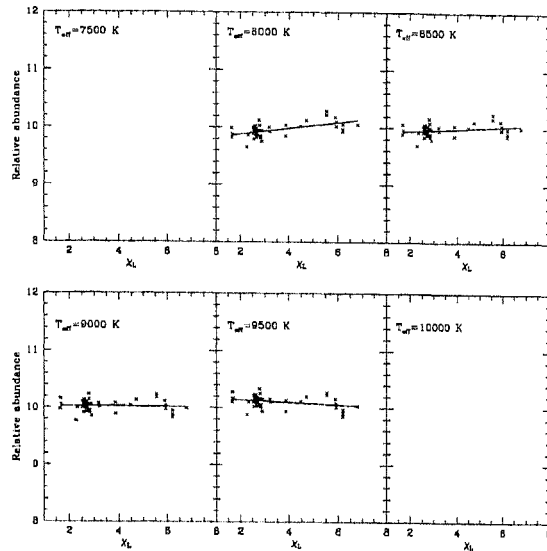


Figure 4.22: Relative abundances from Fe II lines for Fq Aqr, plotted against their χ_L for different values of T_{eff} , showing the estimated T_{exc} is independent of the adopted $\log g$ and C/He. The adopted $\log g$ and C/He are 1.5 and 0.3%, respectively.

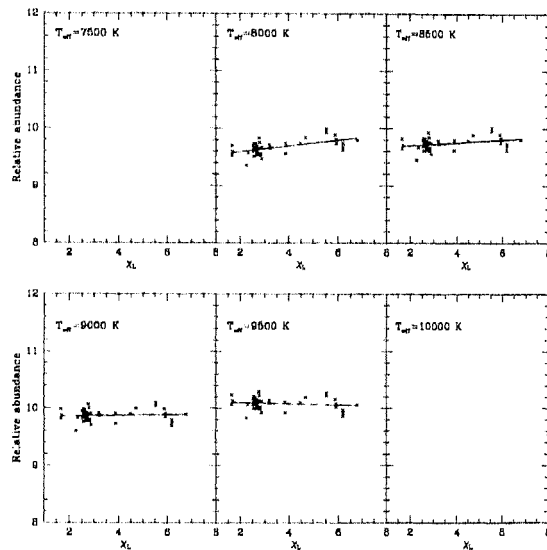


Figure 4.23: Relative abundances from Fe II lines for Fq Aqr, plotted against their χ_L for different values of T_{eff} , showing the estimated T_{exc} is independent of the adopted $\log g$ and C/He. The adopted $\log g$ and C/He are 0.5 and 3%, respectively.

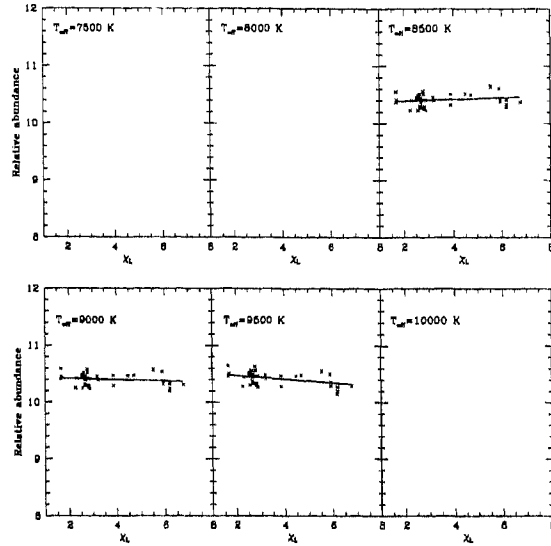


Figure 4.24: Relative abundances from Fe II lines for Fq Aqr, plotted against their χ_L for different values of T_{eff} , showing the estimated T_{exc} is independent of the adopted $\log g$ and C/He. The adopted $\log g$ and C/He are 2.0 and 1%, respectively.

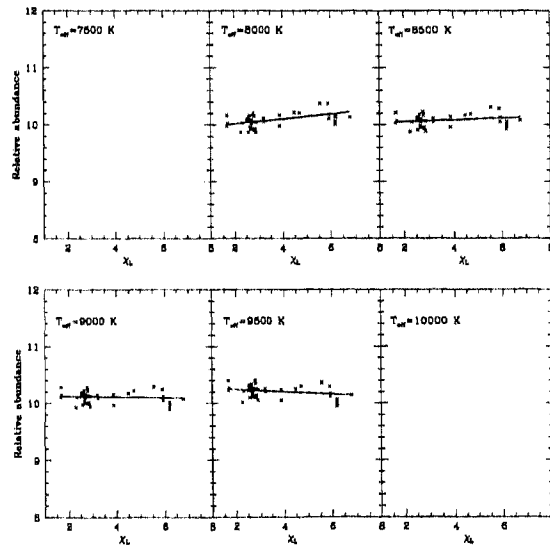


Figure 4.25: Relative abundances from Fe II lines for Fq Aqr, plotted against their χ_L for different values of T_{eff} , showing the estimated T_{exc} is independent of the adopted $\log g$ and C/He. The adopted $\log g$ and C/He are 1.0 and 1%, respectively.

4.4.1 Atomic data

The gf-values and excitation potentials for the lines used in our LTE analysis were taken from the compilations by R. E. Luck (private communication), C. Simon Jeffery (private communication), Thevenin (1989, 1990) and Kurucz and Peytreman (1975). Because of the wide spectral coverage used, we could identify several C I lines in our sample stars. We have used the gf-values of C I lines from Opacity project (Seaton et al. 1994; Luo and Pradhan 1989; Hibbert et al. 1993) for consistency with the analysis of FQ Aqr and LS IV -14° 109 by Lambert et al. (1999). The C I lines and gf-values used for our abundance analysis are given in the Tables 4.6 and 4.7. The sources of gf-values are listed in Tables 4.6 to 4.9. The Stark broadening and radiation broadening coefficients were mostly taken from the compilation by Jeffery (1994).

4.4.2 T_{eff} , $\log g$, ξ and C/He

As already indicated the microturbulence parameter ξ was adjusted until the derived abundances from the same species were independent of line strength, represented by $(\log W_\lambda/\lambda)$.

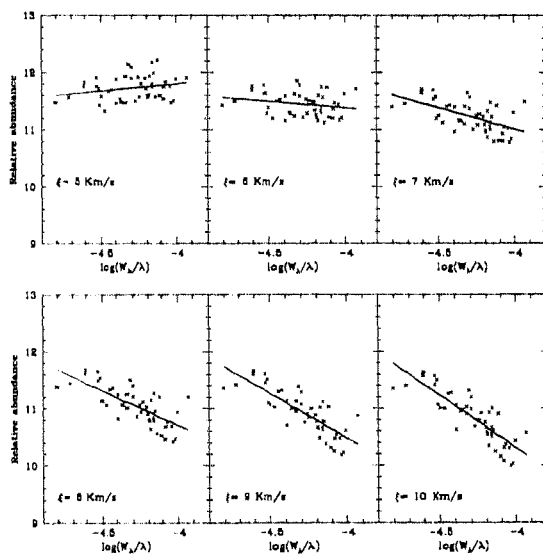


Figure 4.26: Relative abundances from Fe II lines for LS IV -14° 109, plotted against their line strength, represented by $(\log W_\lambda/\lambda)$ for different values of ξ .

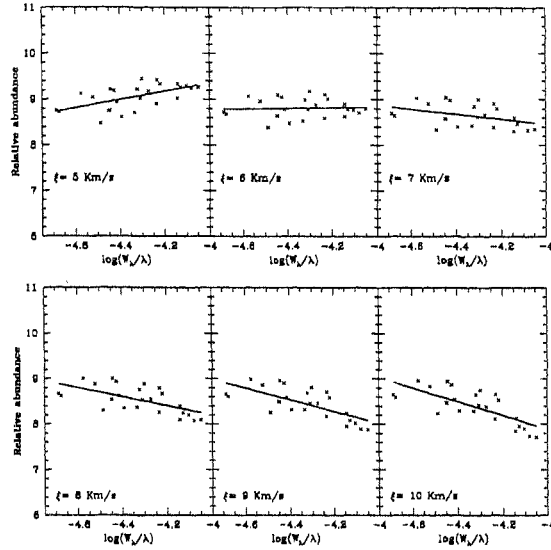


Figure 4.27: Relative abundances from Ti II lines for LS IV $-14^\circ 109$, plotted against their line strength, represented by $(\log W_\lambda/\lambda)$ for different values of ξ .

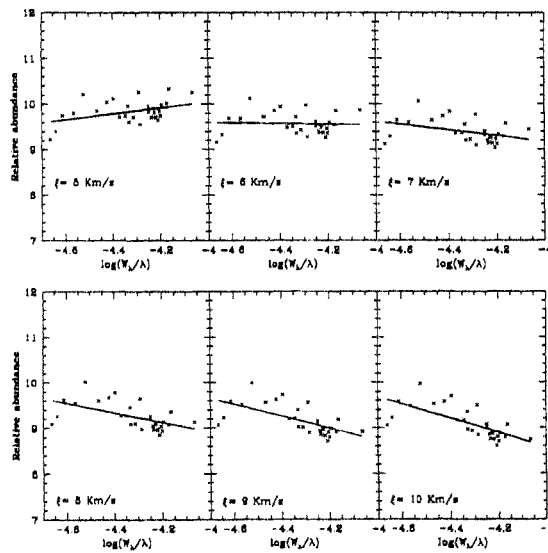


Figure 4.28: Relative abundances from Cr II lines for LS IV $-14^\circ 109$, plotted against their line strength, represented by $(\log W_\lambda/\lambda)$ for different values of ξ .

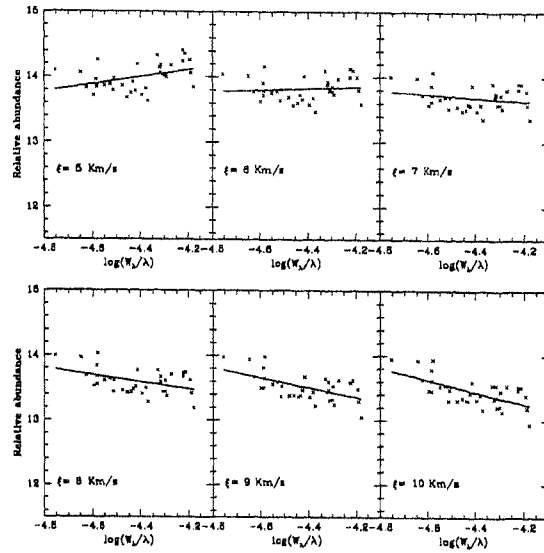


Figure 4.29: Relative abundances from C I lines for LS IV $-14^\circ 109$, plotted against their line strength, represented by $(\log W_\lambda/\lambda)$ for different values of ξ .

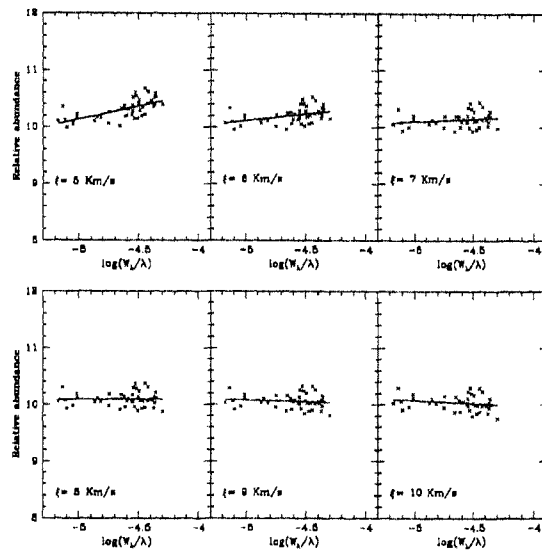


Figure 4.30: Relative abundances from Fe II lines for FQ Aqr, plotted against their line strength, represented by $(\log W_\lambda/\lambda)$ for different values of ξ .

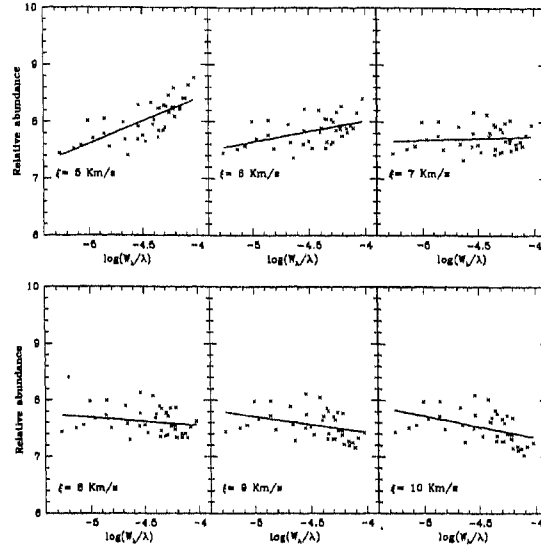


Figure 4.31: Relative abundances from Ti II lines for FQ Aqr, plotted against their line strength, represented by $(\log W_\lambda/\lambda)$ for different values of ξ .

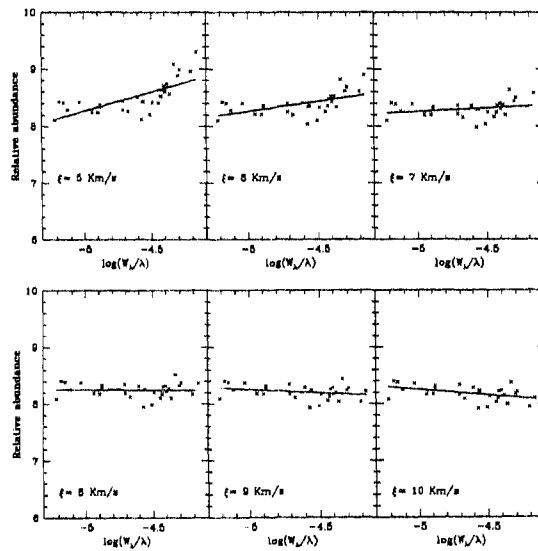


Figure 4.32: Relative abundances from Cr II lines for FQ Aqr, plotted against their line strength, represented by $(\log W_\lambda/\lambda)$ for different values of ξ .

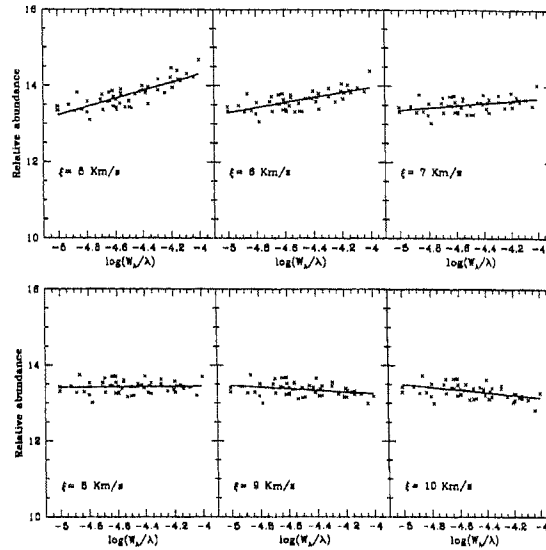


Figure 4.33: Relative abundances from C I lines for FQ Aqr, plotted against their line strength, represented by $(\log W_\lambda/\lambda)$ for different values of ξ .

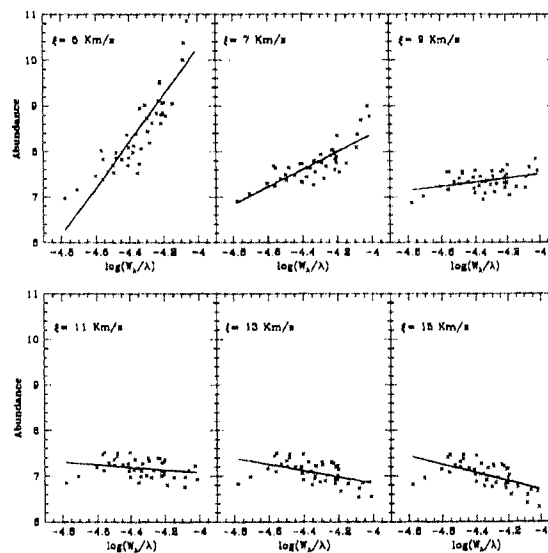


Figure 4.34: Abundances from Fe II lines for BD -1° 3438, plotted against their line strength, represented by $(\log W_\lambda/\lambda)$ for different values of ξ .

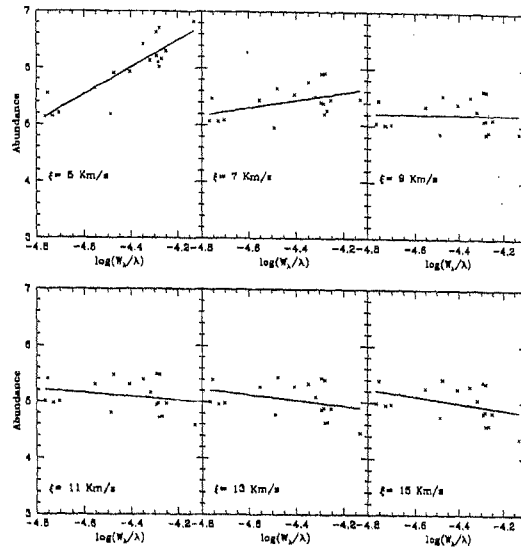


Figure 4.35: Abundances from Ti II lines for BD $-1^\circ 3438$, plotted against their line strength, represented by $(\log W_\lambda/\lambda)$ for different values of ξ .

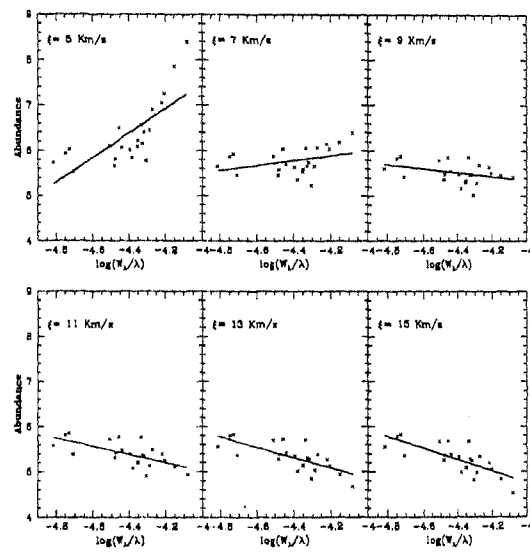


Figure 4.36: Abundances from Cr II lines for BD $-1^\circ 3438$, plotted against their line strength, represented by $(\log W_\lambda/\lambda)$ for different values of ξ .

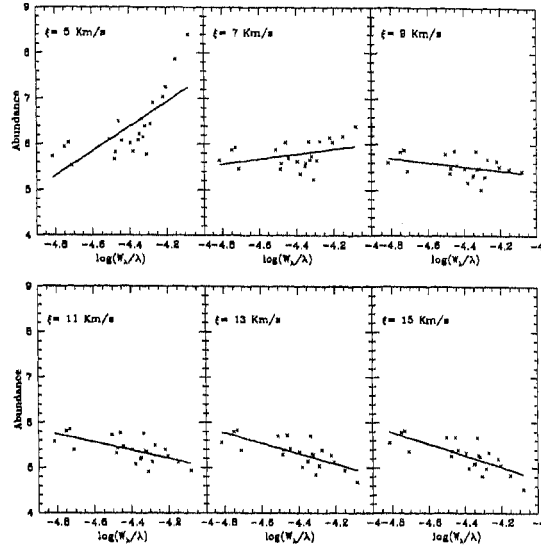


Figure 4.37: Abundances from C I lines for BD -1° 3438, plotted against their line strength, represented by $(\log W_{\lambda}/\lambda)$ for different values of ξ .

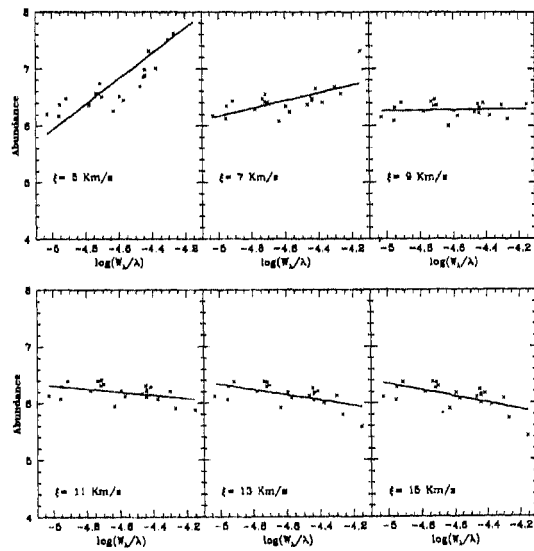


Figure 4.38: Abundances from Fe II lines for LS IV -1° 002, plotted against their line strength, represented by $(\log W_{\lambda}/\lambda)$ for different values of ξ .

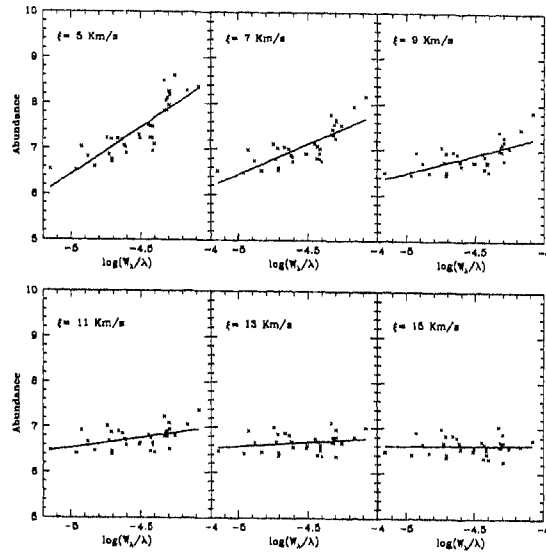


Figure 4.39: Abundances from S II lines for LS IV $-1^\circ 002$, plotted against their line strength, represented by $(\log W_\lambda/\lambda)$ for different values of ξ .

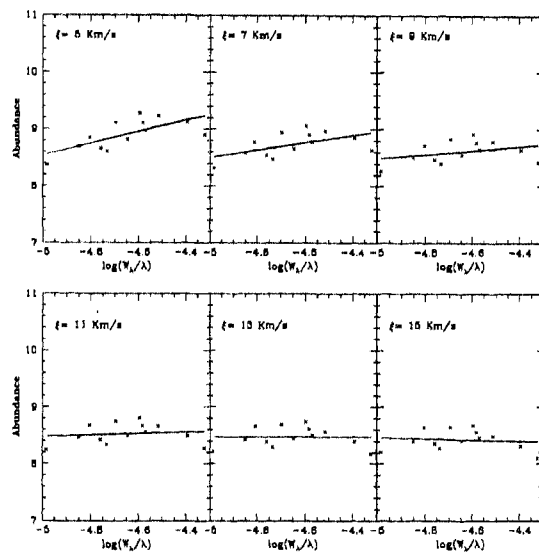


Figure 4.40: Abundances from N II lines for LS IV $-1^\circ 002$, plotted against their line strength, represented by $(\log W_\lambda/\lambda)$ for different values of ξ .

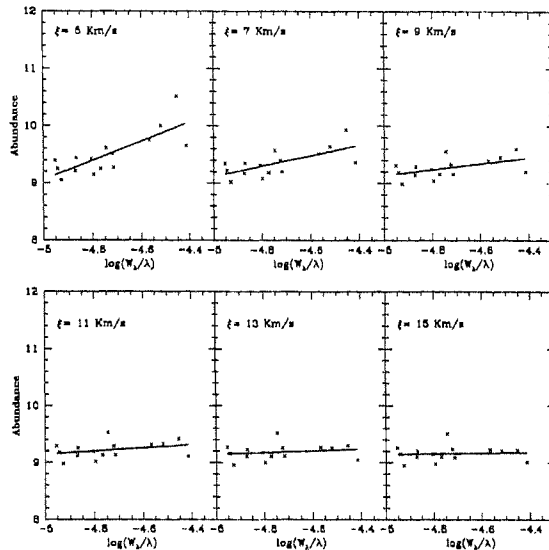


Figure 4.41: Abundances from C I lines for LS IV -1° 002, plotted against their line strength, represented by $(\log W_{\lambda}/\lambda)$ for different values of ξ .

For FQ Aqr, LS IV -14° 109 and BD -1° 3438, we used Fe II, Ti II, Cr II and C I lines, and for LS IV -1° 002, we used Fe II, S II, N II and C I lines for determining the microturbulent velocity ξ . The above species were chosen because many of their lines with a wide range in equivalent widths were available.

In the case of LS IV -14° 109, Fe II, Ti II and Cr II lines give us a value of $\xi = 6$ km s $^{-1}$, and C I lines a value of $\xi = 7$ km s $^{-1}$ (see Figures 4.26 to 4.29). We adopt the average microturbulent velocity ξ in LS IV -14° 109 as 6.5 ± 0.5 km s $^{-1}$, for all species. For FQ Aqr, BD -1° 3438 and LS IV -1° 002 we estimate the microturbulent velocity ξ as 7.5 ± 0.5 km s $^{-1}$, 10.0 ± 1.0 km s $^{-1}$ and 10.0 ± 1.0 km s $^{-1}$, respectively, for all species (see Figures 4.30 to 4.33, 4.34 to 4.37, and 4.38 to 4.41).

Since the ionization equilibrium depends on both surface gravity and temperature, we can find a set of solutions in $\log g$ and T_{eff} which satisfies the equilibrium condition. The ionization equilibrium of the following species (when sufficient lines are available) are used to estimate T_{eff} and $\log g$: S II/S I, Si III/Si II/Si I, N II/N I, Al III/Al II/Al I, C II/C I, Fe III/Fe II/Fe I, Mg II/Mg I and O II/O I. The solutions of T_{eff} and $\log g$ obtained for the programme stars are shown in Figures 4.42, 4.43, 4.44 and 4.45. These figures also show lines of constant $\log(L/M)$ corresponding to 3.75 and 4.5, where most of

the hot EHe stars lie (Jeffery 1996). Note that we have not used these lines of constant $\log(L/M)$ in determining the T_{eff} and $\log g$ for these stars, instead we have used $T_{exc} \sim T_{eff}$ and ionization equilibria for estimating the T_{eff} and $\log g$. The reason for using T_{exc} is that the lines representing the solutions from the ionization equilibria of various species run almost parallel to each other in the $T_{eff} - \log g$ plane for the programme stars.

One of the reasons for the various loci not intersecting in the $T_{eff} - \log g$ plane, and hence not giving a unique set of solutions, could be that we have used ionization equilibria of various species with very little difference in the ionization potentials. The other possible explanation is that the ionization equilibria for various species are satisfied at different depths in the stellar atmosphere. It could also be due to the observational uncertainty in the equivalent width measurement. One can also argue that the model atmospheres used do not adequately represent the actual stellar atmospheres.

The T_{exc} is obtained generally by employing a species having a large number of lines covering a range in excitation potential. The equivalent widths (W_λ) of Fe II lines are plotted against their lower excitation potentials (χ_L) in Figures 4.46 to 4.49. These figures show the wide range in χ_L and W_λ measured for Fe II lines in our sample stars. Since Fe II lines have a wide range in excitation potential, we chose Fe II lines for determining the excitation temperature. The excitation temperature was adjusted until the derived abundances from Fe II lines were independent of the lower excitation potential. In determining T_{eff} , $\log g$ and ξ , models with C/He of 1% have been used. For FQ Aqr and BD -1° 3438, models of C/He equal to 0.3% and 3.0% have also been used for the ionization balance.

FQ Aqr

We have used Fe II lines with equivalent widths less than 200 mÅ while determining the T_{exc} to reduce the line to line scatter in the abundances. The T_{exc} obtained using the excitation equilibria of Fe II lines is 8750 ± 250 K. The ionization balance of S II/S I is given a larger weight because the lines of S II and S I identified in the spectra for abundance determination are weak. C II/C I ionization balance is given a smaller weight because of the carbon problem (see section 6.1.4). A smaller weight is also given to the ionization balance of Al II/Al I because we have only one line of Al I and the source of gf-values for Al II lines is not reliable. Equal weights are given to the ionization balance of N II/N I, Mg II/Mg I and Fe II/Fe I. Using the T_{exc} derived from the excitation balance

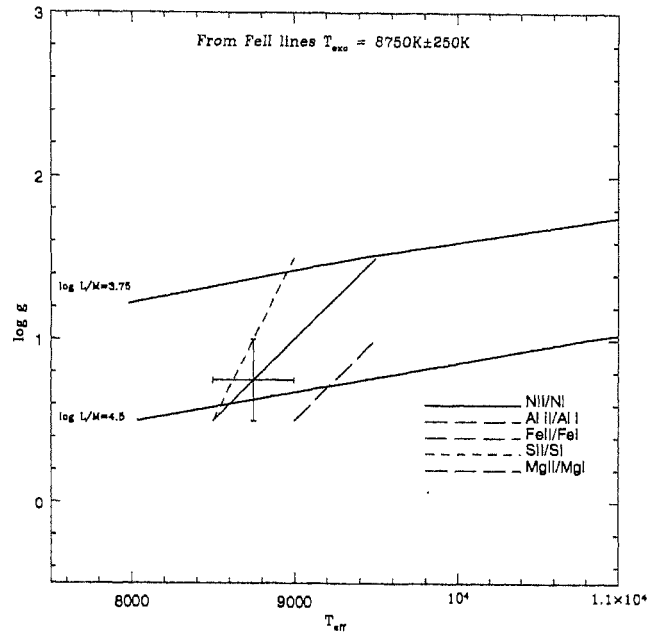


Figure 4.42: Final T_{eff} and $\log g$ of FQ Aqr with error bars.

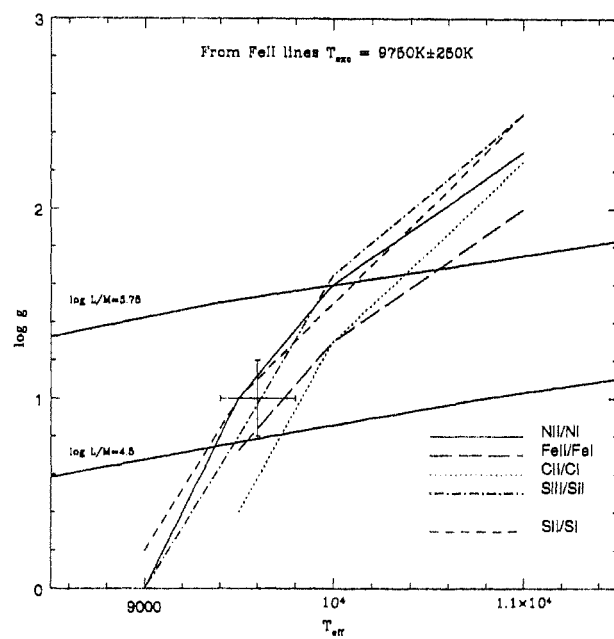


Figure 4.43: Final T_{eff} and $\log g$ of LS IV -14° 109 with error bars.

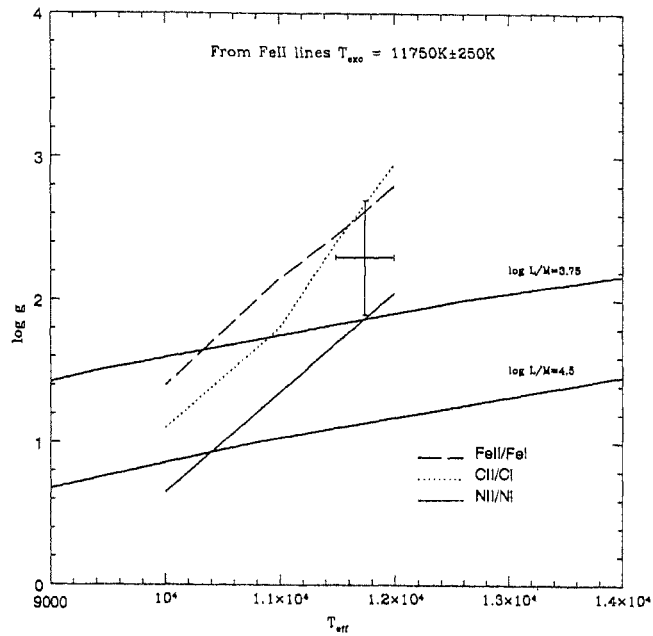


Figure 4.44: Final T_{eff} and $\log g$ of BD -1° 3438 with error bars.

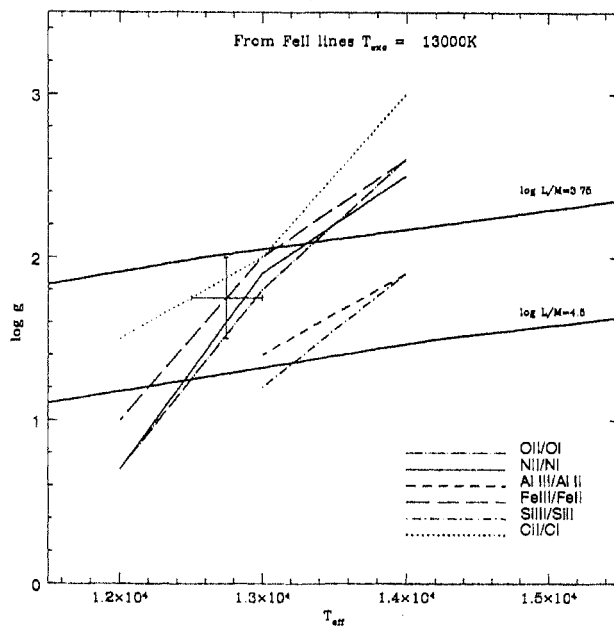


Figure 4.45: Final T_{eff} and $\log g$ of LS IV -1° 002 with error bars.

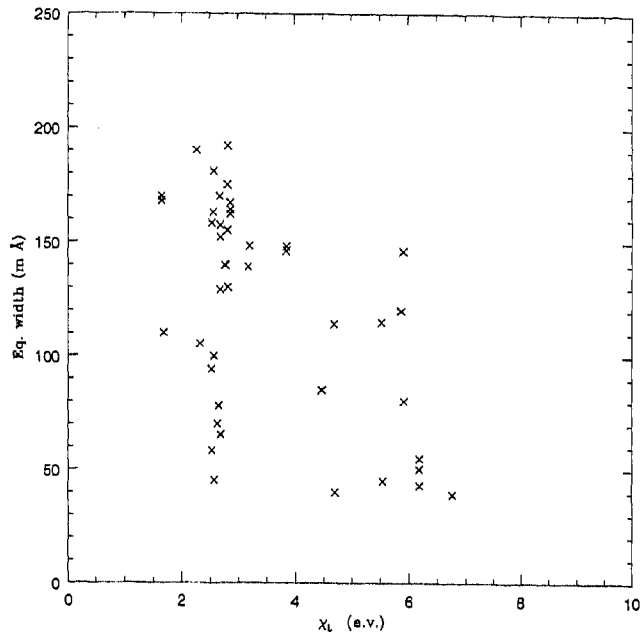


Figure 4.46: The equivalent widths (W_λ) of Fe II lines plotted against their χ_L showing the wide range in χ_L and measured W_λ for FQ Aqr.

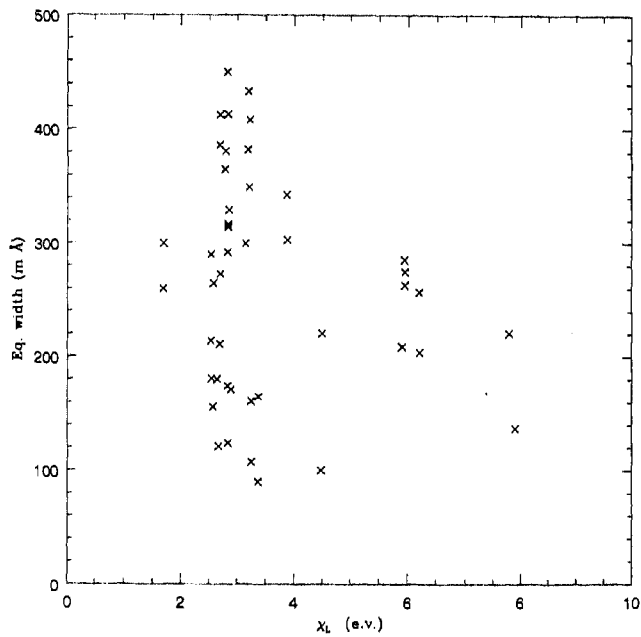


Figure 4.47: The equivalent widths (W_λ) of Fe II lines plotted against their χ_L showing the wide range in χ_L and measured W_λ for LS IV $-14^\circ 109$.

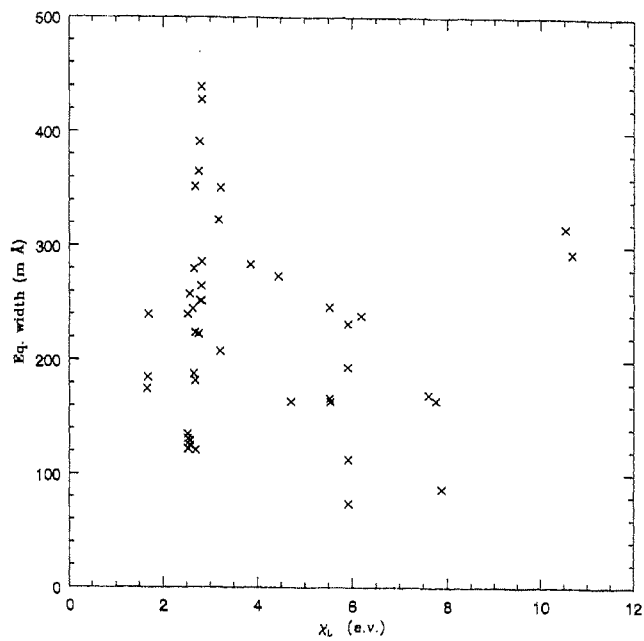


Figure 4.48: The equivalent widths (W_λ) of Fe II lines plotted against their χ_L showing the wide range in χ_L and measured W_λ for BD -1° 3438.

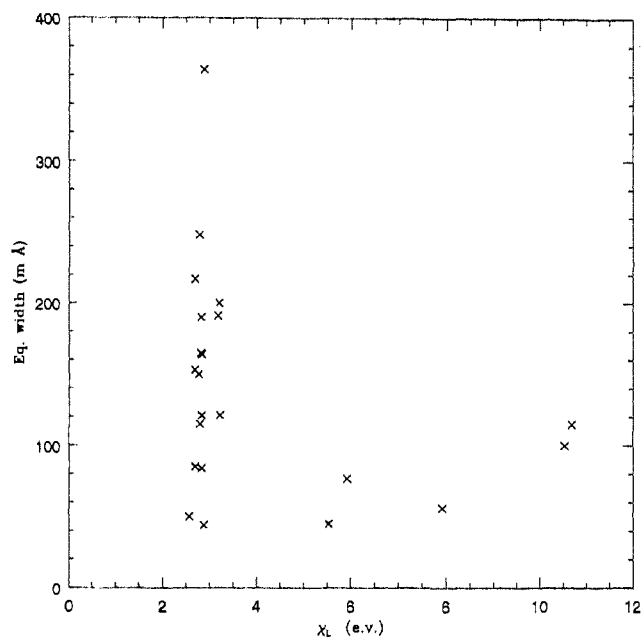


Figure 4.49: The equivalent widths (W_λ) of Fe II lines plotted against their χ_L showing the wide range in χ_L and measured W_λ for LS IV -1° 002.

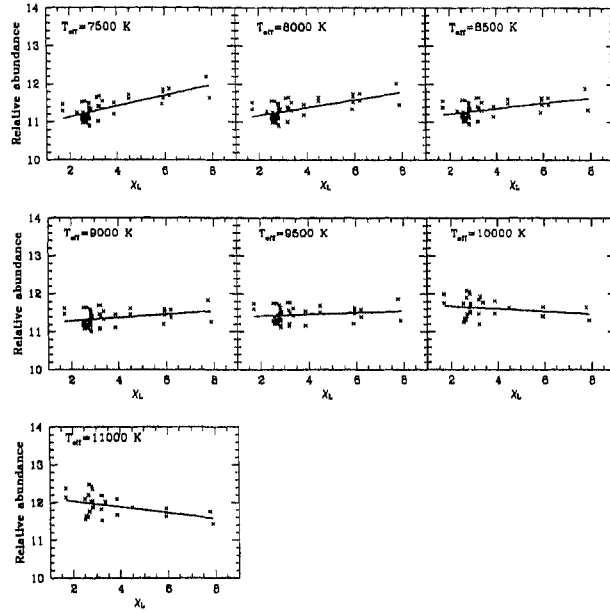


Figure 4.50: Excitation balance for LS IV -14° 109 using Fe II lines

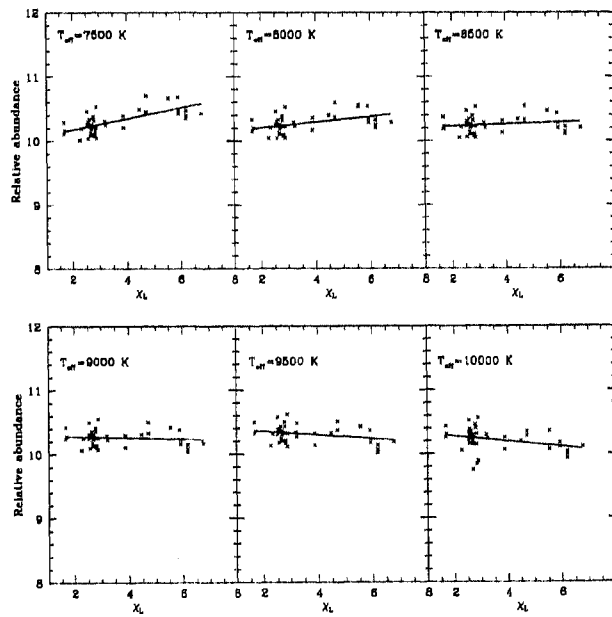


Figure 4.51: Excitation balance for FQ Aqr using Fe II lines.

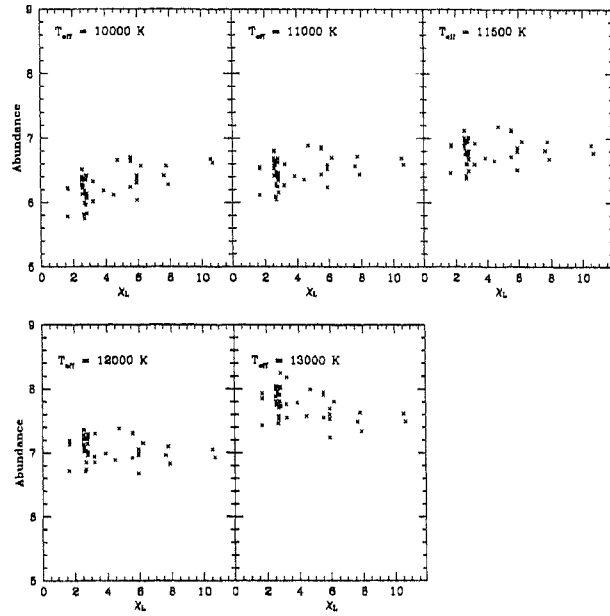


Figure 4.52: Excitation balance for BD -1° 3438 using Fe II lines.

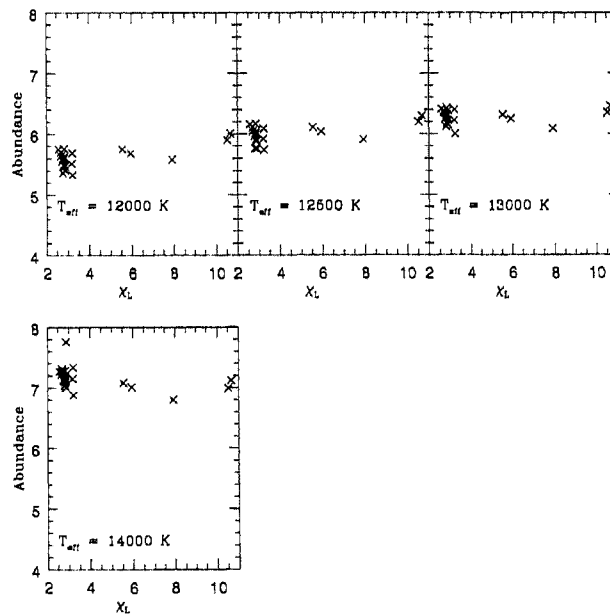


Figure 4.53: Excitation balance for LS IV -1° 002 using Fe II lines.

of Fe II lines and the ionization balance of various species (see Figures 4.42 and 4.51), we arrived at the most probable T_{eff} and $\log g$ which are given in Table 4.1.

The wings of He I λ 5876 Å triplet line depend upon the electron density, and hence upon the surface gravity. We have computed the He I line profiles for various models. Model with $T_{eff} = 8500$ K and $\log g = 0.5$ reproduces the wings as well as the core of He I λ 5876 Å. For C/He = 1%, the synthetic profile of He I λ 6678 Å with the above parameters matches the observed profile better than those with the models, $T_{eff} = 9000$ K, $\log g = 0.5, 1.0$ and 1.5 (Figures 4.54 and 4.55). The uncertainty in T_{eff} and $\log g$ determined from the excitation and ionization equilibria can be constrained from the gravity sensitive He I profiles. We finally estimate $T_{eff} = 8500$ K and $\log g = 0.5$ for FQ Aqr.

The He I lines and the C II lines are affected by Stark broadening and radiation broadening (see section 4.4.1 for references). The Stark broadening seems to be more important relative to radiation broadening for both He I and C II lines. The lines of the other species are less affected by these broadening effects except for zero excitation lines.

The data for computing He I profiles is obtained from various sources. The gf-values are taken from Taylor et al. (private communication), radiation broadening coefficients from Wiese et al. (1966), and electron broadening coefficients from the combination of Griem et al. (1962), Benett and Griem (1971), Bassalo et al. (1980), Dimitrijevic and Sahal-Brechot (1984), and Kelleher (1981). The effects of ion broadening are also included in the broadening due to electrons.

LS IV -14° 109

The T_{exc} estimated using excitation balance of Fe II lines is in the range 9500 ± 250 K (Figure 4.50). Equal weights are given to the ionization balance of N II/N I, Fe II/Fe I, Si II/ Si I and S II/S I. Here again, C II/C I ionization balance is given a smaller weight because of the possibility of carbon problem as mentioned earlier. The final adopted T_{eff} and $\log g$ using the ionization and excitation equilibria (Figures 4.43 and 4.50) is given in Table 4.1.

BD -1° 3438

From the excitation equilibria of Fe II lines, we estimate the T_{exc} of the star to be in the range 11750 ± 250 K. Equal weights are given to the ionization balance of N II/N I,

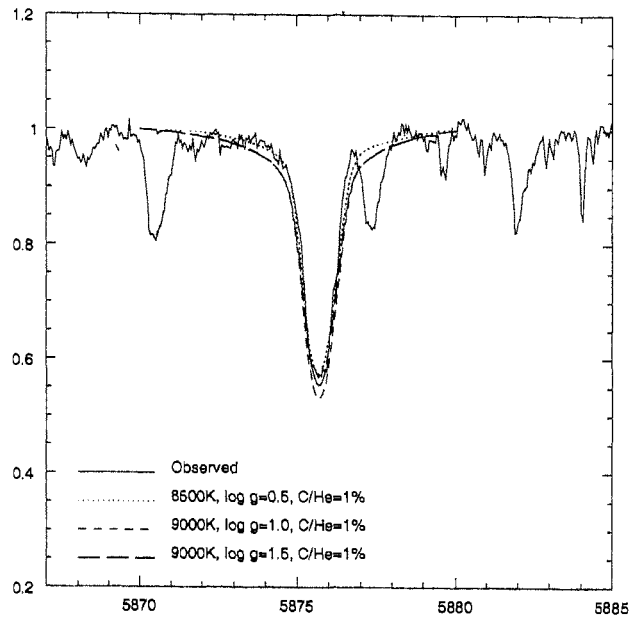


Figure 4.54: Observed and synthesized He I λ 5876 Å triplet line profile of FQ Aqr.

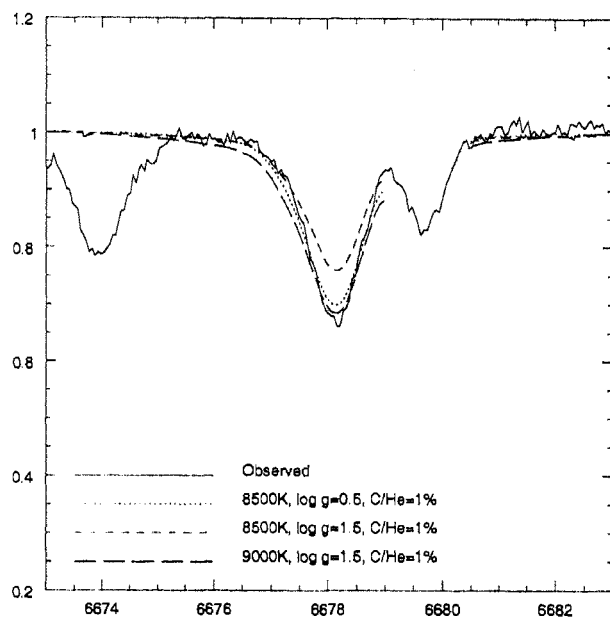


Figure 4.55: Observed and synthesized He I λ 6678 Å line profile of FQ Aqr.

Fe II/Fe I and C II/C I. The final T_{eff} and $\log g$ which we arrive at, using the excitation and ionization balance criteria (Figures 4.52 and 4.44), are given in Table 4.1.

LS IV $-1^\circ 002$

The derived T_{exc} from the excitation balance of Fe II lines is 13000 K. Equal weights are given to the ionization balance of O II/O I, N II/N I, Fe III/Fe II and C II/C I. Smaller weights are given to the ionization balance of Si III/Si II and Al III/Al II because the lines available are very few and the sources of gf-values for these lines are not reliable. The estimated T_{eff} and $\log g$ using the excitation and ionization balance criteria (Figures 4.53 and 4.45), are given in Table 4.1.

Table 4.1
The derived stellar parameters

Star	T_{eff} K	$\log g$ cgs units	ξ km s^{-1}	C/He	R.V km s^{-1}	rotation km s^{-1}
FQ Aqr	8750 \pm 250	0.75 \pm 0.25	7.5 \pm 0.5	1.0%	16 \pm 3 (59)	20
LS IV $-14^\circ 109$	9600 \pm 200	1.00 \pm 0.20	6.5 \pm 0.5	1.0%	5 \pm 2 (47)	15
BD $-1^\circ 3438$	11750 \pm 250	2.30 \pm 0.40	10 \pm 1.0	0.3%	-22 \pm 2 (45)	15
LS IV $-1^\circ 002$	13000 \pm 250	1.75 \pm 0.25	10 \pm 1.0	0.5%	-20 \pm 3 (22)	20

Determination of C/He

For fixing C/He, we adopted the following procedure. Once the T_{eff} and $\log g$ of the star have been determined, we synthesized the theoretical He I profiles using the corresponding grid for different C/He after taking into account Stark broadening, radiation broadening and blending due to other lines. The C/He value is determined from the fit of the synthesized theoretical He I profiles with the observed He I profiles. We used ‘Spectrum’ radiative transfer code for spectrum synthesis. In most of the cases we have used only those He I lines that have good signal-to-noise ratio. We avoided using He I lines in the blue as far as possible because of the poor signal-to-noise ratio of the observed spectra.

All the synthesized spectra were convolved with a Gaussian profile to give a good fit to typical unblended line profiles. Only weak and unblended lines of trace elements were used to fix the full width at half maximum (FWHM) of the Gaussian profile. Note that we have

not used the carbon and helium lines for fixing the FWHM of the Gaussian profile. We find that the FWHM of the Gaussian profile of the stellar lines used is more than the FWHM of the instrumental profile. We attribute this extra broadening to macroturbulence or rotation (Table 4.1).

In the case of FQ Aqr, we have also computed the equivalent widths of the observed He I lines using ‘Eqwrun’ for different C/He, and found that the predicted equivalent widths match best with the measured equivalent widths of the observed He I lines for C/He = 1% (Table 4.2). The helium abundance derived from these lines is 11.53 ± 0.17 , which gives the C/He as $1\% \pm 0.4\%$.

Table 4.2
HeI line Eq. Widths and abundance for FQ Aqr^a

HeI Wavelength (Å)	Eq. Width ^b m Å	Eq. Width ^c m Å	Eq. Width ^d m Å	Abundance ^e
3888.65	318	350	368	11.6
3926.53	145	165	185	11.7
3964.73	190	220	210	11.4
4120.81	160	190	200	11.5
4471.48	325	410	375	11.3
4713.14	187	250	267	11.7

^a For $T_{eff} = 8500$ K and $\log g = 0.5$

^b Computed for C/He = 3%

^c Computed for C/He = 1%

^d Observed

^e Normalized such that $\log \sum \mu_i n_i = 12.15$ where μ_i is the atomic weight

In the case of FQ Aqr, we have synthesized He I profiles of $\lambda\lambda$ 5048, 5876, 6678 Å while for LS IV -14° 109 we have synthesized He I profiles of $\lambda\lambda$ 3872, 5048 Å (Figures 4.56 to 4.60). In the case of LS IV -14° 109 and LS IV -1° 002, He I $\lambda\lambda$ 5876, 6678 Å are not covered in our spectra, and He I λ 7065 Å line is blended with terrestrial H₂O lines.

From He I profiles, we find that the C/He is $1\% \pm 0.4\%$ in FQ Aqr and 0.5% to 1% in

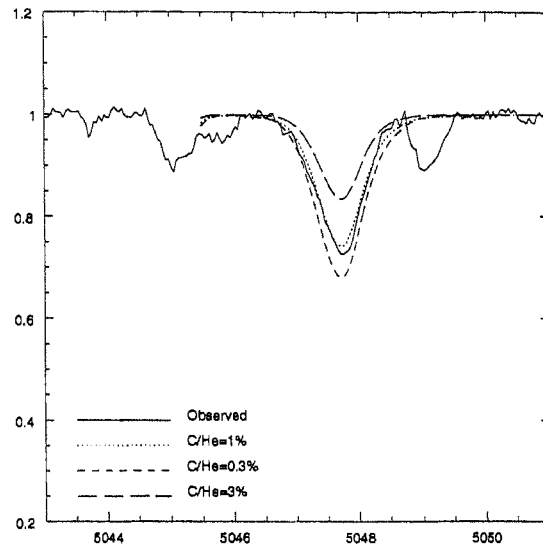


Figure 4.56: Observed and synthesized He I λ 5047.74 Å line profile of FQ Aqr. The He I line profiles are synthesized using model of $T_{eff} = 8500$ K and $\log g = 0.5$, for different values of C/He.

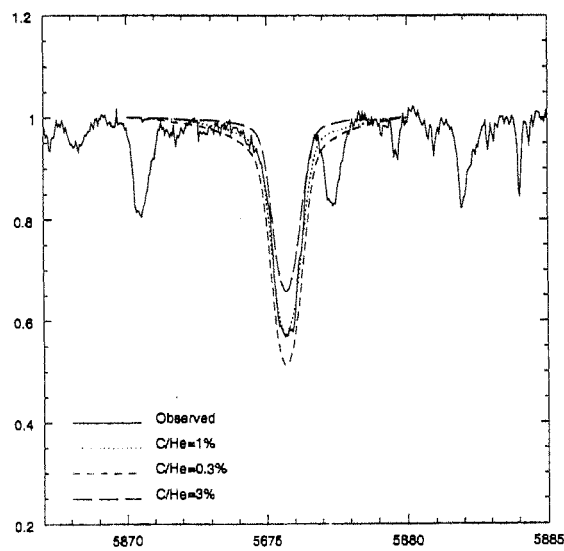


Figure 4.57: Observed and synthesized He I λ 5876 Å triplet line profile of FQ Aqr. The He I line profiles are synthesized using model of $T_{eff} = 8500$ K and $\log g = 0.5$, for different values of C/He.

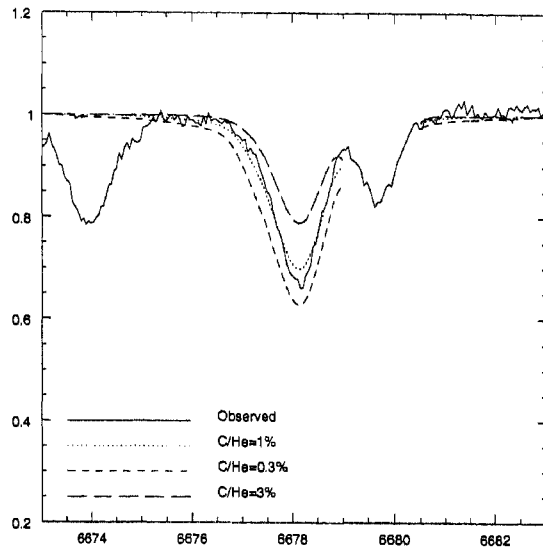


Figure 4.58: Observed and synthesized He I λ 6678 Å line profile of FQ Aqr. The He I line profiles are synthesized using model of $T_{eff} = 8500$ K and $\log g = 0.5$, for different values of C/He.

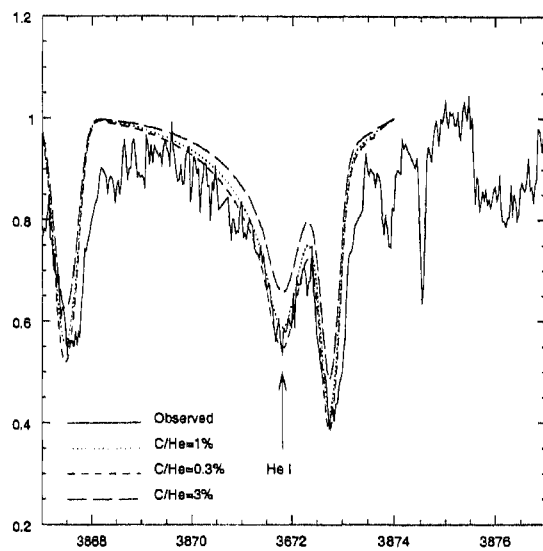


Figure 4.59: Observed and synthesized He I λ 3871.82 Å line profile of LS IV -14° 109. The He I line profiles are synthesized using model of $T_{eff} = 9500$ K and $\log g = 1.0$, for different values of C/He.

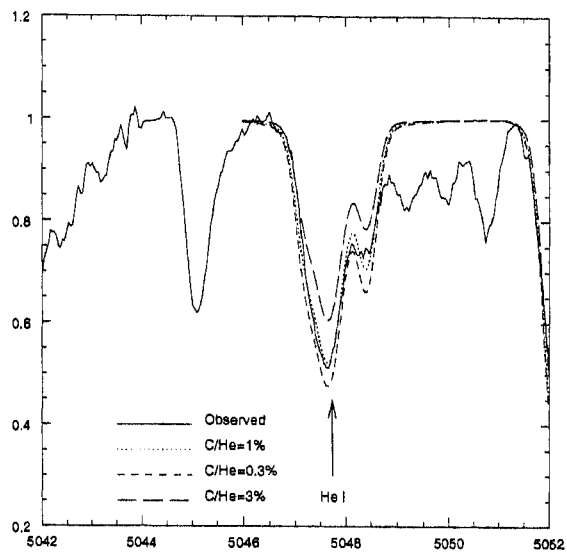


Figure 4.60: Observed and synthesized He I λ 5047.74 Å line profile of LS IV -14° 109. The He I line profiles are synthesized using model of $T_{eff} = 9500$ K and $\log g = 1.0$, for different values of C/He.

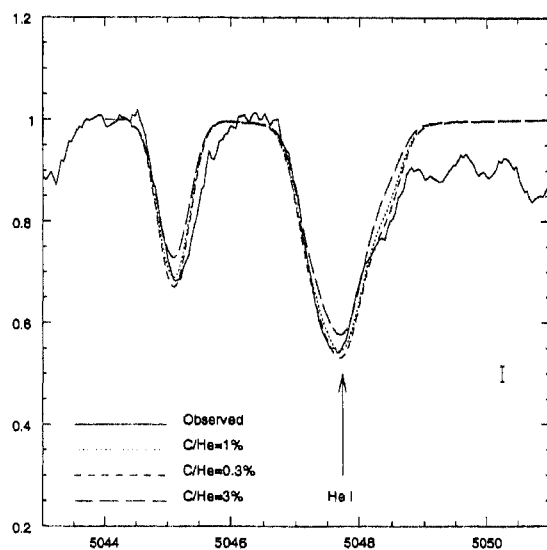


Figure 4.61: Observed and synthesized He I λ 5047.74 Å line profile of BD -1° 3438. The He I line profiles are synthesized using model of $T_{eff} = 11500$ K and $\log g = 1.5$, for different values of C/He. The uncertainty on the ordinate is shown by the error bar.

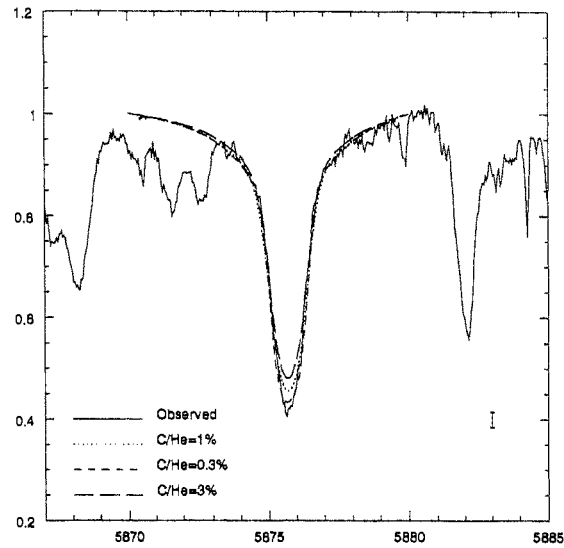


Figure 4.62: Observed and synthesized He I λ 5876 Å triplet line profile of BD -1° 3438. The He I line profiles are synthesized using model of $T_{eff} = 11500$ K and $\log g = 1.5$, for different values of C/He. The uncertainty on the ordinate is shown by the error bar.

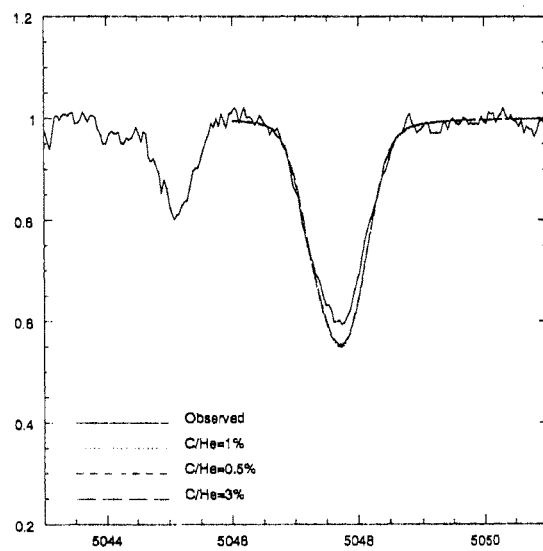


Figure 4.63: Observed and synthesized He I λ 5047.74 Å line profile of LS IV -1° 002. The He I line profiles are synthesized using model of $T_{eff} = 13000$ K and $\log g = 1.5$, for different values of C/He.

LS IV $-14^\circ 109$ (Figures 4.56 to 4.60).

In the case of BD $-1^\circ 3438$ and LS IV $-1^\circ 002$, we find that the observed He I profiles match reasonably well with the synthesized He I profiles for any given C/He (0.3%, 1.0% and 3.0%). The strengths of synthesized He I profiles are independent of the adopted C/He for the hotter stars (see also section 4.2 and 4.3), as clearly demonstrated in Figures 4.61, 4.62 and 4.63.

Using the He I profiles, we find that a C/He of 1% for FQ Aqr and LS IV $-14^\circ 109$. BD $-1^\circ 3438$ and LS IV $-1^\circ 002$ have C/He of 0.3% and 0.5%, respectively; these values are determined using the equivalent widths of C I and C II lines, and not from He I profiles (see section 4.2 and 4.3).

4.5 Abundances

The final abundances were calculated using models of C/He = 1% in the case of FQ Aqr and LS IV $-14^\circ 109$, and 0.3% and 0.5% for BD $-1^\circ 3438$ and LS IV $-1^\circ 002$, respectively. The lines used for the abundance analysis are listed in Tables 4.6, 4.7, 4.8 and 4.9 for FQ Aqr, LS IV $-14^\circ 109$, BD $-1^\circ 3438$ and LS IV $-1^\circ 002$, respectively. These tables also list the lower excitation potential (χ_L), gf-values, measured equivalent widths and the abundance derived for each line.

For the adopted stellar parameters, the individual elemental abundances listed in Table 4.3 are given as $\log n_i$, normalized to such that $\log \sum \mu_i n_i = 12.15$. The abundances determined from the neutral and ionized species of an element are also listed. The He abundance is determined from the computed profiles of He I. In the case of FQ Aqr and LS IV $-14^\circ 109$ we have determined the abundance of helium, also from the equivalent widths of He I lines. The errors quoted are mainly due to line-to-line scatter of the abundances. As a comparison the solar abundances from Grevesse et al. (1996) are also shown in Table 4.3.

Table 4.3

The individual elemental abundances for the analyzed EHe stars^a

	FQ Agr	LS IV -14° 109	BD -1° 3438	LS IV -1° 002	Sun
T_{eff} °K	8500	9500	11500	13000	
$\log g$ (cgs units)	0.5	1.0	2.0	2.0	
C/He	1%	1%	0.3%	0.5%	
ξ km s ⁻¹	8.0	6.0	10.0	10.0	
H	6.3	6.2	5.6	7.1	12.0
He	11.54±0.21	11.54	11.54	11.54	10.99
C (C I, C II)	9.2±0.17, 9.4±0.12	9.3±0.18, 9.5±0.06	9.0±0.17, 8.7±0.3	9.3±0.15, 9.1±0.26	8.55
N (N I, N II)	7.2±0.16, 7.3±0.02	8.6±0.28, 8.6±0.18	8.4±0.20, 8.6±0.15	8.2±0.10, 8.3±0.20	7.97
O (O I, O II)	9.0±0.15, ...	8.5±0.16, ...	8.4±0.19, ...	8.8±0.15, 8.9±0.05	8.87
Ne (Ne I)	8.1±0.27	9.4±0.26	8.8±0.14	9.0±0.13	8.10
Na (Na I)	5.5±0.32	6.8±0.22	6.3 :	6.5 :	6.33
Mg (Mg I, Mg II)	5.5±0.10, 6.2±0.12	6.9±0.26, 7.3±0.10	..., 6.9±0.03	..., 6.9±0.23	7.58
Al (Al II, Al III)	4.8±0.20, ...	7.1±0.20 ; 6.7±0.10	6.0±0.20 ; 6.6±0.07 :	5.4±0.17, 6.3±0.20 :	6.47
Si (Si I, Si II, Si III)	..., 6.5±0.20 ; ...	7.6±0.21, 7.8±0.24,, 6.5±0.14 ; 7.2	..., 5.9±0.10 ; 7.3±0.03	7.55
P (P II)	4.3±0.24	5.3±0.27	5.3 ±0.23	5.1±0.11	5.50
S (S I, S II)	6.1±0.07, 6.0±0.17	7.6±0.24, 7.5±0.40	..., 6.9±0.20	..., 6.7±0.20	7.23
Ca (Ca I, Ca II)	3.9 ; 4.2 :	5.5 ; 5.6±0.22 :	..., 5.5±0.10 :	..., 5.8±0.05 :	6.36
Sc (Sc II)	2.1±0.10	3.3±0.21			3.17
Ti (Ti II)	3.1±0.25	4.3±0.21	4.6±0.28	4.7±0.14	5.02
Cr (Cr I, Cr II)	3.9, 3.7±0.13	..., 5.1±0.24	..., 4.9±0.27		5.69
Mn (Mn II)	4.3±0.20	5.3±0.27	5.1±0.10		5.47
Fe (Fe I, Fe II, Fe III)	5.0±0.11, 5.4±0.13, ...	6.8±0.17, 7.0±0.21, ...	7.1±0.04, 6.7±0.20,, 6.3±0.12, 6.1±0.22	7.50
Ni (Ni I)		6.6±0.17			6.25
Sr (Sr II)	0.4±0.03	2.6±0.05	2.8±0.03 :	2.7±0.20 :	2.97
Y (Y II)		1.9±0.17			2.24
Zr (Zr II)	0.8±0.24	1.9±0.10			2.60
Ba (Ba II)	0.4	1.7±0.13			2.13

^a Uncertain abundances are marked with :

Table 4.4a

Errors due to uncertainty in the stellar parameters

Species	FQ Aqr		LS IV -14° 109	
	$\Delta T_{eff} = -500$	$\Delta \log g = +0.5$	$\Delta T_{eff} = -500$	$\Delta \log g = +0.5$
	[°K]	[cgs]	[°K]	[cgs]
	$\Delta(\log n)$	$\Delta(\log n)$	$\Delta(\log n)$	$\Delta(\log n)$
H I	+0.09	+0.03	-0.10	-0.10
C I/ C II	-0.25/+0.61	-0.17/+0.12	-0.27/+0.22	-0.17/+0.10
N I/ N II	0.00/+0.30	-0.01/+0.17	-0.14/+0.22	-0.11/+0.12
O I	+0.04	0.00	-0.12	-0.08
Ne I	+0.46	+0.24	+0.29	+0.15
Na I	-0.28	-0.18	-0.26	-0.17
Mg I/Mg II	-0.43/+0.10	-0.23/+0.06	-0.50/-0.04	-0.31/0.00
Al I/Al II/Al III	-0.39/+0.21/	-0.18/+0.15/	/-0.09/+0.38	/+0.01/+0.27
Si I/Si II	-0.27/-0.36	-0.20/+0.12	-0.29/+0.13	-0.14/+0.09
P II	+0.22	+0.20	+0.19	+0.19
S I/S II	-0.25/+0.28	-0.16/+0.19	-0.27/+0.21	-0.17/+0.16
Ca I/Ca II	-0.83/-0.26	-0.46/-0.15	-0.86/-0.50	-0.53/-0.22
Sc II	-0.34	-0.04	-0.46	-0.13
Ti II	-0.22	+0.03	-0.33	-0.06
Cr I/Cr II	-0.51/-0.07	-0.22/+0.09	/-0.15	/+0.05
Mn II	-0.04	+0.08	-0.10	+0.05
Fe I/Fe II	-0.46/-0.03	-0.20/+0.12	-0.48/-0.10	-0.24/+0.08
Sr II	-0.57	-0.19	-0.57	-0.20
Y II			-0.53	-0.18
Zr II	-0.30	-0.01	-0.43	-0.10
Ba II	-0.56	-0.19	-0.51	-0.20

4.6 Error Analysis

The major sources of error in deriving the abundances are the line-to-line scatter of the abundances and uncertainty in the adopted stellar parameters (T_{eff} , $\log g$ and ξ). The stellar parameters estimated are accurate within, typically, $\Delta T_{eff} = \pm 300$ K, $\Delta \log g$

$= \pm 0.5$ [cgs] and $\Delta\xi = \pm 1$ km s⁻¹. The errors in abundances corresponding to these uncertainties are given in Tables 4.4a and 4.4b; the errors due to the uncertainty in ξ are negligible when compared to that due to uncertainties in the other parameters.

Table 4.4b
Errors due to uncertainty in the stellar parameters

Species	BD -1° 3438		LS IV -1° 002	
	$\Delta T_{eff} = -500$	$\Delta \log g = +0.5$	$\Delta T_{eff} = -500$	$\Delta \log g = +0.5$
	[°K]	[cgs]	[°K]	[cgs]
	$\Delta(\log n)$	$\Delta(\log n)$	$\Delta(\log n)$	$\Delta(\log n)$
H I	+0.22	-0.32	-0.16	-0.30
C I/ C II	-0.22/-0.04	-0.31/-0.10	-0.09/+0.04	-0.20/+0.05
N I/ N II	+0.24/-0.07	-0.30/+0.12	-0.15/+0.04	-0.23/+0.06
O I/O II	+0.23/	-0.34/	-0.14/+0.06	-0.23/+0.09
Ne I	-0.04	+0.09	-0.10	-0.07
Na I	+0.19	-0.29	-0.12	-0.21
Mg II	+0.25	-0.29	-0.18	-0.23
Al II/Al III	+0.10/-0.14	-0.01/+0.02	-0.12/+0.05	-0.18/+0.10
Si II/Si III	+0.18/-0.08	-0.14/+0.18	-0.18/+0.04	-0.18/+0.10
P II	+0.06	+0.06	-0.07	-0.05
S II	-0.03	+0.08	-0.01	+0.02
Ca II	+0.36	-0.17	-0.66	-0.11
Ti II	+0.38	-0.40	-0.24	-0.24
Cr II	+0.36	-0.35		
Mn II	+0.31	+0.31		
Fe I/Fe II/Fe III	+0.57/+0.35/	-0.22/-0.03/	/-0.16/-0.01	/-0.21/+0.10
Sr II	+0.37	-0.19	-0.19	-0.20
Ba II	+0.33	-0.19	-0.18	-0.20

Abundance ratios are generally less subjected to these uncertainties because most elements are sensitive to the stellar parameters in the same way. The abundance ratios [X/Fe] for the programme stars are given in Table 4.5.

Table 4.5The abundance ratios $[X/Fe]$ for cool EHe stars

	FQ Aqr	LS IV -14° 109	BD -1° 3438	LS IV -1° 002
T_{eff} °K	8500	9500	11500	13000
$\log g$ (cgs units)	0.5	1.0	2.0	2.0
C/He	1%	1%	0.3%	0.5%
ξ km s ⁻¹	8.0	6.0	10.0	10.0
[H/Fe]	-3.6	-5.3	-5.6	-3.7
[C/Fe]	2.8	1.3	1.3	2.0
[N/Fe]	1.3	1.1	1.3	1.4
[O/Fe]	2.2	0.1	0.3	1.1
[Ne/Fe]	2.1	1.8	1.5	2.1
[Na/Fe]	1.3	1.0	0.8	1.4
[Mg/Fe]	0.3	-0.1	0.1	0.5
[Al/Fe]	0.1	0.7	0.3	0.1
[Si/Fe]	0.9	0.8	0.5	1.0
[P/Fe]	0.9	0.3	0.6	0.8
[S/Fe]	1.0	0.9	0.5	0.7
[Ca/Fe]	-0.3	-0.3	-0.1	0.6
[Sc/Fe]	1.0	0.6		
[Ti/Fe]	0.2	-0.2	0.4	0.9
[Cr/Fe]	0.2	-0.1	0.0	
[Mn/Fe]	0.9	0.3	0.4	
[Ni/Fe]		0.9		
[Sr/Fe]	-0.5	0.1	0.6	
[Y/Fe]		0.2		
[Zr/Fe]	0.3	-0.2		
[Ba/Fe]	0.4	0.1		

The final abundances derived from neutral and ionized species of an element are separately given in Table 4.3 for our programme stars.

In the case of BD -1° 3438 and LS IV -1° 002, Al II and Al III lines do not give the same abundance of Al. Since only one or two Al III lines are observed in these stars, we have used Al II lines for the abundance determination. In the spectra of LS IV -14° 109 and BD -1° 3438, Al II lines are strong and saturated, and the abundance of Al derived using these lines is uncertain.

In the spectrum of LS IV -14° 109, both Si I and Si II lines are observed, and we derived the same abundance of Si using Si I and Si II lines. Since the Si I lines present in LS IV -14° 109 are weak and lie on the linear part of the curve of growth, we use these lines for abundance determination. In the spectrum of FQ Aqr no Si I lines were observed. Strong Si II lines are present and these lines fall on the flat part of the curve of growth. The abundance of Si derived using these lines is uncertain and can be treated as an upper limit. The abundance of Si is down by more than 1 dex in FQ Aqr than in LS IV -14° 109 which is hotter than FQ Aqr by approximately 1000 K. Due to the underabundance of Si in FQ Aqr, the Si I lines in FQ Aqr might be very weak and hence difficult to observe. We do not see any Si III lines in the spectra of LS IV -14° 109 and FQ Aqr because most of the Si is in singly ionized state.

In the spectra of BD -1° 3438 and LS IV -1° 002, both Si II and Si III lines are observed. Si I lines are not present in their spectra. Since these stars are hotter than LS IV -14° 109 and FQ Aqr, most of the Si is in singly ionized state and also some amount in doubly ionized state. The Si II lines are very strong in these stars. Therefore we have not used Si II lines for abundance determination, instead we have used weak Si III lines. The Si III lines available for abundance determination are only one or two and hence the abundance of Si derived using these lines is uncertain.

The Ca abundance derived for our programme stars is only an upper limit because the Ca II lines observed in their spectra are very strong and saturated.

The abundances derived using ‘Spectrum’ and ‘Eqwrun’ are in agreement within 0.1 dex for most of the species. We find that the abundances derived using the former are always lower than those derived using the latter. This difference is probably due to the data used for continuous opacity being from two different sources, as described in section 3.2.4.

The model atmospheres of Asplund et al. and Jeffery et al. (private communications) deal with different temperature ranges which do not overlap. We have extrapolated the model atmospheres constructed by Jeffery et al. to 9500 K. The derived abundances using

this extrapolated model atmosphere agree with those derived using the model atmosphere of temperature 9500 K constructed by Asplund et al. within 0.05 dex.

The derived abundances are discussed in the next chapter.

Table 4.6

Lines used to derive elemental abundances for FQ Aqr

$\lambda(\text{\AA})$	$\chi(\text{eV})$	$\log gf$	$W(\text{m\AA})$	Abundance ^a	Reference ^b
H I					
No. of lines=1					
6562.8	10.2	0.71	580.	6.35	Luck
He I					
No. of lines=8					
3888.65	19.73	-0.70	368	11.59	Jeffery
3926.53	21.13	-1.65	185	11.75	Jeffery
3964.73	20.61	-1.30	210	11.39	Jeffery
4120.81	20.87	-1.52	200	11.58	Jeffery
4471.48	20.87	0.04	375	11.33	Jeffery
4713.14	20.87	-1.07	267	11.73	Jeffery
5047.74	14.06	-0.62	Synth ^c	11.54	Jeffery
5875.62	20.96	0.74	Synth ^c	11.54	Jeffery
6678.15	21.21	0.33	Synth ^c	11.54	Jeffery
Mean:				11.53±0.21	
C I					
No. of lines=49					
5813.51	8.87	-2.73	128	9.42	OP
5817.70	8.85	-2.86	69	9.16	OP
5819.50	8.85	-2.73	132	9.44	OP
5850.25	8.77	-2.68	97	9.13	OP
5864.95	8.77	-3.55	47	9.60	OP
5877.31	8.77	-2.14	135	8.81	OP
5963.99	8.65	-2.64	145	9.29	OP
6335.70	8.77	-2.80	63	9.02	OP
6337.20	8.77	-2.33	100	8.82	OP
6342.32	8.77	-2.11	130	8.77	OP
6378.79	8.77	-3.29	68	9.55	OP
6568.71	9.00	-2.17	167	9.18	OP
6591.45	8.85	-2.41	95	8.92	OP
6595.24	8.85	-2.41	78	8.81	OP
6611.35	8.85	-1.84	196	8.90	OP
6641.96	9.03	-3.46	30	9.48	OP
6650.97	8.85	-3.52	35	9.51	OP
6711.29	8.54	-2.69	98	9.04	OP
4735.17	7.95	-3.15	122	9.28	OP
4812.84	7.48	-3.38	152	9.36	OP
4890.65	7.49	-3.35	100	9.06	OP
4898.63	7.49	-3.74	78	9.30	OP
5540.76	8.64	-2.38	142	9.01	OP
5547.27	8.64	-2.25	196	9.16	OP
5996.06	8.64	-2.61	78	8.85	OP
6002.98	8.65	-2.17	191	9.05	OP
6078.40	8.85	-2.27	146	9.06	OP

Table 4.6 (continued)

Lines used to derive elemental abundances for FQ Aqr

$\lambda(\text{\AA})$	$\chi(\text{eV})$	log gf	W(m\AA)	Abundance ^a	Reference ^b
6113.15	8.85	-2.63	120	9.28	OP
6115.85	8.85	-2.51	150	9.31	OP
6120.82	8.85	-2.41	141	9.17	OP
6413.55	8.77	-2.00	178	8.91	OP
6688.78	8.85	-2.13	163	9.03	OP
6671.82	8.85	-1.66	224	8.87	OP
7108.94	8.64	-1.59	295	9.04	OP
7115.19	8.64	-0.94	446	9.11	OP
7116.99	8.65	-0.91	453	9.12	OP
7476.18	8.77	-1.57	290	9.06	OP
7848.25	8.85	-1.73	218	8.87	OP
4371.33	7.68	-1.96	320	9.04	OP
4770.00	7.48	-2.44	307	9.22	OP
4771.72	7.49	-1.87	475	9.66	OP
4775.87	7.49	-2.30	337	9.27	OP
4932.00	7.68	-1.66	402	9.10	OP
5052.12	7.68	-1.30	460	9.05	OP
5551.59	8.64	-1.90	284	9.25	OP
6001.13	8.64	-2.06	260	9.29	OP
6007.18	8.64	-2.06	226	9.11	OP
6010.68	8.64	-1.94	253	9.13	OP
6587.75	8.54	-1.00	458	9.17	OP
Mean:				9.14±0.22	
C II					
No. of lines=2					
3918.98	16.33	-0.55	277	9.47	Jeffery
3920.68	16.33	-0.24	300	9.33	Jeffery
Mean:				9.40±0.1	
N I					
No. of lines=5					
4099.94	10.63	-1.25	50	6.91	Luck
6644.96	11.71	-0.91	46	7.13	Luck
7423.63	10.28	-0.61	220	7.12	Luck
7442.28	10.29	-0.31	309	7.29	Luck
8216.28	10.29	0.16	462	7.31	Luck
Mean:				7.15±0.16	
N II					
No. of lines=2					
3996.00	18.42	0.2	25	7.33	Luck
5679.56	18.4	0.24	18	7.36	Luck
Mean:				7.34±0.02	

Table 4.6 (continued)

Lines used to derive elemental abundances for FQ Aqr

$\lambda(\text{\AA})$	$\chi(\text{eV})$	$\log gf$	$W(\text{m\AA})$	Abundance ^a	Reference ^b
O I					
No. of lines=8					
5330.66	10.69	-0.97	384	8.91	Luck
5436.83	10.69	-1.5	301	8.92	Luck
5554.94	10.94	-1.89	230	9.05	Kur 75
6158.19	10.69	-0.29	513	9.00	Luck
6453.60	10.74	-1.35	388	9.34	Luck
7473.23	14.06	-0.37	142	9.01	Luck
7771.96	9.11	0.32	928	8.84	Luck
7774.18	9.11	0.17	931	9.01	Luck
Mean:	9.01±0.15				
Ne I					
No. of lines=14					
5764.42	18.48	-0.31	93	8.54	Luck
5852.49	16.78	-0.44	101	7.90	Luck
5881.90	16.55	-0.67	84	7.79	Kur 75
6030.00	16.6	-1.04	56	7.84	Kur 75
6074.34	16.6	-0.47	118	8.11	Luck
6143.06	16.55	0.17	153	7.86	Luck
6163.59	16.64	-0.48	88	7.80	Luck
6217.28	16.55	-0.78	74	7.90	Luck
6266.50	16.64	-0.18	148	8.25	Luck
6334.43	16.55	-0.79	121	8.54	Luck
6382.99	16.6	-0.09	155	8.27	Luck
6402.25	16.55	0.35	209	8.35	Luck
6506.53	16.6	0.16	163	8.15	Luck
7032.41	16.55	-0.14	132	8.26	Luck
Mean:	8.11±0.27				
Na I					
No. of lines=2					
5682.65	2.1	-0.71	57	5.76	Luck
8194.84	2.1	0.53	219	5.31	Luck
Mean:	5.53±0.32				
Mg I					
No. of lines=5					
3829.35	2.7	-0.05	190	5.38	Luck
3832.30	2.7	0.70	310	5.40	Luck
5167.32	2.7	-0.86	117	5.60	Luck
5172.68	2.7	-0.38	200	5.52	Luck
5183.60	2.7	-0.16	224	5.39	Luck
Mean:	5.46±0.10				

Table 4.6 (continued)

Lines used to derive elemental abundances for FQ Aqr

$\lambda(\text{\AA})$	$\chi(\text{eV})$	$\log gf$	$W(\text{m\AA})$	Abundance ^a	Reference ^b
Mg II					
No. of lines=6					
3848.24	8.83	-1.60	175	6.29	Luck
4390.58	9.96	-0.53	248	6.23	Luck
4428.00	9.95	-1.21	128	6.08	Luck
4433.99	9.96	-0.90	176	6.09	Luck
7877.06	9.99	0.39	362	6.00	Luck
7896.38	10.0	0.65	450	6.29	Luck
Mean:				6.16±0.12	
Al I					
No. of lines=1					
3944.01	0.0	-0.62	83	4.21	Luck
Al II					
No. of lines=4					
4663.05	10.55	-0.28	145	4.83	Luck
5593.23	13.2	0.41	40	4.56	Kur 75
6226.18	13.01	0.05	44	4.97	Kur 75
6837.14	13.02	0.08	34	4.90	Kur 75
Mean:				4.81±0.18	
Si II					
No. of lines=6					
3853.66	6.83	-1.52	335	6.42	Kur 75
3862.59	6.83	-0.82	415	6.32	Kur 75
4128.05	9.79	0.31	385	6.61	Luck
4130.88	9.8	0.46	403	6.57	Luck
5056.02	10.03	0.44	458	6.86	Luck
5978.93	10.07	-0.06	285	6.26	Luck
Mean:				6.51±0.22	
P II					
No. of lines=2					
6024.17	10.71	0.18	49	4.48	Kur 75
6034.01	10.69	-0.14	16	4.13	Kur 75
Mean:				4.3±0.24	
S I					
No. of lines=3					
6743.58	7.83	-0.85	10	6.14	Luck
6748.79	7.83	-0.53	24	6.18	Luck
6757.16	7.84	-0.24	33	6.05	Luck
Mean:				6.12±0.07	

Table 4.6 (continued)

Lines used to derive elemental abundances for FQ Aqr

$\lambda(\text{\AA})$	$\chi(\text{eV})$	log gf	W(m\AA)	Abundance ^a	Reference ^b
S II					
No. of lines=7					
4815.52	13.61	-0.05	83	6.16	Luck
4917.15	13.94	-0.40	25	5.78	Luck
5453.81	13.61	0.56	110	5.97	Kur 75
5473.59	13.53	-0.12	50	5.85	Kur 75
5509.67	13.56	-0.12	55	5.95	Kur 75
5606.11	13.67	0.16	65	5.90	Kur 75
5659.95	13.62	-0.07	76	6.28	Kur 75
Mean:				5.98±0.17	
Ca I					
No. of lines=1					
4226.73	0.0	0.60	40	3.92	Luck
Ca II					
No. of lines=1					
8248.80	7.51	0.57	161	4.18	Luck
Sc II					
No. of lines=7					
4314.08	0.62	-0.34	330	2.14	Luck
4320.75	0.6	-0.47	290	2.02	Luck
4374.46	0.62	-0.87	268	2.10	Luck
4400.35	0.6	-0.78	217	1.95	Luck
4420.67	0.62	-2.52	18	2.29	Luck
5239.82	1.45	-0.94	94	2.02	Luck
5526.81	1.76	-0.22	210	2.02	Luck
Mean:				2.08±0.11	
Ti II					
No. of lines=49					
3776.06	1.57	-1.34	149	3.15	Luck
3882.28	1.11	-1.71	157	3.22	Luck
3900.55	1.13	-0.45	427	3.69	Luck
3913.46	1.11	-0.31	367	3.12	Luck
3932.01	1.13	-1.78	172	3.36	Luck
4028.33	1.88	-1.00	223	3.33	Luck
4053.81	1.88	-1.21	184	3.33	Luck
4163.64	2.58	-0.40	256	3.34	Luck
4171.90	2.59	-0.56	210	3.26	Luck
4287.89	1.08	-2.02	124	3.25	Kur 75
4290.22	1.16	-1.12	255	3.04	Luck
4300.05	1.18	-0.40	335	2.80	Luck
4301.17	1.16	-1.24	191	2.84	Kur 75
4307.90	1.16	-1.10	223	2.85	Luck
4312.86	1.18	-1.16	240	3.01	Luck
4314.98	1.16	-1.13	215	2.84	Luck

Table 4.6 (continued)

Lines used to derive elemental abundances for FQ Aqr

$\lambda(\text{\AA})$	$\chi(\text{eV})$	$\log gf$	$W(\text{m\AA})$	Abundance ^a	Reference ^b
4337.92	1.08	-1.13	263	3.02	Luck
4395.03	1.08	-0.51	365	2.99	Luck
4399.77	1.23	-1.27	199	2.93	Luck
4407.68	1.22	-2.47	24	2.92	Luck
4411.08	3.08	-1.06	127	3.62	Luck
4417.72	1.16	-1.43	231	3.19	Luck
4421.95	2.05	-1.77	61	3.23	Luck
4441.73	1.18	-2.41	48	3.16	Luck
4443.80	1.08	-0.70	308	2.81	Luck
4450.49	1.08	-2.14	168	3.55	Luck
4468.49	1.13	-0.60	332	2.88	Luck
4488.32	3.11	-0.46	127	3.03	Kur 75
4493.53	1.08	-2.83	44	3.46	Luck
4501.27	1.11	-0.76	309	2.88	Luck
4529.46	1.56	-2.03	95	3.38	Luck
4533.97	1.23	-0.77	429	3.68	Luck
4544.01	1.24	-2.40	33	2.99	Luck
4563.76	1.22	-0.96	276	2.95	Luck
4571.97	1.56	-0.53	285	2.81	Luck
4708.66	1.25	-2.37	40	3.05	Luck
4779.99	2.04	-1.37	104	3.07	Luck
4798.54	1.08	-2.67	67	3.48	Luck
4805.10	2.05	-1.10	152	3.05	Luck
4874.02	3.08	-0.79	75	2.99	Luck
4911.21	3.11	-0.34	113	2.79	Luck
5188.70	1.57	-1.21	175	2.90	Luck
Mean:				3.12±0.25	
Cr I					
No. of lines=49					
4254.35	0.0	-0.11	45	3.93	Luck
Cr II					
No. of lines=30					
3865.59	5.3	-0.78	106	3.66	Kur 75
3979.51	5.65	-0.73	78	3.60	Kur 75
4038.03	6.46	-0.56	46	3.61	Kur 75
4086.14	3.7	-2.42	25	3.49	Kur 75
4252.62	3.84	-2.02	83	3.76	Kur 75
4261.92	3.85	-1.53	138	3.61	Kur 75
4275.57	3.84	-1.71	119	3.67	Kur 75
4539.62	4.02	-2.53	30	3.82	Luck
4555.02	4.05	-1.38	173	3.72	Luck
4558.66	4.06	-0.66	310	3.78	Luck

Table 4.6 (continued)

Lines used to derive elemental abundances for FQ Aqr

$\lambda(\text{\AA})$	$\chi(\text{eV})$	$\log gf$	$W(\text{m\AA})$	Abundance ^a	Reference ^b
4565.78	4.02	-2.11	60	3.74	Luck
4588.22	4.05	-0.63	284	3.58	Luck
4589.89	4.05	-1.22	166	3.51	Luck
4592.09	4.06	-1.22	143	3.41	Luck
4616.64	4.05	-1.29	124	3.36	Luck
4618.83	4.06	-1.11	228	3.73	Luck
4634.11	4.05	-1.24	186	3.63	Luck
4824.13	3.85	-1.22	245	3.78	Luck
4848.24	3.85	-1.14	210	3.51	Luck
4864.32	3.84	-1.37	182	3.59	Kur 75
4876.41	3.84	-1.46	192	3.73	Luck
4884.57	3.84	-2.08	62	3.6	Luck
5237.34	4.06	-1.16	218	3.68	Luck
5246.75	3.7	-2.48	40	3.67	Luck
5249.40	3.74	-2.62	37	3.8	Luck
5274.99	4.05	-1.29	243	3.93	Kur 75
5310.70	4.05	-2.28	49	3.79	Luck
5313.59	4.06	-1.65	132	3.73	Luck
5334.88	4.05	-1.56	114	3.54	Kur 75
5478.35	4.16	-1.91	72	3.68	Kur 75
Mean:				3.66±0.13	
Mn II					
No. of lines=3					
4260.47	1.84	-4.25	44	4.32	Kur 75
4292.25	5.36	-2.23	45	4.47	Kur 75
6122.44	10.14	0.95	50	4.08	Kur 75
Mean:				4.29±0.20	
Fe I					
No. of lines=7					
3825.88	0.91	-0.04	87	4.82	Luck
3827.82	1.55	0.06	79	5.09	Luck
3859.91	0.0	-0.71	100	4.94	Luck
3886.28	0.05	-1.08	65	5.10	Luck
4271.76	1.48	-0.16	60	5.03	Luck
4383.55	1.48	0.20	106	4.96	Luck
4404.75	1.55	-0.14	75	5.15	Luck
Mean:				5.01±0.11	
Fe II					
No. of lines=59					
3779.58	2.53	-3.78	94	5.44	Kur 75
3781.51	4.48	-2.78	85	5.55	Kur 75
3783.35	2.27	-3.16	190	5.24	Kur 75
3821.92	2.33	-3.83	105	5.42	Kur 75

Table 4.6 (continued)

Lines used to derive elemental abundances for FQ Aqr

$\lambda(\text{\AA})$	$\chi(\text{eV})$	$\log gf$	$W(\text{m\AA})$	Abundance ^a	Reference ^b
3824.91	2.57	-3.41	163	5.50	Luck
3872.76	2.69	-3.32	157	5.43	Kur 75
3896.11	2.63	-4.04	70	5.55	Kur 75
3914.48	1.66	-4.05	170	5.57	Luck
3938.29	1.66	-3.89	168	5.40	Luck
3938.97	5.89	-1.85	120	5.66	Luck
3945.21	1.69	-4.25	110	5.44	Luck
3974.16	2.69	-3.51	129	5.43	Luck
4048.83	5.54	-2.14	115	5.68	Kur 75
4122.64	2.57	-3.38	181	5.48	Luck
4124.79	2.53	-4.20	58	5.50	Luck
4138.21	4.71	-3.18	40	5.58	Kur 75
4173.45	2.57	-2.18	330	5.21	Luck
4258.15	2.69	-3.40	170	5.49	Luck
4273.32	2.69	-3.34	152	5.32	Luck
4296.57	2.69	-3.01	234	5.45	Luck
4303.17	2.69	-2.49	310	5.40	Luck
4351.76	2.69	-2.10	376	5.45	Luck
4369.40	2.77	-3.67	140	5.62	Luck
4385.38	2.77	-2.57	240	5.07	Luck
4413.60	2.66	-3.87	78	5.37	Luck
4416.82	2.77	-2.60	308	5.51	Luck
4472.92	2.83	-3.43	130	5.35	Luck
4489.19	2.82	-2.97	224	5.39	Luck
4491.40	2.84	-2.70	230	5.16	Luck
4515.34	2.83	-2.48	299	5.34	Luck
4520.23	2.79	-2.60	295	5.41	Luck
4541.52	2.84	-3.05	212	5.40	Luck
4555.89	2.82	-2.29	360	5.52	Luck
4580.06	2.57	-3.72	100	5.30	Kur 75
4582.83	2.83	-3.10	192	5.33	Luck
4620.51	2.82	-3.28	155	5.31	Luck
4629.34	2.79	-2.37	363	5.58	Luck
4635.33	5.93	-1.65	146	5.51	Luck
4648.93	2.57	-4.39	45	5.52	Kur 75
4666.75	2.82	-3.33	175	5.46	Luck
4731.44	2.88	-3.36	162	5.46	Luck
4871.27	2.69	-4.06	65	5.44	Kur 75
4993.35	2.79	-3.65	140	5.56	Luck
5074.06	6.78	-1.97	39	5.49	Kur 75
5254.92	3.22	-3.23	148	5.44	Kur 75
5272.41	5.93	-2.03	80	5.45	Luck
5275.99	3.19	-1.94	336	5.14	Luck
5284.09	2.88	-3.19	164	5.27	Luck

Table 4.6 (continued)

Lines used to derive elemental abundances for FQ Aqr

$\lambda(\text{\AA})$	$\chi(\text{eV})$	log gf	W(m\AA)	Abundance ^a	Reference ^b
5362.86	3.19	-2.74	248	5.44	Kur 75
5425.27	3.19	-3.36	139	5.49	Luck
5534.86	3.23	-2.93	245	5.64	Luck
6147.73	3.87	-2.72	148	5.33	Kur 75
6149.24	3.87	-2.92	146	5.52	Luck
6175.16	6.2	-1.98	55	5.37	Kur 75
6179.38	5.54	-2.81	45	5.70	Luck
6247.56	3.87	-2.51	204	5.41	Luck
6331.97	6.19	-1.98	50	5.31	Kur 75
6446.43	6.2	-2.16	43	5.43	Luck
4508.28	2.84	-2.21	323	5.23	Luck
Mean:				5.43±0.13	
Ni II					
No. of lines=3					
3849.58	4.01	-1.88	177	4.32	Kur 75
4015.5	4.01	-2.42	95	4.27	Kur 75
4192.07	4.01	-3.06	37	4.34	Kur 75
Mean:				4.31±0.03	
Sr II					
No. of lines=2					
4077.72	0.0	0.15	180	0.45	Luck
4215.54	0.0	-0.16	112	0.41	Luck
Mean:				0.43±0.03	
Zr II					
No. of lines=2					
4149.22	0.80	0.08	51	0.6	Thev 89,90
4359.74	1.23	-0.25	30	0.94	Thev 89,90
Mean:				0.77±0.24	
Ba II					
No. of lines=1					
4554.04	0.0	0.12	50	0.39	Luck

^a Normalized such that $\log \sum \mu_i n_i = 12.15$

^b Sources of gf-values

^c Spectrum synthesis

References:

Jeffery	C. Simon Jeffery (private communication)
Kur 75	Kurucz & Petryemann, 1975
Luck	R. E. Luck (private communication)
OP	Opacity Project (see section 4.4.1)
Thev 89,90	Thevenin 1989, 1990

Table 4.7

Lines used to derive elemental abundances for LS IV -14° 109

$\lambda(\text{\AA})$	$\chi(\text{eV})$	$\log gf$	$W(\text{m\AA})$	Abundance ^a	Reference ^b
H I					
No. of lines=1					
6562.80	10.2	0.71	515	6.30	Luck
He I					
No. of lines=2					
3871.82	21.13	-1.92	Synth ^c	11.54	Jeffery
5047.74	14.06	-0.62	Synth ^c	11.54	Jeffery
C I					
No. of lines=40					
4734.26	7.95	-2.37	191	9.36	OP
4735.17	7.95	-3.15	123	9.67	OP
4766.62	7.48	-2.62	199	9.40	OP
4817.37	7.48	-3.04	182	9.69	OP
4890.65	7.49	-3.35	110	9.52	OP
5023.85	7.95	-2.21	175	9.07	OP
5547.27	8.64	-2.25	131	9.19	OP
5963.99	8.65	-2.64	150	9.71	OP
6002.98	8.65	-2.17	152	9.25	OP
6007.18	8.64	-2.06	157	9.17	OP
6010.68	8.64	-1.94	178	9.19	OP
6078.40	8.85	-2.27	107	9.17	OP
6335.70	8.77	-2.8	106	9.66	OP
6337.20	8.77	-2.33	133	9.37	OP
6397.98	8.77	-1.78	180	9.14	OP
6568.71	9.00	-2.17	150	9.47	OP
6595.24	8.85	-2.41	90	9.21	OP
6611.35	8.85	-1.84	174	9.22	OP
6711.29	8.54	-2.69	95	9.36	OP
7108.94	8.64	-1.59	274	9.50	OP
7111.48	8.64	-1.09	340	9.41	OP
7113.18	8.65	-0.77	364	9.25	OP
7115.19	8.64	-0.94	350	9.32	OP
7116.99	8.65	-0.91	344	9.26	OP
7119.67	8.64	-1.15	334	9.43	OP
7476.18	8.77	-1.57	291	9.65	OP
7483.44	8.77	-1.37	229	9.07	OP
7662.43	8.77	-1.28	255	9.14	OP
7685.20	8.77	-1.52	237	9.26	OP
7832.63	8.85	-1.81	204	9.36	OP
7860.89	8.85	-1.15	291	9.22	OP

Table 4.7 (continued)

Lines used to derive elemental abundances for LS IV -14° 109

$\lambda(\text{\AA})$	$\chi(\text{eV})$	$\log gf$	$W(\text{m\AA})$	Abundance ^a	Reference ^b
4371.33	7.68	-1.96	261	9.39	OP
4770.00	7.48	-2.44	255	9.62	OP
4771.72	7.49	-1.87	309	9.46	OP
4775.87	7.49	-2.3	241	9.38	OP
4932.00	7.68	-1.66	317	9.39	OP
5039.07	7.95	-1.79	308	9.60	OP
5793.12	7.95	-2.06	210	9.13	OP
5052.12	7.68	-1.3	335	9.15	OP
6587.75	8.54	-1.00	332	9.23	OP
Mean:				9.35±0.18	
C II					
No. of lines=3					
3920.68	16.33	-0.24	340	9.46	Yan 87
6578.05	14.45	-0.04	502	9.44	Dahari 84
6582.85	14.45	-0.34	450	9.56	Dahari 84
Mean:				9.48±0.06	
N I					
No. of lines=10					
4099.94	10.63	-1.25	208	8.42	Luck
4114.00	10.64	-1.95	100	8.30	Luck
4151.46	10.29	-1.87	173	8.57	Luck
4914.90	10.63	-2.26	115	8.64	Luck
4935.03	10.64	-1.94	163	8.66	Luck
5999.47	11.55	-1.75	180	9.09	Kur 75
6644.96	11.71	-0.91	255	8.89	Luck
6646.52	11.7	-1.59	138	8.75	Luck
7423.63	10.28	-0.61	476	9.16	Luck
7442.28	10.29	-0.31	505	9.05	Luck
Mean:				8.75±0.29	
N II					
No. of lines=5					
3995.00	18.42	0.2	155	9.16	Luck
4607.15	18.38	-0.5	78	8.81	Luck
4613.87	18.39	-0.64	72	8.87	Luck
4643.09	18.4	-0.35	93	8.90	Luck
5686.21	18.39	-0.55	78	9.10	Luck
Mean:				8.97±0.15	
O I					
No. of lines=8					
5330.66	10.69	-0.97	234	8.42	Luck
5435.76	10.69	-1.65	192	8.77	Luck

Table 4.7 (continued)

Lines used to derive elemental abundances for LS IV -14° 109

$\lambda(\text{\AA})$	$\chi(\text{eV})$	$\log gf$	$W(\text{m\AA})$	Abundance ^a	Reference ^b
6155.99	10.69	-0.66	250	8.21	Luck
6156.78	10.69	-0.44	290	8.28	Luck
6158.19	10.69	-0.29	366	8.68	Luck
7771.96	9.11	0.36	620	8.44	Luck
7774.18	9.11	0.22	578	8.41	Luck
7775.40	9.11	0.0	523	8.33	Luck
Mean:				8.44±0.19	
Ne I					
No. of lines=13					
5852.49	16.78	-0.44	261	9.50	Luck
5881.90	16.55	-0.67	262	9.62	Kur 75
6030.00	16.6	-1.04	190	9.29	Kur 75
6074.34	16.6	-0.47	257	9.44	Luck
6143.06	16.55	0.17	371	9.64	Luck
6163.59	16.64	-0.48	247	9.39	Luck
6217.28	16.55	-0.78	224	9.43	Luck
6266.50	16.64	-0.18	310	9.69	Luck
6334.43	16.55	-0.79	284	10.05	Luck
6382.99	16.6	-0.09	308	9.58	Luck
6402.25	16.55	0.35	388	9.62	Luck
6506.53	16.6	0.16	365	9.74	Luck
7032.41	16.55	-0.14	317	9.83	Luck
Mean:				9.60±0.20	
Na I					
No. of lines=4					
4664.80	2.1	-1.52	69	7.02	Luck
5682.65	2.1	-0.71	135	6.70	Luck
6154.23	2.1	-1.57	70	7.08	Luck
8194.84	2.1	0.53	340	6.58	Luck
Mean:				6.84±0.24	
Mg I					
No. of lines=49					
5183.60	2.7	-0.16	299	6.84	Luck
4702.99	4.33	-0.38	158	7.17	Luck
Mean:				7.00±0.23	
Mg II					
No. of lines=3					
3848.24	8.83	-1.6	275	7.57	Luck
4428.00	9.95	-1.21	248	7.34	Luck
4433.99	9.96	-0.9	303	7.53	Luck
Mean:				7.48±0.12	

Table 4.7 (continued)

Lines used to derive elemental abundances for LS IV -14° 109

$\lambda(\text{\AA})$	$\chi(\text{eV})$	$\log gf$	$W(\text{m\AA})$	Abundance ^a	Reference ^b
Al II					
No. of lines=7					
4663.05	10.55	-0.28	368	7.00	Luck
5593.23	13.2	0.41	282	7.04	Kur 75
6226.18	13.01	0.05	264	7.17	Kur 75
6823.48	13.02	-0.14	271	7.51	Kur 75
6837.14	13.02	0.08	296	7.52	Kur 75
7042.06	11.27	0.35	444	7.24	Kur 75
7063.64	11.27	-0.35	370	7.50	Kur 75
Mean:				7.28±0.23	
Al III					
No. of lines=2					
5696.47	15.64	-0.24	89	6.65	Kur 75
5593.23	13.2	0.41	282	6.80	Kur 75
Mean:				6.73±0.10	
Si I					
No. of lines=5					
5708.44	4.93	-1.47	44	7.50	Luck
6145.08	5.61	-1.48	35	7.77	Luck
6155.14	5.62	-0.75	80	7.51	Tom 97
7932.20	5.96	-0.47	96	7.51	Luck
8556.77	5.87	-0.19	230	7.47	Luck
Mean:				7.60±0.13	
Si II					
No. of lines=2					
4076.78	9.83	0.02	282	7.99	Kur 75
5957.61	10.07	-0.3	414	7.77	Luck
6829.82	12.88	-0.27	207	7.50	Luck
Mean:				7.75±0.24	
P II					
No. of lines=3					
5499.72	10.76	-0.47	74	5.33	Kur 75
6034.01	10.69	-0.14	132	5.66	Kur 75
6165.56	10.76	-0.4	100	5.66	Kur 75
Mean:				5.55±0.19	
S I					
No. of lines=4					
6052.66	7.87	-0.63	85	7.28	Luck
6743.58	7.83	-0.85	120	7.77	Luck
6748.79	7.83	-0.53	140	7.6	Luck
6757.16	7.84	-0.24	211	7.81	Luck
Mean:				7.62±0.24	

Table 4.7 (continued)

Lines used to derive elemental abundances for LS IV -14° 109

$\lambda(\text{\AA})$	$\chi(\text{eV})$	$\log gf$	$W(\text{m\AA})$	Abundance ^a	Reference ^b
S II					
No. of lines=12					
4153.10	15.83	0.4	118	7.11	Kur 75
4716.23	13.56	-0.52	124	7.00	Luck
4779.11	13.61	-1.65	94	7.83	Kur 75
4815.52	13.61	-0.05	191	7.31	Kur 75
4917.15	13.94	-0.4	140	7.28	Luck
5428.64	13.53	-0.01	199	7.39	Luck
5432.77	13.56	0.31	300	8.05	Luck
5453.81	13.61	0.56	329	8.05	Kur 75
5473.59	13.53	-0.12	205	7.56	Kur 75
5509.67	13.56	-0.12	230	7.84	Kur 75
5606.11	13.67	0.16	266	7.97	Kur 75
5664.73	13.6	-0.3	135	7.04	Kur 75
Mean:				7.54±0.40	
Ca I					
No. of lines=1					
4226.73	0.0	0.6	85	5.55	Luck
Ca II					
No. of lines=2					
8542.08	1.69	-0.49	896	5.75	Kur 75
8662.14	1.69	-0.75	779	5.44	Kur 75
Mean:				5.60±0.22	
Sc II					
No. of lines=5					
4400.35	0.6	-0.78	231	3.06	Luck
4305.71	0.59	-1.52	200	3.60	Luck
6604.60	1.55	-1.53	89	3.35	Luck
5684.19	1.5	-1.25	135	3.35	Luck
5526.81	1.76	-0.22	250	3.15	Luck
Mean:				3.30±0.21	
Ti II					
No. of lines=25					
3776.06	1.57	-1.34	228	4.51	Luck
3836.08	0.6	-1.93	178	4.03	Luck
3882.28	1.11	-1.71	157	3.98	Luck
3913.46	1.11	-0.31	350	4.29	Luck
3932.01	1.13	-1.78	230	4.61	Luck
4300.05	1.18	-0.4	359	4.21	Luck
4301.93	1.16	-1.24	250	4.09	Kur 75
4316.81	2.04	-1.42	153	4.14	Luck
4350.83	2.05	-1.4	156	4.14	Luck
4421.95	2.05	-1.77	166	4.55	Luck
4441.73	1.18	-2.41	160	4.60	Luck

Table 4.7 (continued)

Lines used to derive elemental abundances for LS IV -14° 109

$\lambda(\text{\AA})$	$\chi(\text{eV})$	$\log gf$	$W(\text{m\AA})$	Abundance ^a	Reference ^b
4488.32	3.11	-0.46	221	4.27	Kur 75
4544.01	1.24	-2.4	94	4.22	Luck
4545.14	1.13	-1.81	148	3.89	Luck
4563.76	1.22	-0.96	329	4.39	Luck
4571.97	1.56	-0.53	340	4.27	Luck
4708.66	1.25	-2.37	142	4.46	Luck
4779.99	2.04	-1.37	228	4.49	Luck
4798.54	1.08	-2.67	128	4.57	Luck
4874.02	3.08	-0.79	188	4.28	Luck
4911.21	3.11	-0.34	262	4.37	Luck
5072.30	3.11	-0.75	253	4.68	Luck
5418.80	1.57	-2.11	115	4.18	Luck
4501.27	1.11	-0.76	323	4.12	Luck
4443.80	1.08	-0.7	350	4.26	Luck
Mean:				4.30±0.21	
Cr II					
No. of lines=30					
3865.59	5.3	-0.78	200	4.78	Kur 75
3911.32	4.92	-2.06	157	5.44	Kur 75
3979.51	5.65	-0.73	224	5.12	Kur 75
4038.03	6.46	-0.56	182	5.01	Kur 75
4195.41	5.3	-2.32	126	5.62	Kur 75
4256.16	6.46	-1.39	104	5.19	Kur 75
4261.92	3.85	-1.53	246	4.91	Kur 75
4275.57	3.84	-1.71	241	5.03	Kur 75
4539.62	4.02	-2.53	155	5.22	Luck
4555.02	4.05	-1.38	271	5.00	Luck
4558.66	4.06	-0.66	394	5.37	Luck
4565.78	4.02	-2.11	212	5.22	Luck
4616.64	4.05	-1.29	296	5.10	Luck
4618.83	4.06	-1.11	292	4.87	Luck
4634.11	4.05	-1.24	290	4.97	Luck
4812.35	3.85	-1.8	225	4.86	Luck
4824.13	3.85	-1.22	325	5.06	Luck
4836.22	3.84	-2.25	248	5.48	Luck
4848.24	3.85	-1.14	300	4.77	Luck
4864.32	3.84	-1.37	283	4.87	Kur 75
4876.41	3.84	-1.46	335	5.36	Luck
4884.57	3.84	-2.08	208	4.99	Luck
5246.75	3.7	-2.48	114	4.66	Luck
5249.40	3.74	-2.62	198	5.36	Luck
5274.99	4.05	-1.29	311	5.05	Kur 75
5334.88	4.05	-1.56	260	4.93	Kur 75

Table 4.7 (continued)

Lines used to derive elemental abundances for LS IV -14° 109

$\lambda(\text{\AA})$	$\chi(\text{eV})$	$\log gf$	$W(\text{m\AA})$	Abundance ^a	Reference ^b
5420.90	3.74	-2.58	124	4.83	Luck
5620.63	6.46	-1.14	153	5.18	Kur 75
4589.89	4.05	-1.22	278	4.88	Luck
4592.09	4.06	-1.22	277	4.88	Luck
Mean:				5.07±0.24	
Mn II					
No. of lines=11					
5297.06	9.82	0.62	207	5.67	Kur 75
4206.38	5.37	-1.57	168	5.11	Kur 75
4260.47	1.84	-4.25	143	5.52	Kur 75
4292.25	5.36	-2.23	145	5.57	Kur 75
4727.90	5.35	-2.07	134	5.27	Kur 75
4730.36	5.35	-2.15	90	5.04	Kur 75
4755.73	5.37	-1.24	215	5.07	Kur 75
4764.70	5.37	-1.35	203	5.08	Kur 75
6122.44	10.14	0.95	226	5.68	Kur 75
7415.78	3.69	-2.2	295	5.32	Kur 75
7432.27	3.69	-2.5	187	4.95	Kur 75
Mean:				5.30±0.27	
Fe I					
No. of lines=7					
3840.44	0.99	-0.51	170	6.67	Luck
3859.91	0.0	-0.71	230	6.76	Luck
3886.28	0.05	-1.08	150	6.50	Luck
4045.81	1.48	0.28	260	6.90	Luck
4071.74	1.6	-0.02	206	6.77	Luck
4271.16	2.44	-0.35	129	7.00	Luck
4404.75	1.55	-0.14	225	6.91	Luck
Mean:				6.79±0.17	
Fe II					
No. of lines=47					
3779.58	2.53	-3.78	214	6.79	Kur 75
3781.51	4.48	-2.78	220	7.01	Kur 75
3824.91	2.57	-3.41	265	6.89	Luck
3896.11	2.63	-4.04	180	6.74	Kur 75
3930.31	1.69	-4.03	300	7.24	Kur 75
3938.97	5.89	-1.85	209	6.72	Luck
3945.21	1.69	-4.25	260	7.10	Luck
4046.81	4.48	-4.1	100	7.19	Kur 75
4088.75	2.83	-4.81	124	7.14	Kur 75
4122.64	2.57	-3.38	265	6.71	Luck
4124.79	2.53	-4.2	181	6.78	Luck
4177.70	2.53	-3.75	290	7.25	Kur 75
4273.32	2.69	-3.34	273	6.76	Luck

Table 4.7 (continued)

Lines used to derive elemental abundances for LS IV -14° 109

$\lambda(\text{\AA})$	$\chi(\text{eV})$	$\log gf$	$W(\text{m\AA})$	Abundance ^a	Reference ^b
4303.17	2.69	-2.49	386	6.94	Luck
4351.76	2.69	-2.1	413	6.71	Luck
4416.82	2.77	-2.6	365	6.87	Luck
4449.66	7.89	-1.59	137	6.79	Kur 75
4491.40	2.84	-2.7	329	6.62	Luck
4520.23	2.79	-2.6	381	6.97	Luck
4522.63	2.83	-2.03	413	6.67	Luck
4555.89	2.82	-2.29	450	7.13	Luck
4576.33	2.83	-3.04	317	6.80	Luck
4582.83	2.83	-3.1	314	6.83	Luck
4583.83	2.79	-2.02	533	7.22	Luck
4598.53	7.77	-1.5	221	7.36	Kur 75
4601.34	2.88	-4.43	171	7.03	Kur 75
4635.33	5.93	-1.65	285	6.99	Luck
4648.93	2.57	-4.39	156	6.70	Kur 75
4666.75	2.82	-3.33	292	6.84	Luck
4868.82	2.66	-5.16	121	7.26	Kur 75
4871.27	2.69	-4.06	211	6.81	Kur 75
4893.78	2.82	-4.45	174	7.01	Luck
5197.57	3.22	-2.1	408	6.72	Luck
5272.41	5.93	-2.03	263	7.09	Luck
5275.99	3.19	-1.94	433	6.70	Luck
5325.56	3.21	-2.6	349	6.66	Luck
5362.86	3.19	-2.74	382	7.07	Kur 75
5525.14	3.25	-4.61	161	7.28	Kur 75
5591.38	3.25	-4.68	107	7.00	Kur 75
5627.49	3.37	-4.36	165	7.13	Luck
5732.72	3.37	-4.67	90	6.93	Kur 75
5952.55	5.93	-2.03	275	7.13	Kur 75
5991.38	3.14	-3.74	300	7.28	Luck
6147.73	3.87	-2.72	342	7.04	Kur 75
6331.97	6.19	-1.98	257	7.09	Kur 75
6446.43	6.2	-2.16	204	6.89	Luck
7462.38	3.87	-2.73	303	6.66	Kur 75
Mean:				6.95±0.21	
Ni I					
No. of lines=4					
6772.36	3.65	-0.98	28	6.80	Luck
7422.30	3.63	0.07	128	6.63	Luck
4980.16	3.6	-0.1	97	6.62	Luck
4459.04	3.31	-0.06	88	6.39	Thev 89,90
Mean:				6.61±0.17	

Table 4.7 (continued)

Lines used to derive elemental abundances for LS IV -14° 109

$\lambda(\text{\AA})$	$\chi(\text{eV})$	$\log gf$	$W(\text{m\AA})$	Abundance ^a	Reference ^b
Sr II					
No. of lines=2					
4077.72	0.00	0.15	310	2.60	Luck
4215.54	0.00	-0.16	277	2.53	Luck
Mean:				2.56±0.05	
Y II					
No. of lines=3					
4309.62	0.13	-0.74	55	1.87	Luck
4854.87	0.99	-0.38	35	1.77	Luck
4900.13	1.03	-0.09	104	2.09	Luck
Mean:				1.91±0.17	
Zr II					
No. of lines=2					
4149.22	0.8	0.08	113	1.85	Thev 89,90
4359.74	1.23	-0.25	56	1.99	Thev 89,90
Mean:				1.92±0.10	
Ba II					
No. of lines=3					
4554.04	0.0	0.12	95	1.61	Luck
4934.09	0.0	-0.16	72	1.68	Luck
6141.73	0.7	-0.08	60	1.86	Luck
Mean:				1.72±0.13	

^a Normalized such that $\log \sum \mu_i n_i = 12.15$

^b Sources of gf-values

^c Spectrum synthesis

References:

Kur 75 Kurucz & Petryemann, 1975
 Luck R. E. Luck (private communication)
 OP Opacity Project (see section 4.4.1)
 Thev 89,90 Thevenin 1989, 1990
 Tom 97 Tomkin et al., 1997
 Yan 87 Yan, Taylor & Seaton, 1987

Table 4.8

Lines used to derive elemental abundances for BD -1° 3438

$\lambda(\text{\AA})$	$\chi(\text{eV})$	$\log gf$	$W(\text{m\AA})$	Abundance ^a	Reference ^b
H I					
No. of lines=1					
6562.80	10.15	0.71	234	5.61	Luck
He I					
No. of lines=2					
5047.74	14.06	-0.62	Synth ^c	11.54	Jeffery
5875.62	20.96	0.74	Synth ^c	11.54	Jeffery
Mean:					
C I					
No. of lines=28					
3942.22	7.680	-2.398	190	9.09	Kur 75
4064.20	7.450	-2.699	110	9.22	Heb 83
4064.20	7.460	-2.699	113	9.24	Heb 83
4371.33	7.680	-2.097	171	8.93	Heb 83
4766.62	7.450	-2.398	111	8.84	Heb 83
4770.00	7.450	-2.301	157	8.97	Heb 83
4771.72	7.460	-1.699	233	8.75	Heb 83
4775.87	7.460	-2.301	154	8.94	Heb 83
4817.33	7.460	-2.523	120	9.00	Heb 83
4826.73	7.460	-2.155	184	8.96	Heb 83
4890.64	7.490	-3.35	35	9.19	Luck
4932.00	7.650	-1.770	212	8.82	Heb 83
5793.11	7.950	-2.046	105	8.68	Luck
6010.67	8.640	-2.000	115	9.05	Kur 75
6013.21	8.650	-1.469	225	9.07	Kur 75
6014.84	8.640	-1.721	175	9.06	Kur 75
7108.93	8.640	-1.602	190	9.03	Luck
7111.47	8.640	-1.071	215	8.62	Luck
7113.18	8.650	-0.762	300	8.72	Luck
7115.18	8.650	-0.900	287	8.80	Luck
7116.90	8.650	-1.081	270	8.90	Luck
7119.67	8.640	-1.310	294	9.24	Luck
7476.17	8.770	-1.638	202	9.20	Luck
7483.43	8.770	-1.444	200	8.99	Luck
7662.43	8.770	-1.328	175	8.76	Luck
7685.19	8.770	-1.569	146	8.86	Luck
7832.62	8.850	-1.678	146	9.00	Luck
7860.88	8.850	-1.155	250	8.91	Luck
Mean:				8.95±0.17	

Table 4.8 (continued)

Lines used to derive elemental abundances for BD -1° 3438

$\lambda(\text{\AA})$	$\chi(\text{eV})$	log gf	W(m\AA)	Abundance ^a	Reference ^b
C II					
No. of lines=4					
3918.98	16.333	-0.545	335	8.82	Yan 87
3920.69	16.334	-0.244	370	8.73	Yan 87
4744.77	13.720	-2.523	109	8.35	Dahari 84
6098.51	22.570	0.243	60	9.05	Dahari 84
Mean:				8.74±0.3	
N I					
No. of lines=11					
4099.94	10.630	-1.244	145	8.05	Kur 75
4114.00	10.640	-1.959	64	8.25	Kur 75
4151.46	10.290	-1.886	134	8.46	Luck
4914.90	10.630	-2.301	55	8.46	Luck
4935.03	10.640	-1.959	109	8.54	Luck
6644.96	11.710	-0.910	214	8.56	Luck
6646.52	11.710	-1.585	108	8.70	Luck
7423.63	10.280	-0.611	435	8.59	Luck
7442.28	10.290	-0.311	473	8.49	Luck
8567.74	10.630	-0.699	400	8.40	Kur 75
8594.01	10.630	-0.300	440	8.16	Kur 75
Mean:				8.4±0.2	
N II					
No. of lines=9					
4607.16	18.464	-0.483	119	8.54	Bec 89
4630.54	18.484	0.093	221	8.70	Bec 89
4643.09	18.484	-0.385	122	8.48	Bec 89
5666.64	18.461	0.009	187	8.70	Wiese 66
5679.56	18.478	0.279	227	8.71	Wiese 66
5686.21	18.461	-0.474	110	8.62	Wiese 66
5710.76	18.483	-0.470	142	8.87	Jeffery
3955.85	18.391	-1.149	80	8.77	Luck
3995.00	18.498	0.225	215	8.41	Bec 89
Mean:				8.6±0.15	
O I					
No. of lines=6					
5330.66	10.690	-0.971	232	8.30	Luck
5435.76	10.690	-1.658	151	8.58	Luck
5436.83	10.690	-1.495	175	8.55	Luck
6155.99	10.690	-0.701	250	8.15	Heb 83
6155.99	10.690	-0.701	315	8.46	Heb 83
6158.19	10.690	-0.332	329	8.16	Heb 83
Mean:				8.36±0.19	

Table 4.8 (continued)

Lines used to derive elemental abundances for BD -1° 3438

$\lambda(\text{\AA})$	$\chi(\text{eV})$	$\log gf$	$W(\text{m\AA})$	Abundance ^a	Reference ^b
Ne I					
No. of lines=9					
5764.41	18.480	-0.314	299	9.01	Luck
5881.90	16.550	-0.701	312	8.58	Wiese 66
6030.00	16.600	-0.987	276	8.68	Wiese 66
6074.34	16.600	-0.467	358	8.67	Wiese 66
6163.59	16.640	-0.476	362	8.72	Luck
6217.28	16.550	-0.870	300	8.71	Wiese 66
6266.49	16.640	-0.180	419	8.77	Luck
6334.43	16.550	-0.388	405	8.85	Wiese 66
6598.95	16.780	-0.187	442	8.97	Luck
Mean:				8.8±0.14	
Na I					
No. of lines=1					
8194.83	2.1	0.53	300	6.27	Luck
Mean:				6.27±0.00	
Mg II					
No. of lines=3					
3848.25	8.830	-1.585	242	6.89	Heb 83
4428.00	9.950	-1.201	212	6.83	Heb 83
4434.00	9.960	-0.900	273	6.85	Heb 83
Mean:				6.86±0.03	
Al II					
No. of lines=8					
4663.05	10.550	-0.301	326	5.63	Wiese 66
8640.70	11.770	0.100	393	5.83	Kur 75
6226.18	13.010	0.049	230	5.96	Kur 75
6231.78	13.020	0.400	345	6.23	Kur 75
6243.36	13.020	0.669	400	6.26	Kur 75
6823.48	13.020	-0.140	218	6.09	Kur 75
6837.14	13.020	0.079	262	6.10	Kur 75
5593.23	13.200	0.410	248	5.76	Kur 75
Mean:				6.0±0.2	
Al III					
No. of lines=2					
5696.47	15.642	0.236	172	6.68	Jeffery
5722.65	15.642	-0.069	118	6.57	Jeffery
Mean:				6.63±0.07	
Si II					
No. of lines=5					
3853.66	6.858	-1.377	420	6.43	Duf 83
3862.60	6.858	-0.682	520	6.41	Duf 83

Table 4.8 (continued)

Lines used to derive elemental abundances for BD -1° 3438

$\lambda(\text{\AA})$	$\chi(\text{eV})$	log gf	W(m\AA)	Abundance ^a	Reference ^b
4130.89	9.839	0.545	605	6.52	Bec 90
5055.98	10.070	0.517	725	6.62	Bec 90
6829.82	12.880	-0.270	175	6.74	Kur 75
Mean:				6.54±0.14	
Si III					
No. of lines=1					
4567.87	19.018	0.06	100	7.21	Bec 90
Mean:				7.21±0.00	
P II					
No. of lines=3					
5499.72	10.799	-0.717	82	5.03	Hib 88
6034.01	10.690	-0.140	166	5.39	Kur 75
6165.56	10.760	-0.400	126	5.46	Kur 75
Mean:				5.3±0.23	
S II					
No. of lines=18					
3923.40	16.130	-0.328	77	6.87	Jeffery
3993.52	14.230	-0.810	135	6.98	Kur 75
4153.10	25.831	0.681	183	6.52	Jeffery
4230.98	17.370	-0.022	45	6.78	Jeffery
4483.42	15.830	-0.429	117	7.20	Wiese 69
4486.66	15.800	-0.400	50	6.60	Wiese 69
4524.95	15.000	0.061	285	7.15	Jeffery
4716.23	13.560	-0.520	177	6.73	Wiese 69
4792.02	16.070	-0.120	98	6.88	Wiese 69
4815.52	13.610	-0.050	257	6.79	Wiese 69
4917.20	14.003	-0.400	172	6.78	Jeffery
4925.32	13.530	-0.471	259	7.18	Luck
5428.64	13.530	-0.010	267	6.81	Kur 75
5473.61	13.584	-0.122	250	6.84	Jeffery
5509.71	13.617	-0.117	296	7.13	Jeffery
5556.01	13.560	-0.570	126	6.51	Kur 75
5606.11	13.733	0.041	315	6.78	Jeffery
5664.73	13.660	-0.301	198	6.75	Jeffery
Mean:				6.85±0.2	
Ca II					
No. of lines=2					
8542.08	1.69	-0.492	695	5.57	Kur 75
8662.14	1.69	-0.754	632	5.43	Kur 75
Mean:				5.5±0.1	

Table 4.8 (continued)

Lines used to derive elemental abundances for BD -1° 3438

$\lambda(\text{\AA})$	$\chi(\text{eV})$	$\log gf$	$W(\text{m\AA})$	Abundance ^a	Reference ^b
Ti II					
No. of lines=18					
3913.46	1.110	-0.312	290	4.10	Heb 83
4163.64	2.580	-0.300	233	4.50	Heb 83
4171.90	2.590	-0.370	217	4.50	Heb 83
4290.22	1.160	-1.292	206	4.65	Heb 83
4301.93	1.160	-1.237	140	4.30	Heb 83
4312.86	1.180	-1.553	220	4.99	Heb 83
4314.98	1.160	-1.523	227	4.97	Heb 83
4399.77	1.230	-1.553	173	4.80	Heb 83
4421.95	2.050	-1.770	78	4.92	Luck
4450.49	1.080	-1.921	149	4.96	Heb 83
4501.27	1.110	-0.762	236	4.21	Heb 83
4545.14	1.130	-1.824	78	4.49	Luck
4563.76	1.220	-0.959	233	4.44	Luck
4571.97	1.560	-0.530	246	4.24	Heb 83
4779.99	2.040	-1.367	134	4.80	Heb 83
4805.10	2.061	-1.102	215	4.90	Luck
4874.02	3.080	-0.790	91	4.49	Luck
5072.30	3.110	-0.752	100	4.52	Luck
Mean:				4.6±0.28	
Cr II					
No. of lines=23					
4812.35	3.850	-1.796	174	4.96	Luck
4824.13	3.850	-1.222	290	4.87	Luck
4848.24	3.850	-1.143	249	4.61	Luck
4864.32	3.840	-1.377	217	4.70	Kur 75
4876.41	3.840	-1.456	260	4.97	Luck
5249.40	3.740	-2.699	98	5.33	Luck
4275.57	3.840	-1.721	172	4.90	Kur 75
4284.21	3.840	-1.854	143	4.93	Kur 75
4555.02	4.060	-1.377	218	4.85	Luck
4558.66	4.060	-0.310	378	4.41	Luck
4565.78	4.020	-2.097	142	5.23	Luck
4588.22	4.050	-0.650	324	4.61	Heb 83
4592.09	4.060	-1.222	191	4.58	Luck
4616.64	4.050	-1.292	204	4.69	Luck
4618.83	4.060	-0.979	287	4.75	Heb 83
5478.35	4.160	-1.921	191	5.25	Kur 75
3865.59	5.300	-0.660	190	4.46	Kur 75
3979.51	5.650	-0.733	187	4.92	Kur 75
4098.44	5.310	-1.469	80	4.92	Kur 75
4038.03	6.460	-0.558	133	4.87	Kur 75

Table 4.8 (continued)

Lines used to derive elemental abundances for BD -1° 3438

$\lambda(\text{\AA})$	$\chi(\text{eV})$	$\log gf$	$W(\text{m\AA})$	Abundance ^a	Reference ^b
4070.90	6.460	-0.752	188	5.33	Kur 75
4256.16	6.460	-1.398	76	5.36	Kur 75
5620.63	6.460	-1.143	86	5.11	Kur 75
Mean:				4.9±0.27	
Mn II					
No. of lines=4					
4343.98	5.370	-1.097	246	5.19	Kur 75
4755.72	5.370	-1.244	178	5.00	Kur 75
4764.70	5.370	-1.357	160	5.03	Kur 75
6122.43	10.140	0.950	198	5.19	Kur 75
Mean:				5.10±0.1	
Fe I					
No. of lines=4					
3840.44	0.990	-0.506	63	7.02	Heb 83
3859.91	0.000	-0.710	120	7.10	Heb 83
3886.28	0.050	-1.076	60	7.10	Heb 83
4071.74	1.600	-0.020	110	7.12	Heb 83
Mean:				7.08±0.04	
Fe II					
No. of lines=45					
3914.48	1.660	-4.05	245	6.86	Luck
3930.31	1.690	-4.03	240	6.83	Kur 75
3938.28	1.660	-3.89	175	6.39	Luck
3945.21	1.690	-4.25	185	6.80	Kur 75
3896.11	2.630	-4.04	125	6.79	Kur 75
3974.16	2.690	-3.51	182	6.55	Luck
4119.53	2.530	-4.17	122	6.83	Heb 83
4122.64	2.570	-3.38	258	6.68	Heb 83
4124.79	2.530	-4.20	131	6.90	Heb 83
4177.70	2.530	-3.75	240	6.94	Heb 83
4273.32	2.690	-3.34	224	6.53	Heb 83
4303.17	2.690	-2.523	352	6.30	Kro 87
4314.29	2.660	-3.000	280	6.35	Heb 83
4369.40	2.770	-3.67	223	6.88	Luck
4413.60	2.660	-3.91	188	6.91	Heb 83
4416.82	2.770	-2.523	365	6.51	Heb 83
4489.16	2.820	-3.53	265	6.94	Heb 83
4515.34	2.830	-2.398	428	6.71	Kro 87
4520.23	2.790	-2.523	391	6.65	Heb 83
4522.63	2.830	-2.046	439	6.40	Kro 87
4582.84	2.830	-3.000	286	6.60	Kro 87
4648.93	2.570	-4.39	129	7.05	Kur 75
4666.75	2.820	-3.33	252	6.66	Heb 83

Table 4.8 (continued)

Lines used to derive elemental abundances for *BD -1° 3438*

$\lambda(\text{\AA})$	$\chi(\text{eV})$	$\log gf$	$W(\text{m\AA})$	Abundance ^a	Reference ^b
4871.27	2.690	-4.05	121	6.73	Kur 75
4993.35	2.790	-3.65	252	6.94	Luck
5254.92	3.220	-3.000	208	6.52	Luck
5362.86	3.190	-2.699	323	6.51	Kur 75
5534.86	3.230	-3.000	351	6.84	Luck
6147.73	3.870	-2.699	284	6.62	Kur 75
3845.18	4.460	-2.222	274	6.58	Heb 83
4138.21	4.710	-3.000	164	7.11	Kur 75
4048.83	5.540	-1.921	247	6.65	Heb 83
4070.03	5.890	-4.33	135	7.06	Kur 75
4111.90	5.930	-2.398	113	6.72	Heb 83
4446.24	5.930	-2.398	74	6.44	Kur 75
4625.91	5.930	-2.155	194	6.75	Kur 75
4953.97	5.550	-2.699	164	7.04	Kur 75
5272.41	5.930	-2.046	232	6.78	Luck
6179.37	5.540	-2.699	167	7.06	Luck
6175.15	6.200	-2.000	239	6.87	Kur 75
4354.35	7.620	-1.398	170	6.75	Kur 75
4449.66	7.890	-1.585	87	6.62	Kur 75
4598.53	7.770	-1.495	165	6.88	Heb 83
5247.95	10.531	0.629	316	6.80	Luck
5961.71	10.678	0.689	294	6.69	Luck
Mean:				6.73±0.2	
Sr II					
No. of lines=2					
4077.72	0.000	0.149	244	2.78	Luck
4215.54	0.000	-0.160	170	2.74	Luck
Mean:				2.76±0.03	
Ba II					
No. of lines=1					
4554.00	0.000	0.12	50	2.20	Luck

^a Normalized such that $\log \sum \mu_i n_i = 12.15$

^b Sources of gf-values

^c Spectrum synthesis

References:

- | | |
|-----------|------------------------------------------|
| Bec 89 | Becker & Butler, 1989 |
| Bec 90 | Becker & Butler, 1990 |
| Dahari 84 | Dahari & Osterbrock, 1984 |
| Duf 83 | Dufton et al., 1983 |
| Heb 83 | Heber, 1983 |
| Hib 88 | Hibbert, 1988 |
| Jeffery | C. Simon Jeffery (private communication) |
| Kro 87 | Kroll & Kock, 1987 |
| Kur 75 | Kurucz & Petryemann, 1975 |
| Luck | R. E. Luck (private communication) |
| Wiese 66 | Wiese, Smith & Glennon, 1966 |
| Wiese 69 | Wiese, Smith & Miles, 1969 |
| Yan 87 | Yan, Taylor & Seaton, 1987 |

Table 4.9

Lines used to derive elemental abundances for LS IV -1° 002

$\lambda(\text{\AA})$	$\chi(\text{eV})$	log gf	W(m \AA)	Abundance ^a	Reference ^b
H I					
No. of lines=1					
6562.80	10.15	0.71	500	7.05	Luck
He I					
No. of lines=1					
5047.74	14.06	-0.62	Synth ^c	11.54	Jeffery
C I					
No. of lines=15					
4063.57	7.450	-3.78	73	9.61	Heb 83
4766.62	7.450	-2.398	64	9.20	Heb 83
4770.00	7.450	-2.301	81	9.21	Heb 83
4771.72	7.460	-1.699	184	9.22	Heb 83
4775.87	7.460	-2.222	92	9.21	Heb 83
4817.33	7.460	-2.523	55	9.25	Heb 83
4826.73	7.460	-2.301	57	9.05	Heb 83
6010.67	8.640	-2.000	67	9.36	Kur 75
6013.21	8.650	-1.469	163	9.42	Kur 75
6014.84	8.640	-1.721	114	9.38	Kur 75
6587.75	8.500	-1.337	199	9.44	Heb 83
7108.93	8.640	-1.602	111	9.27	Luck
7116.90	8.650	-1.081	250	9.51	Luck
7476.17	8.770	-1.638	101	9.32	Luck
5380.24	7.680	-2.046	86	9.09	Kur 75
Mean:				9.30±0.15	
C II					
No. of lines=11					
3918.98	16.333	-0.545	405	8.94	Yan 87
3920.69	16.334	-0.244	450	8.88	Yan 87
4317.26	23.120	-0.009	107	9.36	Yan 87
4318.60	23.120	-0.409	67	9.40	Yan 87
4372.35	24.650	0.057	105	9.37	Yan 87
4374.27	24.650	0.634	120	9.11	Yan 87
4737.97	13.720	-3.000	122	8.76	Dahari 84
4744.77	13.720	-2.523	156	8.65	Dahari 84
4802.70	21.000	-0.411	145	9.2	Yan 87
6098.51	22.570	0.243	70	8.94	Dahari 84
Mean:				9.06±0.26	

Table 4.9 (continued)

Lines used to derive elemental abundances for LS IV -1° 002

$\lambda(\text{\AA})$	$\chi(\text{eV})$	log gf	W(m\AA)	Abundance ^a	Reference ^b
N I					
No. of lines=6					
4099.94	10.630	-1.244	42	7.99	Kur 75
4151.46	10.290	-1.886	25	8.23	Luck
4935.03	10.640	-1.959	13	8.14	Luck
6644.96	11.710	-0.910	56	8.27	Luck
7423.63	10.280	-0.611	199	8.18	Luck
7442.28	10.290	-0.311	283	8.23	Luck
Mean:				8.17±0.1	
N II					
No. of lines=14					
3955.85	18.391	-1.149	62	8.50	Luck
3995.00	18.498	0.225	190	8.06	Bec 89
4041.31	23.128	0.830	42	7.94	Bec 89
4447.03	20.411	0.238	82	8.12	Bec 89
4607.16	18.464	-0.483	104	8.33	Bec 89
4613.87	18.468	-0.607	80	8.27	Bec 89
4630.54	18.484	0.093	187	8.28	Bec 89
4643.09	18.484	-0.385	125	8.38	Bec 89
5045.09	18.460	-0.389	132	8.48	Bec 89
5666.64	18.461	0.009	173	8.41	Wiese 66
5676.02	18.462	-0.340	144	8.59	Jeffery
5679.56	18.478	0.279	249	8.57	Wiese 66
5686.21	18.461	-0.474	80	8.29	Wiese 66
5710.76	18.483	-0.470	115	8.55	Jeffery
Mean:				8.34±0.2	
O I					
No. of lines=3					
5330.66	10.690	-0.971	204	8.75	Luck
6158.19	10.690	-0.332	324	8.68	Heb 83
6653.83	14.470	-0.400	55	8.96	Luck
Mean:				8.80±0.15	
O II					
No. of lines=5					
4345.56	22.973	-0.344	45	8.87	Bec 88
4349.43	22.993	0.057	89	8.96	Bec 88
4641.82	22.973	0.093	87	8.99	Bec 88
4649.14	22.993	0.340	111	8.95	Bec 88
4661.63	22.973	-0.259	45	8.90	Bec 88
Mean:				8.93±0.05	

Table 4.9 (continued)

Lines used to derive elemental abundances for *LS IV -1° 002*

$\lambda(\text{\AA})$	$\chi(\text{eV})$	log gf	W(m \AA)	Abundance ^a	Reference ^b
Ne I					
No. of lines=9					
5748.29	18.480	-1.018	138	8.79	Luck
5764.41	18.480	-0.314	271	8.75	Luck
5852.48	16.780	-0.445	446	9.04	Luck
5881.90	16.550	-0.701	423	9.07	Wiese 66
5944.83	16.550	-0.556	450	9.08	Wiese 66
5965.47	18.650	-1.125	167	9.13	Luck
6030.00	16.600	-0.987	326	8.88	Wiese 66
6217.28	16.550	-0.870	351	8.88	Wiese 66
6598.95	16.780	-0.187	490	9.03	Luck
Mean:				8.96±0.13	
Na I					
No. of lines=1					
8194.83	0.000	0.529	200	6.45	Luck
Mg II					
No. of lines=6					
3848.25	8.830	-1.585	120	6.97	Heb 83
4390.60	9.960	-0.500	180	6.62	Heb 83
4428.00	9.950	-1.201	92	6.87	Heb 83
4434.00	9.960	-0.900	138	6.82	Heb 83
4481.13	8.863	0.568	718	6.95	Wiese 66
4851.10	11.580	-0.682	144	7.32	Kur 75
Mean:				6.90±0.23	
Al II					
No. of lines=8					
4663.05	10.550	-0.301	190	5.45	Wiese 66
8640.70	11.770	0.100	157	5.24	Kur 75
6226.18	13.010	0.049	76	5.58	Kur 75
6231.78	13.020	0.400	142	5.61	Kur 75
6243.36	13.020	0.669	160	5.43	Kur 75
6823.48	13.020	-0.140	45	5.49	Kur 75
6837.14	13.020	0.079	76	5.55	Kur 75
5593.23	13.200	0.410	56	5.12	Kur 75
Mean:				5.43±0.17	
Al III					
No. of lines=4					
4528.91	17.818	-0.294	103	6.18	TOPbase
5696.47	15.642	0.236	185	6.48	Jeffery
5722.65	15.642	-0.069	131	6.48	Jeffery
4512.54	17.808	0.405	51	6.07	TOPbase
Mean:				6.30±0.2	

Table 4.9 (continued)

Lines used to derive elemental abundances for LS IV -1° 002

$\lambda(\text{\AA})$	$\chi(\text{eV})$	$\log gf$	$W(\text{m\AA})$	Abundance ^a	Reference ^b
Si II					
No. of lines=3					
3853.66	6.858	-1.377	232	5.92	Duf 83
4130.89	9.839	0.545	381	5.95	Bec 90
5055.98	10.070	0.517	380	5.77	Bec 90
Mean:					5.88±0.09
Si III					
No. of lines=2					
4567.82	19.018	0.061	137	7.27	Bec 90
4574.76	19.018	-0.416	78	7.31	Bec 90
Mean:					7.3±0.03
P II					
No. of lines=3					
5425.93	10.799	0.241	113	5.01	Hib 88
6034.01	10.690	-0.140	86	5.19	Kur 75
6165.56	10.760	-0.400	54	5.22	Kur 75
Mean:					5.14±0.11
S II					
No. of lines=35					
3993.52	14.230	-0.810	75	6.71	Kur 75
3998.79	16.180	0.049	59	6.48	Wiese 69
4032.81	16.180	0.241	100	6.60	Wiese 69
4153.10	15.880	0.681	165	6.41	Jeffery
4217.23	15.880	-0.150	46	6.44	Wiese 69
4230.98	17.370	-0.022	50	6.94	Jeffery
4294.43	16.070	0.560	165	6.61	Wiese 69
4483.42	15.830	-0.429	81	7.02	Wiese 69
4486.66	15.800	-0.400	32	6.50	Wiese 69
4524.95	15.000	0.061	174	6.64	Jeffery
4656.74	13.530	-0.810	114	6.70	Wiese 69
4716.23	13.560	-0.520	175	6.74	Wiese 69
4792.02	16.070	-0.120	63	6.68	Wiese 69
4815.52	13.610	-0.050	267	6.74	Wiese 69
4824.07	16.200	0.021	105	6.90	Wiese 69
4885.63	13.940	-0.642	118	6.73	Kur 75
4917.20	14.003	-0.400	175	6.81	Jeffery
4925.32	13.530	-0.471	248	7.04	Luck
4942.47	13.530	-0.963	115	6.88	Luck
4991.94	13.613	-0.650	233	7.18	Wiese 66
5009.54	13.613	-0.284	240	6.85	Wiese 66
5014.03	14.063	0.033	244	6.74	Wiese 66
5027.19	13.040	-0.721	157	6.64	Luck

Table 4.9 (continued)

Lines used to derive elemental abundances for LS IV -1° 002

$\lambda(\text{\AA})$	$\chi(\text{eV})$	log gf	$W(\text{m\AA})$	Abundance ^a	Reference ^b
5103.30	13.668	-0.108	188	6.45	Wiese 66
5320.70	15.000	0.459	249	6.75	Luck
5432.77	13.560	0.310	369	6.88	Kur 75
5453.81	13.610	0.560	451	7.08	Kur 75
5473.61	13.584	-0.122	278	6.87	Jeffery
5509.71	13.617	-0.117	270	6.84	Jeffery
5556.01	13.560	-0.570	109	6.47	Kur 75
5606.11	13.729	0.041	283	6.44	Wiese 66
5616.63	13.600	-0.471	110	6.40	Kur 75
5659.95	13.620	-0.070	219	6.56	Kur 75
5664.73	13.660	-0.301	174	6.59	Jeffery
5819.22	14.01	-0.759	113	6.88	Kur 75
Mean:				6.72±0.2	
Ca I					
No. of lines=2					
8542.08	0.000	-0.492	510	5.80	Kur 75
8662.14	0.000	-0.754	450	5.72	Kur 75
Mean:				5.76±0.05	
Ti II					
No. of lines=5					
3900.55	1.130	-0.631	158	4.82	Heb 83
3913.46	1.110	-0.740	97	4.61	Heb 83
4443.80	1.080	-1.237	69	4.87	Heb 83
4563.76	1.220	-0.959	55	4.53	Luck
4571.97	1.560	-0.740	93	4.74	Heb 83
Mean:				4.70±0.14	
Fe II					
No. of lines=22					
4048.83	5.540	-1.921	45	6.39	Heb 83
4122.64	2.570	-3.000	50	6.48	Heb 83
4296.57	2.690	-3.000	85	6.43	Heb 83
4303.17	2.690	-2.523	153	6.44	Kro 87
4351.76	2.690	-2.097	217	6.39	Kro 87
4416.82	2.770	-2.301	150	6.30	Heb 83
4508.28	2.840	-2.301	164	6.37	Heb 83
4515.34	2.830	-2.398	121	6.23	Kro 87
4520.23	2.790	-2.523	115	6.33	Heb 83
4522.63	2.830	-2.046	190	6.22	Kro 87
4555.89	2.820	-2.301	165	6.34	Kro 87
4576.33	2.830	-3.000	84	6.49	Heb 83
4583.83	2.790	-1.824	248	6.12	Luck
4635.33	5.930	-1.409	77	6.32	Heb 83
4731.44	2.880	-3.000	44	6.20	Heb 83

Table 4.9 (continued)

Lines used to derive elemental abundances for LS IV -1° 002

$\lambda(\text{\AA})$	$\chi(\text{eV})$	log gf	W(m\AA)	Abundance ^a	Reference ^b
5081.92	7.910	-0.585	56	6.16	Kur 75
5169.03	2.891	-0.870	364	6.18	Luck
5197.56	3.220	-2.097	121	6.05	Luck
5234.62	3.221	-2.046	200	6.42	Luck
5247.95	10.531	0.629	100	6.42	Luck
5275.99	3.190	-1.959	191	6.25	Kur 75
5961.71	10.678	0.689	115	6.52	Luck
Mean:				6.30±0.12	
Fe III					
No. of lines=2					
4419.59	8.210	-1.699	103	5.97	Jeffery
4395.78	8.220	-2.155	74	6.28	Jeffery
Mean:				6.13±0.22	
Sr II					
No. of lines=2					
4077.72	0.000	0.149	64	2.81	Luck
4215.54	0.000	-0.160	20	2.54	Luck
Mean:				2.675±0.2	
Ba II					
No. of lines=1					
4554.04	0.000	0.12	7.0	2.22	Luck

^a Normalized such that $\log \sum \mu_i n_i = 12.15$

^b Sources of gf-values

^c Spectrum synthesis

References:

Bec 88	Becker & Butler, 1988	Luck	R. E. Luck
Bec 89	Becker & Butler, 1989		(private communication)
Bec 90	Becker & Butler, 1990	TOPbase	Canuto & Mendoza, 1992
Dahari 84	Dahari & Osterbrock, 1984	Wiese 66	Wiese, Smith & Glennon, 1966
Duf 83	Dufton et al., 1983	Wiese 69	Wiese, Smith & Miles, 1969
Heb 83	Heber, 1983	Yan 87	Yan, Taylor & Seaton, 1987
Hib 88	Hibbert, 1988		
Jeffery	C. Simon Jeffery		
	(private communication)		
Kro 87	Kroll & Kock, 1987		
Kur 75	Kurucz & Petryemann, 1975		

Chapter 5

Emission–line spectrum of MV Sgr

5.1 Description of the spectrum

The spectrum of MV Sgr is a mix of absorption and emission lines. The absorption line component which we attribute to the stellar photosphere is similar to that described by Jeffery et al (1988). Absorption lines are mainly due to Al III, Si III, C II (higher multiplets), N II, O II, and possibly Ne I. Permitted or forbidden emission lines from the following atoms and ions are readily identifiable: H, He I, Li I, C I, C II, [N II], [O I], Ne I, Na I, Mg I, Si II, Ti II, Fe I, Fe II, and Ni I. Table 5.1 provides a list of the identified emission lines. Diffuse interstellar absorption bands (Herbig 1975b) are seen in the spectrum. The bands at $\lambda\lambda$ 5487, 5780, 5797, 6011, 6196, 6203, 6269, 6376, 6379, and 6613 are clearly present.

Sample portions of the spectrum are provided in Figures 5.1 and 5.2 to show the fascinating mix of absorption and emission profiles. Figure 5.1 shows an emission line attributed to the Li I 6707 Å doublet and also Ca I 6717 Å along with the absorption line of O II 6721 Å. We believe this is the first astrophysical detection of the Li I resonance feature at 6707 Å in emission. Figure 5.2 shows C II ($\lambda\lambda$ 6780, 6784, 6787, 6791, 6798, 6800 and 6812) in absorption and Ni I 6767 Å in emission. Selected emission line profiles are displayed in Figures 5.3, 5.4, 5.5 and 5.6. Figure 5.3 shows the emission line of H α , a strong Fe II line, a weak C I line and the prominent Si II at 6347 Å. Figure 5.4 shows the [N II] and [O I] profiles. Figure 5.5 shows profile of Li I with those of the Ca I] 6572 Å, Fe I 5501 Å, and Ni I 6767 Å.

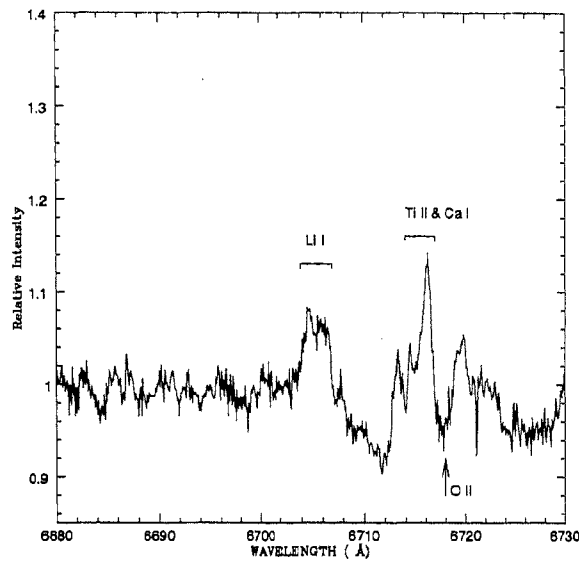


Figure 5.1: Spectrum of MV Sgr showing the Li I 6707 Å , Ca I and Ti II lines in emission and O II 6721 Å line in absorption.

Profiles of four Fe II lines from the multiplet RMT46 are shown in Figure 5.6. The Fe II emission lines clearly show two components with a minimum centred at about the stellar (photospheric) velocity (see below). Weaker lines (Figure 5.5) tend to show flat-topped profiles with a width similar to that of the stronger and double-peaked lines. A central minimum may be present but higher signal-to-noise spectra are needed to derive definitive profiles for these weaker lines.

5.2 Radial velocities

The absorption lines of Al III, Si III, N II, and C II give a velocity of $-93 \pm 4 \text{ km s}^{-1}$ which we refer to as the stellar velocity. This value agrees well with the earlier measurements of -91 ± 7 and $-96 \pm 4 \text{ km s}^{-1}$ by Jeffery et al. (1988) and one of $-95 \pm 8 \text{ km s}^{-1}$ by Rao et. al (1990). If, as is likely, MV Sgr experiences atmospheric pulsations, their amplitude would seem to be just a few kilometres per second.

The diffuse interstellar bands at 5796, 6195, 6202 and 6613 give a mean radial velocity of -8 km s^{-1} ; the rest wavelengths are taken from Herbig (1975b). An absorption component at this velocity is seen in the Na I D lines. Our spectra show that this Na I D component consists of at least 2 unresolved components. There is another absorption component of

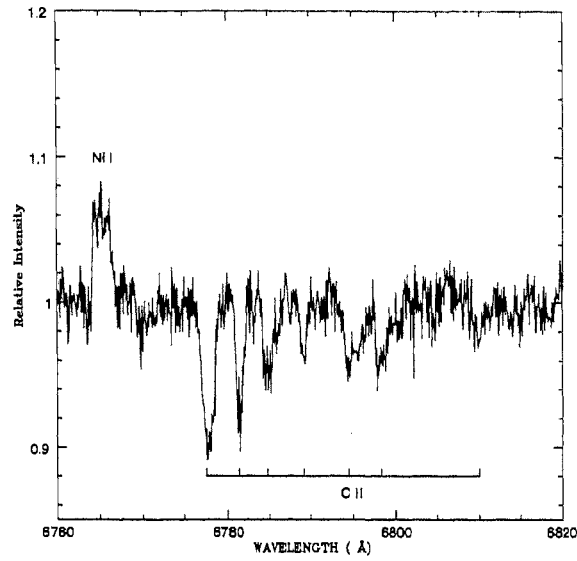


Figure 5.2: Spectrum of MV Sgr showing the C II (RMT14) absorption lines and Ni I $\lambda 6767$ emission.

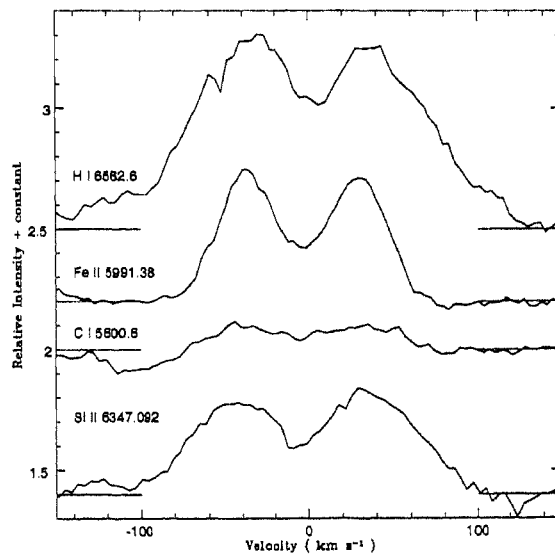


Figure 5.3: Comparison of emission lines of $H\alpha$, Fe II $\lambda 5991$ C I $\lambda 5800$ and Si II $\lambda 6347$. The zero of the velocity scale refers to the photospheric velocity. The position of the mean continuum for each spectrum segment is indicated by the line marked.

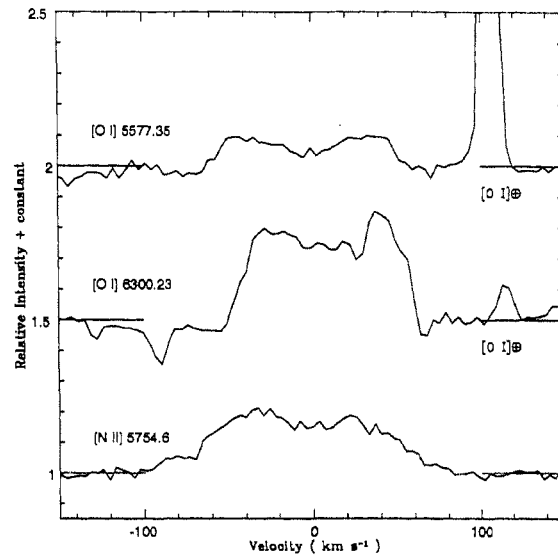


Figure 5.4: Comparison of forbidden emission lines of O I and N II. The abscissa is similar to Fig. 5.3. The mean continuum for each spectrum segment is indicated by the line marked.

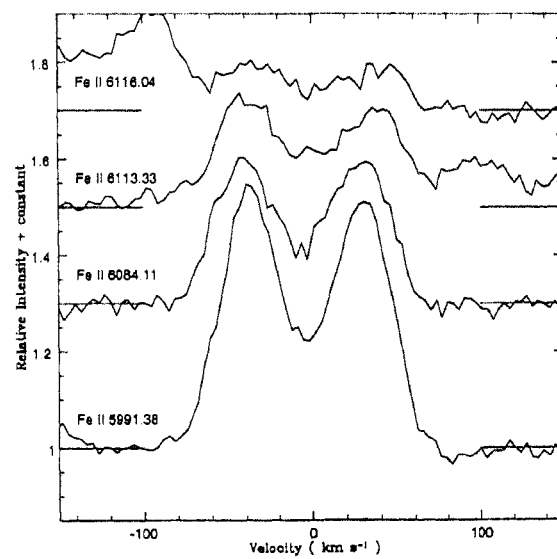


Figure 5.5: Comparison of Fe I emission lines from RMT46. The velocity scale is similar to Fig. 5.4. The mean continuum for each spectrum segment is marked as in Fig. 5.3.

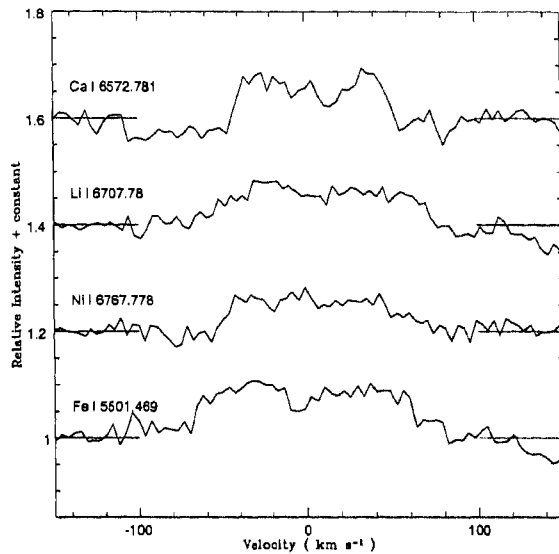


Figure 5.6: Comparison of Li I 6707 Å emission line profile and other low excitation weak permitted lines. The velocity scale is similar to Fig. 5.4. The mean continuum for each spectrum segment is marked as in Fig. 5.3.

the Na I D lines at a radial velocity of 29 km s^{-1} . Jeffery et al. (1988) find absorption components for Ca II H and K lines at 20 km s^{-1} which they attribute to the interstellar medium. This velocity is consistent with a cloud at approx 4 kpc.

The emission lines are centred on the stellar velocity. Lines with a clear central minimum between the two emission peaks have their central minimum at $-92 \pm 5 \text{ km s}^{-1}$ (from 20 lines). In cases where the central minimum is not obvious, the centre of the line coincides with the stellar velocity. The velocity separation between the blue and red peaks is $68 \pm 4 \text{ km s}^{-1}$ from 15 Fe II lines. This splitting agrees with the estimate of 68 km s^{-1} reported by Jeffery et al. (1988). It would seem that the emission line spectrum has not changed significantly.

5.3 Emission lines

We have assumed that the split lines are formed from two components, red-shifted and blue-shifted, which have been measured independently where possible. The measured equivalent widths of the emission lines (both components) have been converted to line

fluxes using the UBVRI colors from Landolt (1979) to define the continuum flux. A reddening correction of $E(B-V) = 0.45$ is adopted from Heber and Schönberner (1981) who compared the observed and predicted colours. Drilling et al. (1984) give $E(B-V) = 0.38$ based on the strength of the 2200 Å interstellar bump. Our principal conclusions are unaffected by adoption of this slightly lower reddening. Seaton's (1979) reddening curve is used to correct the observed fluxes to their unreddened values.

5.3.1 Forbidden lines

The [O I] lines at 5577, 6300, and 6363 Å and [N II] 5755 Å lines are clearly present. Their profiles (Figure 5.4) are almost flat-topped but a central minimum is probably present. Since these lines are most probably optically thin, the profiles reflect the velocity distribution of the emitting gas. These forbidden lines are diagnostics of this gas. In the following analysis we consider the entire line profile and do not attempt to treat the blue and red components separately. From Table 5.1 we can say that the blue and the red components of the emission lines are symmetric. [O I] and [N II] emission indicates the presence of a nebula around the star. The overall symmetry and similarity of the profiles suggest that the physical conditions of the 'blue' and 'red' gas are not very different.

In considering the [O I] lines, we assume the 6363 Å line to have its predicted flux which is one-third the observed flux of the stronger 6300 Å line; the 6363 Å line is present but difficult to measure accurately. Then, the flux ratio involving the [O I] lines is given by

$$F[\text{OI}] = \frac{F(6300) + F(6363)}{F(5577)} = 1.9 \pm 0.3.$$

Here $F(\lambda) = W(\lambda) F_c(\lambda)$, with $F(\lambda)$ the flux in the line, $W(\lambda)$ its equivalent width and $F_c(\lambda)$ the continuum flux corrected for interstellar reddening.

The [N II] lines have an analogous flux ratio involving the 5755 Å line, which is strong and readily measured (Figure 5.4), and the line pair 6548 and 6583 Å. Unfortunately, the latter pair are blended with other lines: 6548 Å with a Fe I line and 6583 Å with a C II line. A rough estimate of the flux in the 6548 and 6583 lines is made in the following way. The redward component of the 6548 Å line can be seen and measured. We assume that the blue component has the same strength, a symmetry clearly satisfied by the majority of the emission lines (see Table 5.1. and Figures 5.4, 5.5, and 5.6). Since the relative strength of the 6583 Å to the 6548 Å line is fixed by their Einstein A coefficients, the

total flux in the pair of lines is obtained by this procedure. The flux ratio involving the [N II] lines is given by

$$F[\text{N II}] = \frac{F(6548)+F(6583)}{F(5755)} = 0.45 \pm 0.15.$$

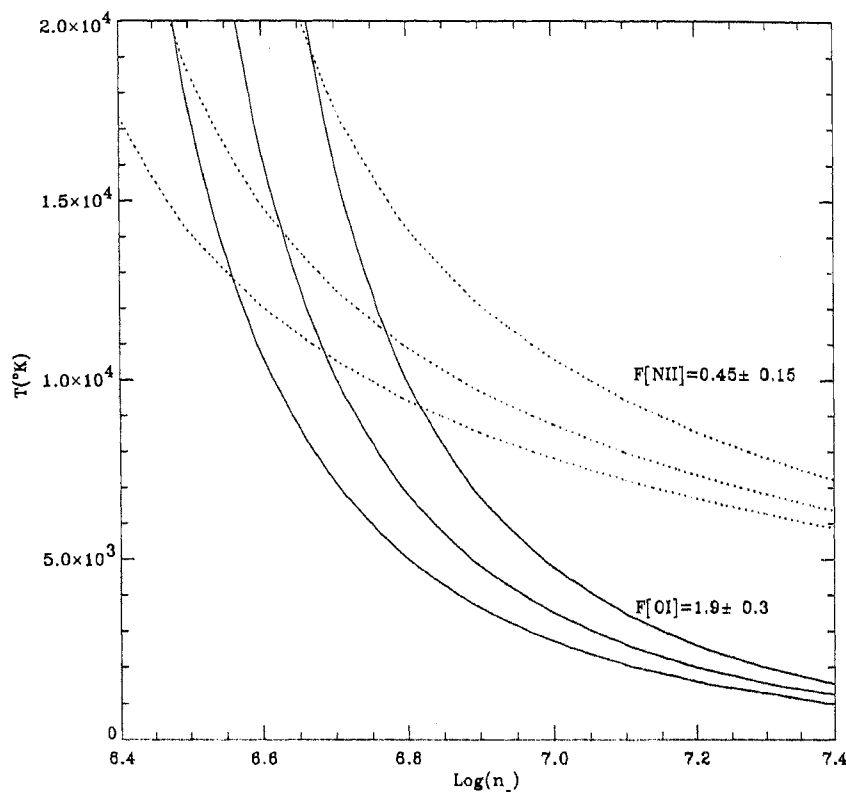


Figure 5.7: The $\log(n_e) - T$ plane showing the loci corresponding to the flux ratios $F[\text{N II}]$ and $F[\text{O I}]$ - see text. A combination $T \sim 1.5 \times 10^4$ K and $\log(n_e) \sim 6.6$ satisfies the two observed ratios.

Osterbrock (1989) provides predictions of $F(\text{N II})$ as a function of the temperature (T) and electron density (n_e) of the emitting gas. A solution for the population of the various levels of [O I] and the emitted relative line strengths by them, was formulated along the lines of the discussion in Osterbrock (1989). The numerical values of the collision strengths and transition probabilities for [O I] were taken from Mendoza (1983). Figure 5.7 represents the $\log(n_e) - T$ plane for flux ratios of [O I] (solid lines) and [N II] (broken lines). The common region represents the range of solutions as $n_e = (3 - 7) \times 10^6 \text{ cm}^{-3}$ for $T = 8500 - 20000$ K.

Table 5.1
Emission lines

λ	Ident.	Equiv.Width ^a		Flux ^b	Rad. vel.	Base width
		(mÅ)				
		blue	red			
6562.83	HI	1689	1612	3.5	-94.0	214.0
5875.63	HeI			5.5	-95.0	346.0
6678.15	HeI			3.3	-100.0	366.0
6707.78	LiI	195		3.3		139.0
5969.33	CI	65	35	5.1	-90.0	118.0
5805.19	CI	59	64	5.8	-90.0	130.0
5800.59	CI	100	109	5.8	-95.0	142.0
6855.55	CI	52	64	3.1	-87.0	134.0
6828.12	CI	237	246	3.1	-91.0	137.0
6655.51	CI	131	79	3.3	-90.0	149.0
6016.45	CI	54	37	4.9	-93.0	129.0
6001.13	CI	49	32	5.0	-91.0	136.0
6013.22	CI	52	82	4.9	-89.0	132.0
6663.04	CI	54	83	3.3	-99.0	145.0
6688.79	CI	43	42	3.3	-91.0	131.0
6671.84	CI			3.3	-99.0	212.0
6662.73	CI	47	75	3.3	-85.0	141.0
6100.46	CI	71	48	4.6	-94.0	128.0
6583.45	[NII]			3.5		
5754.80	[NII]	316	232	6.0	-106.0	140.0
6548.08	[NII]		40	3.5		
6300.23	[OI]	312	312	4.1	-81.0	115.0
6363.88	[OI]			4.0	-102.0	125.0
5577.35	[OI]	109	99	7.0	-89.0	125.0
6163.59	NeI			4.4		
6506.53	NeI			3.6		

^a The numbers refer to the blue and red components.

^b Continuum Flux- Units: $W \text{ cm}^{-2} \mu\text{m}^{-1} \times 10^{-17}$

λ	Ident.	Equiv.Width ^a		Flux ^b	Rad. vel.	Base width
		(mÅ)				
		blue	red			
6074.34	NeI			4.7		
6030.00	NeI			4.9		
6334.43	NeI			4.0		
6143.06	NeI			4.5		
6402.25	NeI			3.8		
6351.86	NeI			3.9		
5881.89	NeI			5.4		
5889.95	NaI			5.4		
5895.92	NaI			5.4		
5528.41	MgI	93	95	7.2	-89.6	135.0
5978.97	SiII	184	172	5.0	-94.0	190.0
6347.09	SiII	532	541	3.9	-103.0	195.0
6572.78	CaI		177	3.5		102.0
6122.23	CaI		122	4.6		144.0
6439.07	CaI		176	3.7		104.0
5956.70	FeI	180	225	5.1	-73.0	150.0
5501.47	FeI	92	87	7.4	-77.0	130.0
5497.52	FeI	59	38	7.4	-98.0	95.0
5506.78	FeI	35	38	7.4	-80.0	100.0
6318.02	FeI	484	500	4.0	-100.0	170.0
6191.56	FeI	90	70	4.4	-113.0	125.0
6270.24	FeI	195	130	4.1	-103.0	135.0
5615.65	FeI	73	54	6.7	-97.0	105.0
5586.76	FeI	65	70	6.9	-80.0	115.0
5624.55	FeI	37	26	6.7	-100.0	130.0

^a The numbers refer to the blue and red components.

^b Continuum Flux- Units: $W \text{ cm}^{-2} \mu\text{m}^{-1} \times 10^{-17}$

λ	Ident.	Equiv.Width ^a		Flux ^b	Rad. vel.	Base width
		(mÅ)				
		blue	red			
6432.65	FeII	637	576	3.8	-92.0	135.0
6516.05	FeII	688	761	3.6	-92.0	153.0
6129.71	FeII	123	142	4.5	-92.0	120.0
5991.38	FeII	475	474	5.0	-92.0	130.0
6084.11	FeII	276	269	4.7	-92.0	130.0
6113.33	FeII	165	140	4.6	-92.0	135.0
6116.04	FeII	74	69	4.6	-92.0	125.0
5534.86	FeII	375	368	7.2	-92.0	140.0
5525.40	FeII	95	105	7.3	-100.0	120.0
5627.49	FeII	116	122	6.7	-92.0	120.0
6456.38	FeII	842	746	3.7	-92.0	170.0
6247.56	FeII	290	320	4.2	-95.0	140.0
6147.74	FeII			4.5	-92.0	140.0
6416.91	FeII	284	406	3.8	-92.0	140.0
6149.24	FeII			4.5	-90.0	140.0
6407.30	FeII	125	226	3.8	-92.0	140.0
6219.54	FeII	256	198	4.3	-75.0	140.0
6179.38	FeII	91	107	4.4	-92.0	120.0
5813.67	FeII	103	90	5.7	-92.0	151.4
6482.21	FeII	53	64	3.7	-80.0	160.0
6331.97	FeII	149	203	4.0	-95.0	120.0
6175.16	FeII			4.4	-92.0	145.0
6103.54	FeII	173	112	4.6	-90.0	130.0
6627.28	FeII	217	228	3.4	-100.0	135.0
6108.12	NiI	79		4.6		133.0
6767.78	NiI	158		3.2		127.0

^a The numbers refer to the blue and red components.

^b Continuum Flux- Units: $W \text{ cm}^{-2} \mu\text{m}^{-1} \times 10^{-17}$

5.3.2 Fe I and Fe II lines

The relatively large number of measurable Fe I and Fe II lines encouraged us to determine their excitation temperatures (T_{exc}). Extraction of T_{exc} from a set of line fluxes is straight forward for lines emitted by optically thin gas. Jeffery et al. (1988) suggested, however, that the gas emitting the Fe II lines was optically thick. This suggestion was prompted largely by their interpretation of the central minimum as a self-reversal. We consider the emitting gas to be optically thin if lines from a single multiplet scale with their Einstein A coefficients. In the optically thin limit, the line flux is given by

$$\log \{W(\lambda) F_c(\lambda)\} - \log gf + 3 \log \lambda = \log N_2/g_2 + \log C,$$

where $W(\lambda)$ is the equivalent width, $F_c(\lambda)$ is the continuum flux corrected for interstellar reddening, N_2 is the upper level population and g_2 is the statistical weight of that level, and C is a constant. Within a multiplet the left hand side of the above expression, which we denote by G , should be fairly constant unless the gas is optically thick or the excitation is exceptionally peculiar (i.e., selective fluorescence is involved). The left hand side will not be constant if the lines come from optically thick gas for which the line flux may be almost independent of the gf -values.

Four lines of the strong Fe II multiplet RMT46 in the red are shown in Figure 5.6. By inspection it is seen that the equivalent widths (hence, the line fluxes for these lines of similar wavelength) vary greatly across the multiplet, as expected for optically thin lines. This qualitative indicator of optical thinness is readily transformed to a quantitative measure by computing the left hand side G of the above expression. We adopt the gf -values given by Giridhar and Ferro (1995); the range in $\log gf$ is from -3.74 for the strongest line (5991 \AA) to -4.56 (6116 \AA). We perform the test separately on the blue and red components of the lines by computing $G(\text{blue})$ and $G(\text{red})$ for each line. In arbitrary units, we find values $G(\text{blue})$ of 1.45, 1.44, 1.55 and 1.45 for the lines in the order of largest to smallest gf . Similarly for $G(\text{red})$, they are 1.45, 1.43, 1.47, and 1.42. That the values within a multiplet are equal to within the measurement errors (say ± 0.1 dex) is evidence that the emitting gas is optically thin to the lines; $\log gf$ spans a range of 0.82 dex across these lines and G would have varied by about this amount if the gas were optically thick.

The excitation temperature T_{exc} is provided by plotting G versus the excitation potential of the upper level (χ). This plot for the Fe II lines is shown in Figure 5.8 where

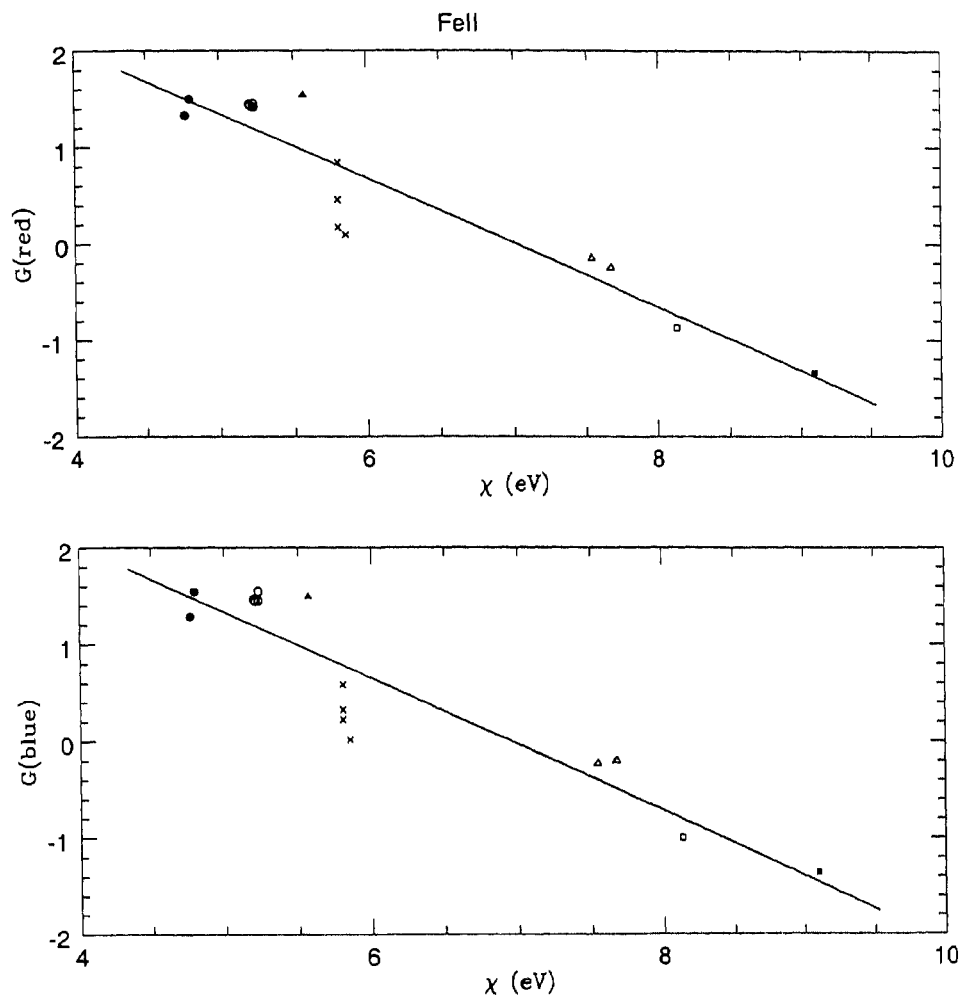


Figure 5.8: Excitation of the Fe II red and blue emission line components. See text for definition of G . χ is the excitation potential of the upper level responsible for an emission line. Filled circles represent RMT40, open circles represent RMT46, cross represents RMT47, open triangles represent RMT163, open squares represent RMT199, filled squares represent RMT210 and filled triangles represent RMT57.

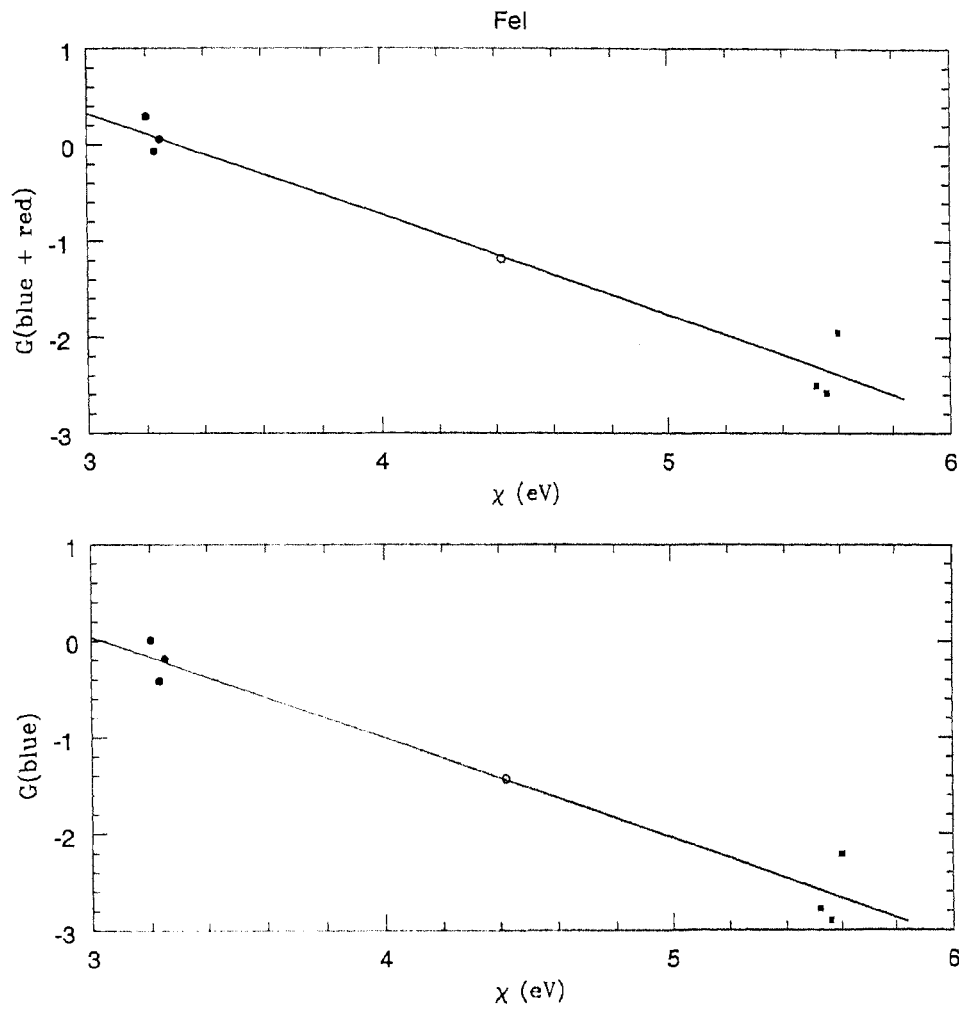


Figure 5.9: Excitation of the Fe I red and blue emission line components. See text for definition of G . χ is the excitation potential of the upper level responsible for an emission line. Filled circles represent RMT15, open circles represent RMT169 and filled squares represent RMT686.

measurements from 6 multiplets are combined and the excitation potential (χ) spans about 4 eV. Blue and red components of the lines are shown separately. The line fitted to the points corresponds to $T_{\text{exc}} = 7400 \pm 400$ K. The same temperature fits the red and blue components. The gf -values are again taken from Giridhar and Ferro (1995). The corresponding plot for the measurable Fe I lines is shown in Figure 5.9 for which the gf -values were taken from Giridhar and Ferro (1989) and the estimated excitation temperature is $T_{\text{exc}} = 4850 \pm 400$ K. Since the Fe I profiles are not so obviously double we show the plot for the integrated line profile. These results fully confirm Herbig's (1975a) suggestion about the excitation and colour temperatures. The total number of Fe II can be calculated assuming that the excitation temperature applies to the unobserved and populous low lying levels. If the same temperature is assumed for the Fe I lines, the ratio $N(\text{Fe II})/N(\text{Fe I})$ gives $n_e = 9 \times 10^7 \text{ cm}^{-3}$ when Saha's equation is adopted with $T = 7300$ K. If $T = 5000$ K is assumed for the excitation and ionization, $n_e = 2 \times 10^5 \text{ cm}^{-3}$ is found. These estimates indicate the lower and the upper limits on the electron density of the emitting regions. The [N II] and [O I] lines give us an estimate to electron density which agrees well with the estimated range of electron density from Fe lines.

5.3.3 Li I emission at 6707 Å

A novel result of this study is the discovery of emission at 6707.8 Å corresponding to Li I resonance doublet. No plausible alternative identification has been found. With the presence of Na I, Ni I, Ca I and other low excitation lines in emission the identification of Li I looks secure. The shape and width of the Li I profile closely resembles that of the other low excitation lines.

An estimate of the abundance of Li/Ca can be made by using the Ca I intercombination line at 6572 Å. We assume that the emitting gas is optically thin to both lines. Certainly the profiles are similar in shape and quite similar to the profiles of stronger lines from more abundant elements. If the excitation temperatures are taken to be similar, the observed flux ratio with the well determined Einstein A coefficients of the lines gives $\log N(\text{Li I})/N(\text{Ca I}) = -4.2$. Since Li and Ca atoms have similar first ionization potentials, we assume the abundance ratio of the neutral atoms to be the elemental abundance ratio. If the Ca abundance is the solar value, $\log \text{Li} = 2.1$ for MV Sgr on the usual scale on which $\log \text{H} = 12.0$. Compared to the solar abundance the sulphur and silicon abundance determined by Jeffery et al. (1988) are deficient by 0.7 dex, if Ca is also deficient to the

same extent then $\log \text{Li} = 1.5$. Solar Li abundance is 3.13 (from meteorites).

5.3.4 $\text{H}\alpha$, He I and C II profiles

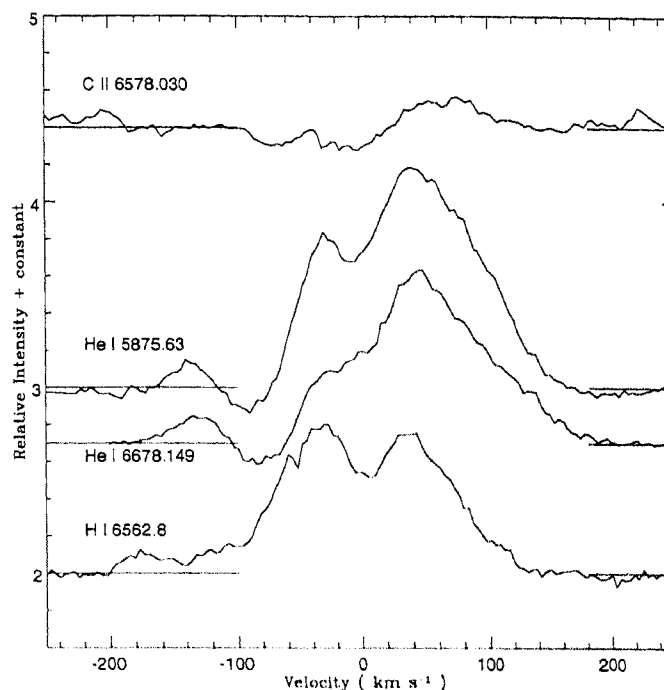


Figure 5.10: Comparison of emission line profiles of high excitation lines of C II, He I, and $\text{H}\alpha$. The velocity scale is similar to Fig. 5.4. The mean continuum for each spectrum segment is marked as in Fig. 5.3.

Profiles of $\text{H}\alpha$, the He I $\lambda 5875$ and $\lambda 6678$, and the C II $\lambda 6578$ lines are shown in Figure 5.10. These emission profiles are considerably broader than those of Fe II and other lines; the emission in the red wing extends to about 100 km s^{-1} in contrast to 50 km s^{-1} for the Fe II lines. This difference suggests that $\text{H}\alpha$ and the other lines given above come in large part from gas that is moving faster than that providing the Fe II and similar lines. Another difference between He I and C II lines, and the Fe II family of lines is the presence of blue shifted absorption in the former profiles. The He I lines show an absorption component at a relative velocity of about -80 km s^{-1} apparently superimposed on the broad emission. The C II $\lambda 6578$ profile shows a faint absorption component at -20 km s^{-1} relative to the stellar velocity. This in part may be the photospheric absorption line filled in by

lines). An apparent exception is provided by the Na I D lines which have a larger blue component's width (120 km s^{-1}) than other resonance lines for which a width of 60 km s^{-1} is representative. We suppose this difference reflects the higher optical depth in the Na D lines relative to the weak resonance (e.g., the Ca I] 6572 \AA) or low excitation lines providing the points in Figure 5.11.

Chapter 6

Results and discussion

6.1 EHe stars

6.1.1 Elemental abundances

H: The hydrogen deficiency in these stars gives us a clue that the composition of their atmospheres have been modified from their original values and are dominated by the nuclear processed material. The amount of hydrogen present in the atmospheres of FQ Aqr, LS IV -14° 109 and BD -1° 3438 is approximately 1 dex lower than that present in LS IV $+6^{\circ}$ 002, the most hydrogen-deficient candidate among the eleven EHe stars analyzed earlier (Jeffery 1996). LS IV -1° 002 is hydrogen deficient almost to the same degree as LS IV $+6^{\circ}$ 002. As in the case of minority and majority class R CrB, and hot EHe stars, we find that the S abundance, which is also an indicator of metallicity (see section 6.1.3), has a range in the programme stars. From Figure 6.1, which is a plot of H/S against the corresponding S, we find that the minority and majority class R CrB, programme stars and hot EHe stars exhibit a range in both H/S and S. The iron group and the α group elements might be the least affected by nuclear processing, and hence can give us an idea of the initial metallicity in these stars, provided they are not affected by dust gas separation.

He: From the present spectroscopic analysis, we find that helium is the most abundant species present in the atmospheres of the programme stars. Helium is 98% or even more by mass in their atmospheres.

C: Carbon is the most abundant species after helium in the cool EHe stars studied. We find that the carbon abundance relative to Fe is enhanced when compared to solar. FQ Aqr and LS IV -1° 002 have $[C/Fe] \approx 2.4$ dex, similar to minority class R CrB, while LS IV -14° 109 and BD -1° 3438 have $[C/Fe] \approx 1.3$ dex, like majority class R CrB. The enhancement of carbon indicates the presence of material processed through triple- α burning, assuming that the abundances relative to iron were initially solar. The high $[C/Fe]$ ratios in the cases of FQ Aqr and LS IV -1° 002 could be a result of differential condensation of iron on to dust grains (Lambert 1996), but no evidences for the presence dust shells around these objects have been found so far (Walker¹⁹⁸⁵-1995).

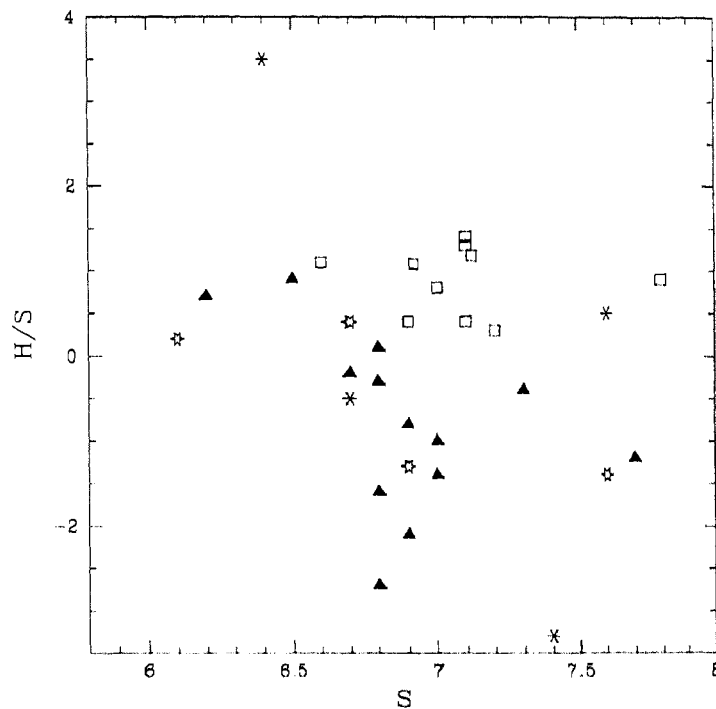


Figure 6.1: H/S versus S, showing a range in H/S and S: symbol stars represent cool EHe, solid triangles majority class R CrB, * minority class R CrB, and open squares hot EHe stars.

N: Nitrogen abundance relative to Fe is enhanced with respect to solar by approximately 1.2 dex. Most of the EHe stars studied so far also show $[N/Fe]$ close to 0.9. The majority class R CrB are known to share a common $[N/Fe]$ of 1.7. The enhancement in

nitrogen indicates that helium must have been produced from hydrogen burning by CNO cycle. There is a strong correlation between N and Fe abundances in the present sample of cool EHe stars as in the case of R CrB stars. As shown in Figure 6.2, these stars lie approximately on the locus of the line corresponding to the complete conversion of the sum of CNO nuclei to N for various metallicities (i.e., Fe abundance), which implies that the carbon resulting from triple- α burning has not been further converted to N. The hot EHe stars lie below this line implying the incomplete conversion of CNO nuclei to N. On the contrary, R CrB stars lie above this line, indicating a complete conversion of CNO nuclei to N and a further conversion of C from triple α to N in these stars.

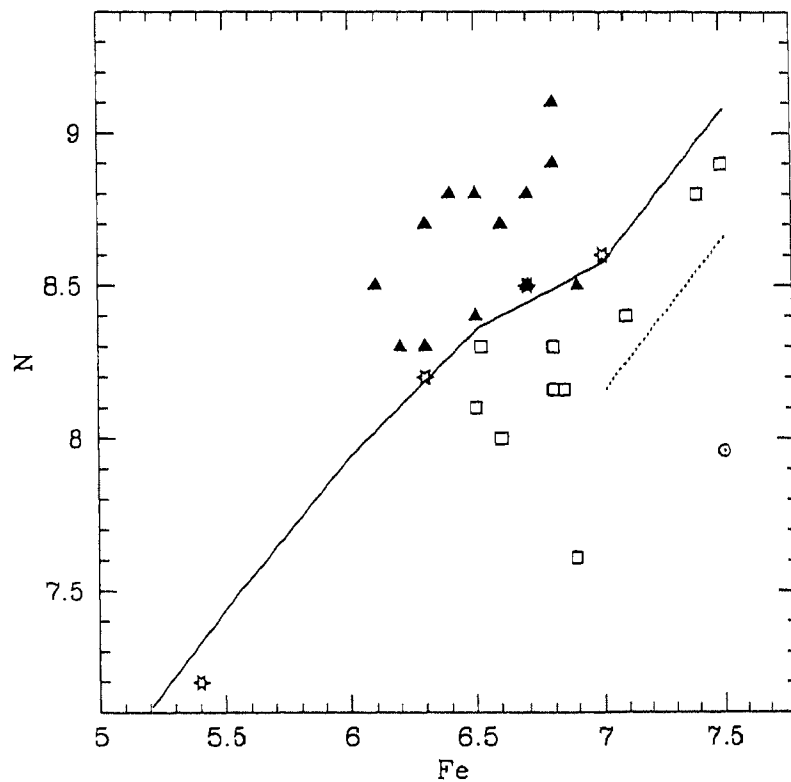


Figure 6.2: Abundance of N versus Fe: symbols stars represent cool EHe, solid triangles majority class R CrB, and open squares hot EHe stars. The Sun is denoted by \odot . The solid line represents the locus of the sum of initial C, N, O converted to N for various Fe (metallicity) abundances. The dashed line represents conversion of the initial sum of C and N to N.

O: [O/Fe] is around 0.2 in LS IV $-14^\circ 109$ and BD $-1^\circ 3438$, while it is quite large in FQ Aqr and LS IV $-1^\circ 002$. Oxygen abundance relative to Fe is like solar in LS IV $-14^\circ 109$ and BD $-1^\circ 3438$. A large dispersion in [O/Fe] is seen in these cool EHe stars, as in the case of R CrB and hot EHe stars. FQ Aqr and LS IV $-1^\circ 002$ show high [O/Fe] ratios like minority class R CrB stars. The large dispersion in [O/Fe] ratios could be the result of variable dilution of ON cycles and alpha processed material, as suggested by Rao and Lambert (1996).

Ne: Neon abundance relative to Fe is enhanced with respect to solar. [Ne/Fe] for our sample stars ranges from 1.5 to 2.1. Ne is overabundant in all the EHe stars analyzed so far. Neon is normally produced by the simple α -capture, $^{16}\text{O}(\alpha, \gamma)^{20}\text{Ne}$. This reaction is supposed to be ineffective during core helium burning. A second α -capture, $^{20}\text{Ne}(\alpha, \gamma)^{24}\text{Mg}$ during shell burning destroys the Ne nuclei. Neon can also be produced in early stages of helium burning by the reaction, $^{14}\text{N}(\alpha, \gamma)^{18}\text{F}(\beta^+ \nu)^{18}\text{O}(\alpha, \gamma)^{22}\text{Ne}$.

Na: Sodium abundance relative to Fe is enhanced with respect to the solar value by approximately 1 dex in the cool EHe stars presently studied, suggesting the synthesis of Na. Na is possibly synthesized by the reaction $^{22}\text{Ne}(p, \gamma)^{23}\text{Na}$ at the site of the ON cycle at $T \approx 3 \times 10^7$ K (Rao and Lambert 1996). Majority class R CrB stars also show an enhancement roughly by the same amount as in these stars.

Mg: Relative to Fe, Mg is like solar for all the four programme stars.

Al: Relative to Fe, Al is like solar in FQ Aqr, BD $-1^\circ 3438$ and LS IV $-1^\circ 002$, while in LS IV $-14^\circ 109$ [Al/Fe] is 0.7. The enhancement in this star could be because of the reaction $^{25}\text{Mg}(p, \gamma)^{26}\text{Al}$. Majority R CrB stars show [Al/Fe] = 0.5 ± 0.3 . Hot EHe stars also show the relative Al abundance like solar.

Si, S and Ca: The R CrB stars show a linear relation between the abundances of Si and S relative to Fe with [Si/Fe] \approx [S/Fe] (Rao and Lambert 1996, Lambert et al. 1999). As mentioned earlier the R CrB stars are divided into two groups, majority R CrB and

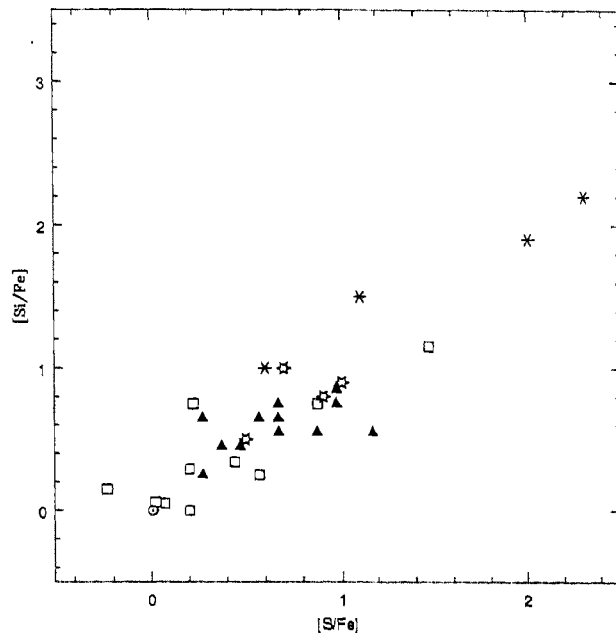


Figure 6.3: $[\text{Si}/\text{Fe}]$ versus $[\text{S}/\text{Fe}]$ for cool EHe, majority and minority class R CrB and hot EHe stars. The symbols are as in Figure 6.2 with addition for minority class R CrB stars (*).

minority R CrB, according to their $[\text{Si}/\text{Fe}]$ and $[\text{S}/\text{Fe}]$ ratios. The majority R CrB stars show $[\text{Si}/\text{Fe}] \approx [\text{S}/\text{Fe}] \approx 0.6$, while the minority R CrB stars show much higher $[\text{Si}/\text{Fe}]$ and $[\text{S}/\text{Fe}]$ ratios (see Figure 6.3). Our sample of cool EHe stars have $[\text{S}/\text{Fe}]$ of 0.8 ± 0.2 and $[\text{Si}/\text{Fe}]$ of 0.88 ± 0.2 . Relative to Fe, Ca is like solar for all these stars, except for LS IV -1° 002.

P: $[\text{P}/\text{Fe}]$ ranges from 0.3 to 0.9 for these stars. Relative to Fe, P is slightly enhanced with respect to solar. Phosphorus can be produced from the α -capture $^{27}\text{Al}(\alpha, \gamma)^{31}\text{P}$. However, there is no evidence that there has been a sufficient production of ^{27}Al to seed this process.

s-process elements: Very few lines of light s-process elements, like Sr, Y and Zr, and heavy s-process elements, like Ba are present in our sample of cool EHe stars. FQ Aqr and LS IV -14° 109 appear to show the abundances of both the light and heavy s-process elements, relative to Fe similar to the solar value. Since the s-process elements show a

large error of 0.6 dex in their abundances due to the uncertainty in the stellar parameters used, it is difficult to be sure whether the s-process elements relative to Fe are really enhanced with respect to solar or not. We have only one Ba II line for estimating the abundance, and hence it is rather difficult to obtain accurate abundance ratio of light s-process elements to heavy s-process elements in the four cool EHe stars considered. In majority and minority class R CrB stars, the s-process elements are enriched relative to Fe, the light s-elements being more enhanced than the heavy s-elements.

6.1.2 Comparison with R CrB stars and hot EHe stars

The mean abundance ratios $[X/Fe]$ for the three groups, majority class R CrB stars, cool EHe stars and hot EHe stars are given in the Table 6.1. In the case of R CrB stars, the C/He is not determined accurately. Since the abundance ratios such as X/Fe (here X excludes C and He) are not sensitive to the adopted C/He as explained in section 4.1, we use these ratios for a comparative study. The abundances relative to Fe are given in Table 6.1. The abundance ratios in the majority class R CrB stars are taken from Lambert et al. (1999) while those in the hot EHe stars are taken from Jeffery (1996, 1998), Jeffery et al. (1998) and Drilling et al. (1998).

Table 6.1

Comparison of abundance ratios in R CrB stars, cool EHe stars and hot EHe stars

Element ratio	majority R CrB stars ^a	cool EHe stars ^b	EHe stars ^c
$[X/Fe]$			
$[N/Fe]$	1.7 ± 0.3	1.2 ± 0.1	0.9 ± 0.3
$[O/Fe]$	0.4 ± 0.6	0.9 ± 0.8	0.3 ± 0.7
$[Na/Fe]$	0.8 ± 0.1	1.1 ± 0.2	
$[Al/Fe]$	0.5 ± 0.3	0.3 ± 0.2	0.2 ± 0.4
$[Si/Fe]$	0.6 ± 0.2	0.8 ± 0.2	0.4 ± 0.5
$[S/Fe]$	0.6 ± 0.3	0.8 ± 0.2	0.3 ± 0.5
$[Ca/Fe]$	0.0 ± 0.2	0.0 ± 0.4	0.4 ± 0.3

^a Mean abundance ratios from Lambert et al. (1999)

^b Mean abundance ratios from present study.

^c Mean abundance ratios from Jeffery (1996), Jeffery (1998), Jeffery et al. (1998) and Drilling et al. (1998).

Hydrogen: If we compare the mean hydrogen abundance of each group—R CrB, cool EHe and hot EHe stars—we find that hydrogen deficiency increases in the order of hot EHe, cool EHe and R CrB stars, i.e., the hydrogen deficiency increases with decrease in temperature. This could be understood as follows: To begin with, hydrogen is the major constituent of the star, and the hydrogen deficiency is the result of its evolution. Since hydrogen is consumed but never synthesized in the star, the degree of hydrogen deficiency reflects its evolutionary status. This phenomenon is observed in Sakurai's object, which showed a continuous decrease in hydrogen abundance as it evolved towards cooler temperatures (Asplund 1999). Mean hydrogen abundance is 6.3 ± 0.9 for majority class R CrB stars (a total of 13 stars), 6.3 ± 0.5 for cool EHe stars (our sample) and 8.0 ± 0.5 for hot EHe stars (10 objects, Jeffery 1996; Jeffery 1998; Jeffery et al. 1998; Drilling et al. 1998). We have excluded V652 Her, HD 144941, and the three hot R CrB stars DY Cen, MV Sgr and V348 Sgr while averaging. There is a large scatter in the hydrogen abundance from star to star within a group, but they seem to show a relation with temperature, when mean hydrogen abundance as a group is considered (Figures 6.4 and 6.5).

Carbon, nitrogen and oxygen: The carbon to helium ratio for R CrB stars, cool EHe stars and hot EHe stars lies in the range of 0.3% to 1.0%. Since carbon is the major source of continuum opacity for R CrB stars, we can not compare the carbon abundance of these stars with cool EHe stars and hot EHe stars. But it is clear from the carbon abundance that helium burning (triple α) has taken place in these stars.

The average value of $[N/Fe]$ is 1.7 ± 0.3 , 1.3 ± 0.1 and 0.9 ± 0.3 for majority class R CrB, cool EHe and hot EHe stars, respectively. Here the hot EHe stars refer to the 10 hot EHe stars mentioned above. As the temperature decreases from hot EHe to cool EHe to majority class R CrB stars, the nitrogen abundance relative to iron increases (see Figure 6.6). The abundance of nitrogen gives us a clue to the evolutionary status of these stars. Enrichment of nitrogen is a result of nuclear processing and mixing. The nuclear processed material is brought to the surface as a result of mixing (dredge-up). In the course of its evolution the star dredges-up more and more nuclear processed material (here nitrogen) to the surface at various stages of its evolution. From the trend observed in nitrogen abundance relative to iron in these groups, we feel that the sequence of evolution is from

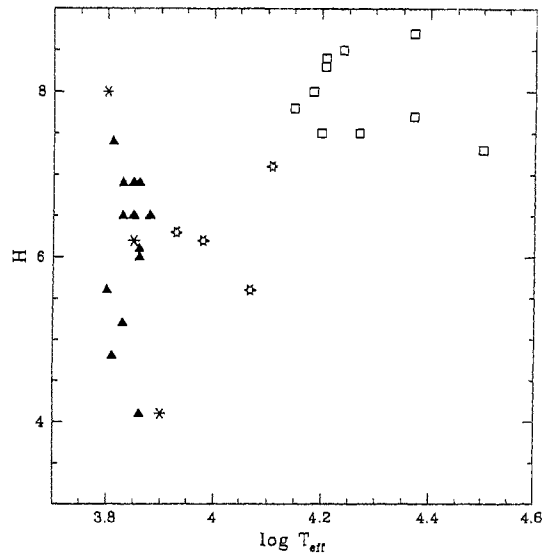


Figure 6.4: H versus $\log T_{eff}$ for cool EHe, majority and minority class R CrB , and hot EHe stars. The symbols are as in Figure 6.3.

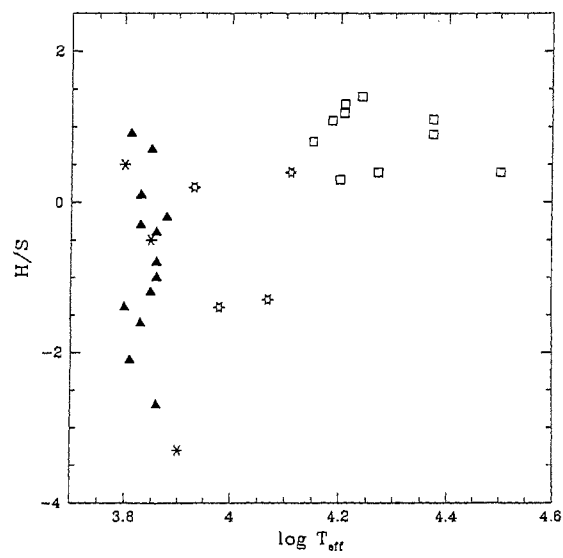


Figure 6.5: H/S versus $\log T_{eff}$ for cool EHe, majority and minority class R CrB , and hot EHe stars. The symbols are as in Figure 6.3.

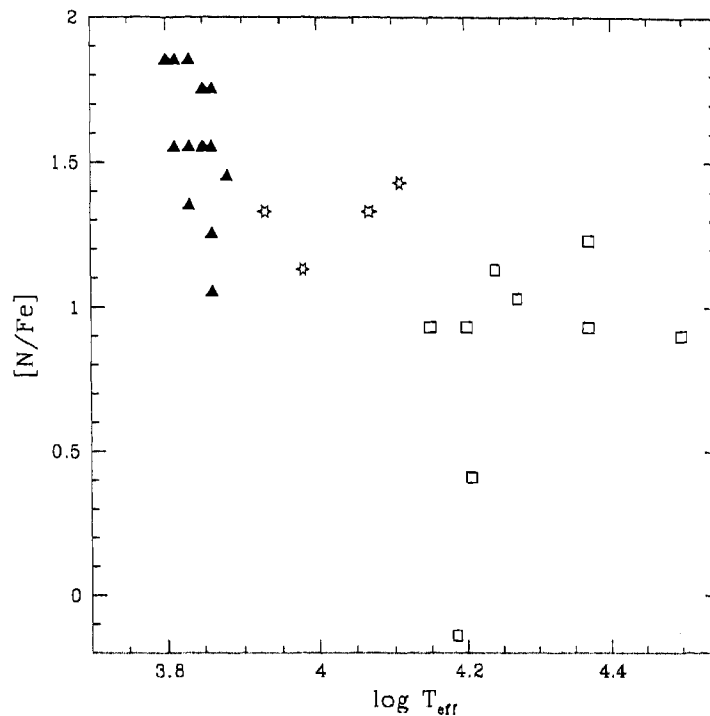


Figure 6.6: $[N/Fe]$ versus $\log T_{eff}$ for cool EHe, majority class R CrB and hot EHe stars. The symbols are as in Figure 6.2.

hot EHe to cool EHe and then to majority class R CrB stars. Schönberner (1996), and Lambert (1996) had earlier suggested that the evolution is from cool to hot stars, but from the behaviour of $[N/Fe]$ ratios in these groups of stars, which shows a clear relationship with temperature, it appears that as the star evolves it becomes cooler.

A large scatter in the $[O/Fe]$ ratios in the stars makes the ordering of these three groups with respect to the oxygen abundance impossible.

Sodium and aluminium: The material which is severely exposed to hydrogen burning results in the enrichment of Na and Al. Relative to Fe, Na is enriched in these objects: $[Na/Fe]$ is approximately 1.1 for cool EHe stars and 0.8 for majority class R CrB stars. Abundance of Na is not available for hot EHe stars. The intrinsic scatter in $[Na/Fe]$ for cool EHe stars is ~ 0.2 dex (see Figure 6.7). Majority class R CrB stars also show negligible intrinsic scatter in $[Na/Fe]$ ratios. Average value of Na relative to Fe is enriched approximately by the same amount in cool EHe and majority class R CrB stars. All the

three groups show scatter in $[Al/Fe]$ ratios. Relative to Fe, Al is enhanced approximately by the same amount on an average in all the three groups. Na seems to be more enhanced when compared with Al, in all the three groups.

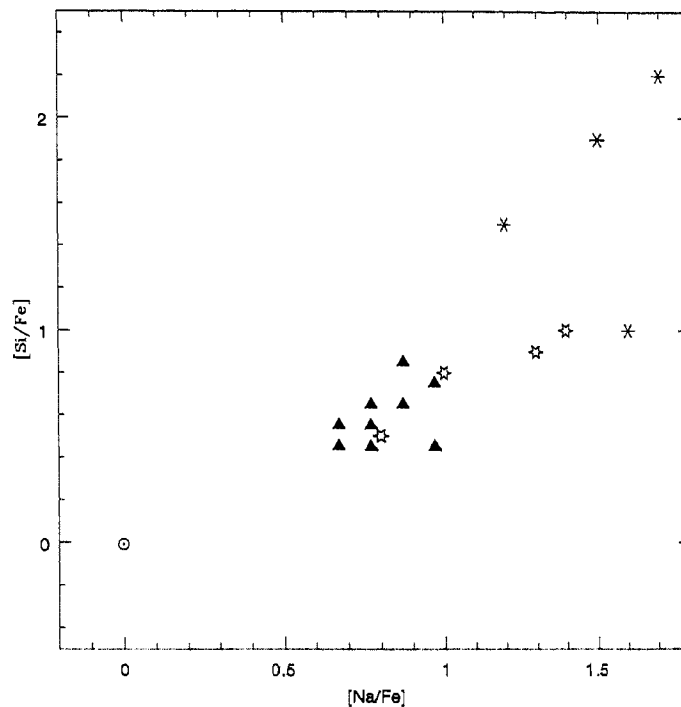


Figure 6.7: $[Si/Fe]$ versus $[Na/Fe]$ for cool EHe, majority and minority class R CrBs and hot EHe stars. The symbols are as in Figure 6.3.

Silicon, sulphur and calcium: It is evident from Figure 6.3 that the programme stars also obey a linear relation between $[Si/Fe]$ and $[S/Fe]$, like majority class R CrB stars, minority class R CrB stars and hot EHe stars. The programme stars are more similar to majority class R CrB stars in $[Si/Fe] \approx [S/Fe]$ ratios. FQ Aqr and LS IV $-1^\circ 002$, being low metallicity stars (low Fe abundance), have slightly higher $[Si/Fe]$ and $[S/Fe]$ ratios when compared to majority class R CrB stars. The average value of $[Si/Fe] \approx [S/Fe]$ is 0.4 for hot EHe stars, 0.6 for majority class R CrB stars and 0.8 for cool EHe stars. The cool EHe stars and majority R CrB stars exhibit a small spread in the values of $[Si/Fe]$ and $[S/Fe]$ about their respective averages, while the hot EHe stars show a large spread about its average value. In FQ Aqr the abundance of Si is derived from strong and saturated

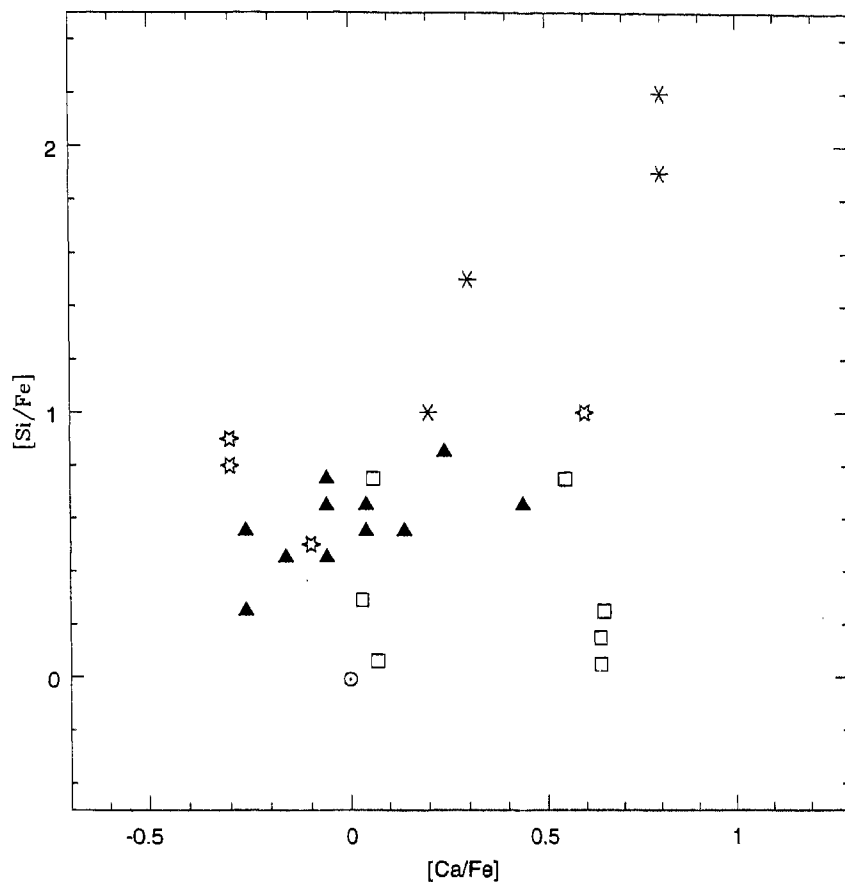


Figure 6.8: $[Si/Fe]$ versus $[Ca/Fe]$ for cool EHe, majority and minority class R CrB and hot EHe stars. The symbols are as in Figure 6.3.

lines of Si II, and hence is uncertain. $[Ca/Fe]$ ratios in the stars studied are like those in majority class R CrB. LS IV $-1^{\circ} 002$ is an exception to this. Here it may be noted that it is more close to hot EHe stars in temperature. The $[Ca/Fe]$ ratio, which is approximately 0.6, seen in this star is similar to that seen in hot EHe stars (Figure 6.8). $[Ca/Fe]$ ratio is larger in hot EHe stars when compared to that in cool EHe and majority class R CrB stars. This implies that Ca is either enriched in hot EHe stars or it is depleted in R CrB stars as a result of condensation on to dust grains. Ca abundance is estimated using strong Ca II $\lambda\lambda$ 8542, 8662 Å lines. Since these lines lie on the flat part of the curve of growth the uncertainty in the Ca abundance is more.

s-process elements: The abundances of s-process elements are not available for hot EHe stars. Out of the four cool EHe stars studied, FQ Aqr and LS IV $-14^\circ 109$ show abundances of s-process elements relative to Fe very similar to that of sun, indicating that the photospheric material has not been exposed to s-processing. The abundances of s-process elements in the other two stars, BD $-1^\circ 3438$ and LS IV $-1^\circ 002$, are uncertain due to the lack of sufficient number of lines and the large errors involved in determining the stellar parameters. Relative to Fe, s-process elements are enriched when compared with the solar abundance in the case of majority class R CrB stars, implying the presence of material exposed to s-process in their photospheres. Since majority class R CrB stars show material exposed to s-processing while the cool EHe stars do not, the former might be more evolved than the latter. From a consideration of the abundances of s-process elements, we suggest that cool EHe stars (FQ Aqr and LS IV $-14^\circ 109$) might evolve to majority class R CrB stars.

6.1.3 Metallicity

Iron content of the star is an indicator of its metallicity. There is a likelihood that iron might have condensed on to dust grains at an earlier phase of evolution, thereby depleting its initial photospheric iron abundance. Since α -nuclei (Mg, Si, S, Ca, etc.) also reflect the metallicity approximately, we use sulphur abundance as the metallicity indicator as it is least depleted (Lambert 1996). In carbon rich atmospheres the sulphur products are few and lower in abundance when compared with the products of carbon, nitrogen, silicon, etc., (Goeres 1996). Therefore, it is quite likely that sulphur is one of the least depleted in carbon rich atmospheres.

Lambert et al. (1999) have determined the metallicity of R CrB stars from Fe/C ratio, where C is the spectroscopic carbon abundance derived from C I lines. Since carbon is produced in the star and iron could have been affected by the dust gas separation, Fe/C might not give us the true metallicity of R CrB stars. Using sulphur abundance as the metallicity indicator, majority class R CrB stars show metallicity $[Z(S)]$, in the range -1.0 to 0.47 . The metallicities $[Z(S)]$ for FQ Aqr, LS IV $-14^\circ 109$, BD $-1^\circ 3438$ and LS IV $-1^\circ 002$ are -1.13 , 0.37 , -0.33 and -0.53 , respectively. For hot EHe stars metallicity $[Z(S)]$ lies in the range -0.63 to 0.57 . We find a continuity in range in the metallicity for majority class R CrB, cool EHe and hot EHe stars.

6.1.4 The “carbon problem”

In the case of R CrB stars it is found that the abundances derived from the C I line strengths are far below (by 0.62 dex) the input abundance used in the model atmospheres. If we use a model atmosphere of input abundance of carbon as 9.5 dex, the carbon abundance derived from C I line strengths turns out to be about 8.9 dex. If one uses a model atmosphere of input abundance of carbon as 8.9 dex, the C I line strengths still return an abundance which is about 0.6 dex lower than the input abundance of carbon, i.e., 8.3 dex. This difference is defined as “carbon problem” (Gustafsson and Asplund

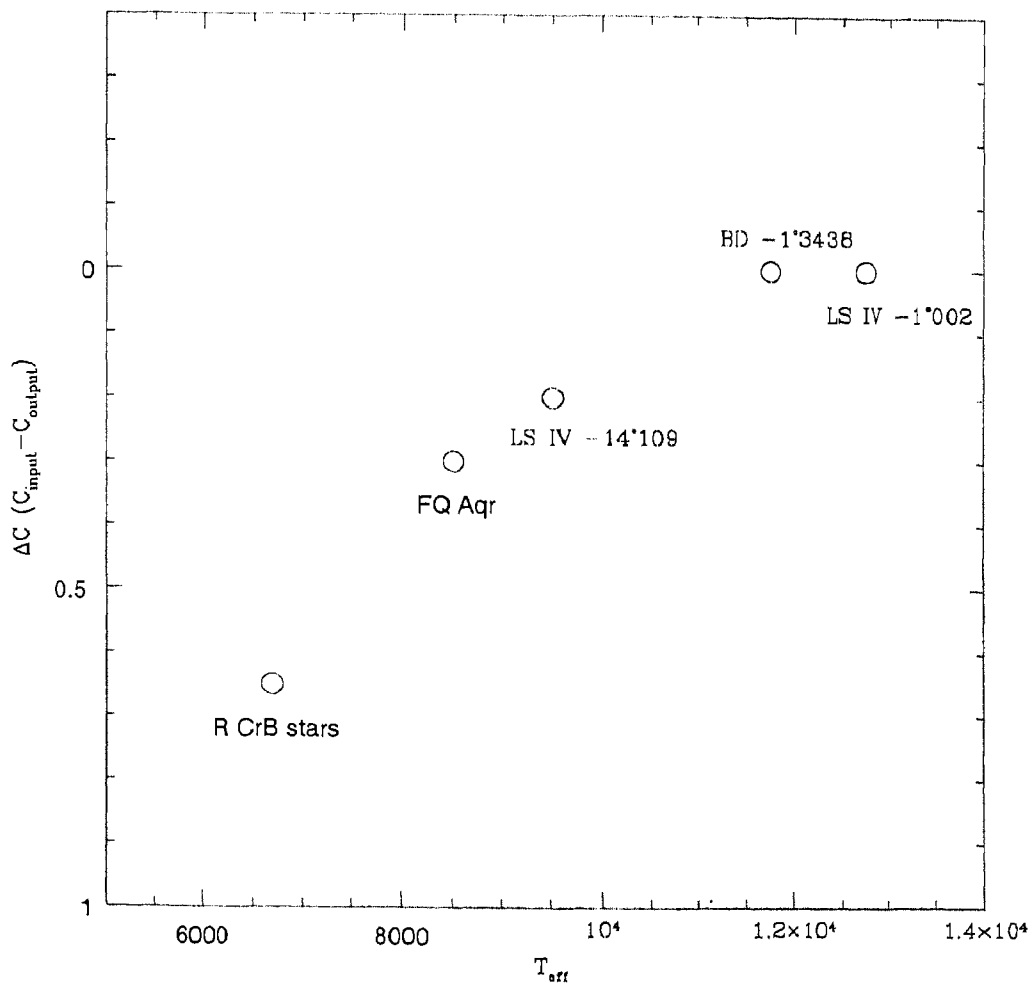


Figure 6.9: ΔC ($C_{input} - C_{output}$) versus T_{eff} for R CrB and cool EHe stars.

1996; Gustafsson 1997; Lambert et al. 1999). The “carbon problem” has been nagging

the R CrB investigators for quite sometime. In our cool EHe stars we find that the “carbon problem”, though exists, is not as severe as in the case of R CrB stars. The strength of C I lines in FQ Aqr and LS IV $-14^{\circ} 109$ give carbon abundance of 9.2 and 9.3, respectively (Tables 4.6 and 4.7), for an input carbon abundance of 9.5, which translates to a “carbon problem” of 0.3 to 0.2 dex. For BD $-1^{\circ} 3438$ and LS IV $-1^{\circ} 002$ we do not find any “carbon problem” because the equivalent widths of carbon lines (C I and C II) give the same abundance as the input used for the model atmosphere. The difference between the input and output carbon abundances, ΔC , is plotted against the temperature in Figure 6.9. It can be seen that ΔC , which is significantly large at lower temperatures, decreases with increase in temperature, and hence the magnitude of the “problem” is reduced at higher temperatures. This behaviour can be interpreted in terms of the role played by carbon, which is the major source of continuum opacity at the cool end.

Lambert et al. (1999) explain the “carbon problem” in terms of underestimation of the measured equivalent widths, errors in atomic data for C I, and photoionization of C I not being the dominant contributor to the continuous opacity. In the present work we have estimated the contributions to the continuum opacity from various sources (C I, He I, e^- , He $^-$ and N I) at different temperatures (see section 4.2 and 4.3 and Figures 4.1, 4.2 and 4.3). We find that the dominant source of continuum opacity changes from C I to e^- to He I, as we go from the cool to the hot end. The discrepancy between the input and output carbon abundance is more severe at the cool end. Thus it appears that the “carbon problem” is related to the role of C I as the major source of continuum opacity. In model atmospheres which are hotter than R CrB stars (>8000 K) continuum opacity due to e^- dominates over C I. Probably, the change in the dominant source of continuum opacity from C I to e^- as the temperature increases results in reducing the “problem”. Lambert et al. (1999) argue that the “carbon problem” is due to the atmospheric structure adopted in the model atmospheres.

Rao et al. (1999) have found that “carbon problem” is 0.3 dex when R CrB was observed on 1995 Sep 30, just before a light decline. A value of 0.3 dex is considered to be a “carbon problem” of low magnitude. They also find that the abundance of other elements derived from the 1995 Sep 30 spectra of R CrB are consistently higher than that derived at other times by about 0.3 to 0.5 dex. They attribute this difference in chemical composition, to the atmospheric disturbance that subsequently initiated the decline. The problem could also be in the model atmospheres used because the atmospheric disturbance

that subsequently initiated the decline is not taken into account while constructing these models.

6.1.5 Evolutionary aspects

The discussion on abundances and their interpretation are mainly based on the various processes which may have been responsible in producing the observed chemical composition of these stars. It is clear that these stars are in the late stages of evolution and the observed abundances appear to have been affected by nucleosynthesis taking place in the course of their evolution.

Evolutionary scenarios

The two scenarios, FF and DD, proposed for the origin of R CrB and EHe stars are described in section 1.5.1 and 1.5.2. We have also discussed the pros and cons of these two scenarios when the predictions based on these models are compared with the observations. A direct comparison of observed abundances in the case of cool EHe stars is not possible because of the lack of detailed prediction of abundances resulting from these two scenarios.

DD scenario explains the high He and N abundances, but fails to account for the observed H and C abundances. Lambert et al. (1999) speculate that the rp-process might synthesize the intermediate mass elements Na - S. In that case Mg and Ca should also be produced in significant amounts, but the observed Mg/Fe and Ca/Fe ratios are like solar for the cool EHe stars. The merging of an He white dwarf and a C-O white dwarf also may initiate repeated α -captures producing significant amounts of ^{28}Si and ^{32}S (Lambert et al. 1999).

FF scenario successfully accounts for the observed H, C, N and He abundances, but it is not able to explain the non-solar Si/Fe and S/Fe ratios for cool EHe stars. The high S/Fe ratio could be explained in terms of dust-gas separation but the high Si/Fe ratio cannot be explained by this chemical process. For cool EHe stars the derived C/He is 0.3% to 1% by number, much lower than that of C/He \approx 5% to 10% predicted by the FF scenario (Schönberner 1996; Iben and MacDonald 1995). Recent calculations by Herwig et al. (1999) show the resulting surface mass fraction C/He to be \approx 1. These calculations are in agreement with the surface abundance pattern observed in [WC] and PG 1159 stars.

It is clear from the above discussion that it is difficult to pinpoint whether cool EHe stars are the outcome of DD scenario or FF scenario. Since the FF scenario can eventually produce hydrogen-deficient stars with surface composition of C/He ≈ 1 by mass (Herwig et al. 1999), one would expect to see objects having a surface composition of C/He ≈ 0.01 at an intermediate stage after the final helium shell flash has taken place. Such hydrogen-deficient stars with C/He ≈ 0.01 would appear to be similar to R CrB/EHe stars in their surface composition. It could be possible that R CrB/EHe stars ultimately evolve to [WC] and PG 1159 stars.

Comparison with halo stars

For BD $-1^\circ 3438$, the α -elements and iron peak elements are consistent with the composition of disk and halo dwarfs with [Fe] = -0.8 . For FQ Aqr, LS IV $-14^\circ 109$ and LS IV $-1^\circ 002$, the [Si/Fe] and [S/Fe] ratios are high when compared with disk and halo dwarfs for their metallicities (McWilliam 1997). The radial velocities of our cool EHe stars, which we have determined using Fe II, lines are listed in Table 4.1. These velocities are much lower than those of R CrB stars and hot EHe stars.

Evolutionary link

In the $\log g$ - $\log T_{eff}$ diagram our sample EHe stars are located along a band bounded by the loci of constant $\log(L/M)$ values of about 3.75 and 4.5, similar to R CrB and hot EHe stars. In Figure 6.10, which shows the $\log g$ - $\log T_{eff}$ diagram, symbol stars indicate the cool EHe stars, open squares the hot EHe stars, and filled triangles the R CrB stars. Solid lines in Figure 6.10 show the hydrogen and helium main-sequences, the horizontal branch and the Eddington limit for pure Thomson scattering in a helium atmosphere. Broken lines show the loci of stars with $\log L/M$ values of 3.75 and 4.5.

From the observed dependence of hydrogen abundance, nitrogen abundance relative to Fe and abundance of s-process elements relative to Fe on temperature, we have already mentioned that there is a clear indication of an evolution from hot EHe to cool EHe to majority class R CrB stars. In the $\log g$ - $\log T_{eff}$ diagram (Figure 6.10), we find that the hot EHe stars, cool EHe stars and majority class R CrB stars form a near-continuous sequence indicating a possible evolutionary link between them.

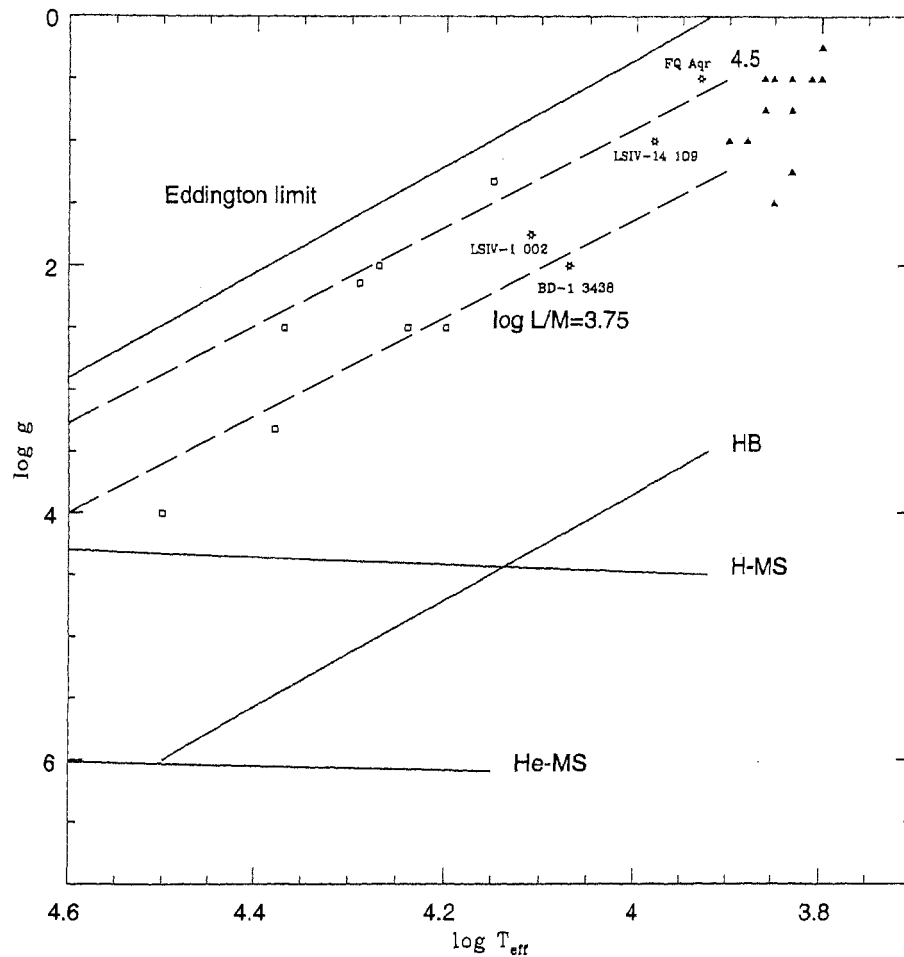


Figure 6.10: $\log g$ - $\log T_{eff}$ diagram for cool EHe, R CrB and hot EHe stars. The symbols are as in Figure 6.2. Solid lines show the hydrogen and helium main-sequences, the horizontal branch and the Eddington limit for pure Thomson scattering in a helium atmosphere. Broken lines show the loci of stars with the given $\log L/M$.

6.2 MV Sgr

The double-peaked Fe II (and other) emission lines suggest that the emitting gas in MV Sgr is confined either to a rotating envelope or to a bipolar flow. In both models the more excited lines are presumed to come from the inner regions closest to the star where the

rotation velocities or the wind velocities are the highest. Keplerian motion about MV Sgr seems a feasible explanation for the velocity separation of the emission lines, red and blue components. The expected Keplerian velocities are v (km s^{-1}) $\simeq 120R_h^{-0.5}$ where R_h is the distance from the stellar center expressed in stellar radii. We estimate the stellar radius to be $R_* \simeq 13R_\odot$ from the assumptions that $M_{bol} \simeq -5$ and $T_{eff} \simeq 15000K$. A circular velocity of $\pm 30 \text{ km s}^{-1}$, as indicated by the displacement of the blue and red peaks, is attained at $R_h \sim 15R_*$. The observed separation includes an unknown projection factor, so $R_h \leq 15R_*$ is suggested. This gas is well inside the dusty region ($R_{dust} \sim 40R_*$, Walker 1985) responsible for the infrared emission characterized by a 1600 K blackbody. The fact that the strong emission lines appear doubled suggests that the emitting gas is in a flattened system if the line splitting is due to rotation. In turn, this may suggest that there is a preferred direction for the gas outflow from the star.

In considering alternatives to the rotating envelope, the two peaks (optically thin) of the emission profiles could simply imply (indicate) flows in two directions, towards and away from the observer irrespective of the presence of the dust-disk (or torus) as long as the projected size of the dust-disk is small compared to the resulting flow size. The high excitation lines (e.g., He I) may sample the inner volume between the star and the disk, and the receding gas on the ‘far’ side of the disk may be visible. This will account for the larger widths of these lines. The blue-shifted absorption in the He I and C II lines is probably formed close to the star where the wind is fastest. This model in which one component of the dust, presumably the warmer component ($T = 1600 \text{ K}$), is concentrated into a disk implies a preferred direction for the ejection of gas and dust. The colder dust may be more spherically distributed.

Chapter 7

Conclusions and future prospects

7.1 Cool EHe stars

Investigations of EHe stars in the disc of the Galaxy by several authors have revealed the existence of a small group of cool objects among them. Preliminary analysis existing in the literature have indicated that these stars might be transition objects which might evolve either to R CrB or to hot EHe stars. In the present investigation, we have obtained high resolution, high signal-to-noise ratio spectra of four hydrogen-deficient stars classified as EHe stars. These stars, which have effective temperatures in the range 8000 K to 13000 K, are hotter than R CrB stars but cooler among the EHe stars. The spectra of these stars are characterized by neutral carbon lines, singly ionized carbon lines, neutral helium lines, and of course weak, or absent Balmer lines. We have carried out a detailed abundance analysis which provides us with clues to establish the kinship of these cool EHe stars with R CrB stars and hot EHe stars.

The continuum opacity, directly or indirectly, in all the normal stars is controlled by hydrogen, which is not the case for hydrogen-deficient stars. Therefore, it becomes very important to identify the dominant sources of continuum opacity to derive meaningful elemental abundances in cool EHe stars. He and C being the most abundant elements in the atmospheres of these stars contribute significantly to the continuum opacity. Earlier investigations have shown that photoionization of C I is the major source of continuum opacity in the temperature domain of R CrB stars. In our analysis of cool EHe stars, we have shown that C I is still the major source of continuum opacity at the cool end (8000

K to 10000 K) and He I at the hot end (12000 K to 14000 K) by two independent ways: (i) by calculating the individual sources of continuum opacity as a function of optical depth (τ) in the temperature domain of these stars, and (ii) by a study of the predicted equivalent widths of C I, C II and He I lines using model atmospheres across a grid of T_{eff} , $\log g$ and C/He in the temperature range of these stars. We find that the predicted equivalent widths of C I and C II lines are independent of C/He at the cool end while the predicted equivalent widths of He I lines are independent of C/He at the hot end. We have interpreted such a behavior in terms of the changes in the dominant source of continuum opacity with temperature.

We find that the dominant sources of continuum opacity at the cool end (FQ Aqr and LS IV $-14^\circ 109$) are the photoionization of neutral carbon and electron scattering. Most of the carbon is in singly ionized state and contributes 50% of the total free electrons. A superposition of the spectra of V3795 Sgr (R CrB type, $T_{eff} = 8000$ K), FQ Aqr (cool EHe star) and LS IV $-14^\circ 109$ (cool EHe star) shows that the C I lines ($\lambda\lambda$ 5817.7, 5864.95 Å) have approximately the same strength in all these stars. This implies that the continuous opacity in the line-forming regions of FQ Aqr and LS IV $-14^\circ 109$ is dominated by the photoionization of C I, making the C I line strength insensitive to carbon abundance. At the hot end (for BD $-1^\circ 3438$ and LS IV $-1^\circ 002$) photoionization of neutral helium is the major source of continuum opacity.

The spectroscopic determination of carbon to helium ratio for cool EHe stars is essential in the context of their evolutionary status and in the estimation of continuum opacity due to C I and He I. Our observations of EHe stars with a fairly wide range in temperature (8000 K to 14000 K) have helped us in understanding the importance of the dominant role played by continuous opacity due to carbon and electrons at the cool end, and due to helium at the hot end. Our study has shown how the sources of continuum opacity vary across the temperature range. C I being the minor source of continuum opacity at the hot end, equivalent widths of C I and C II lines could be used to derive unambiguously the carbon content of the star. At the cool end C I is the major source of continuum opacity and He I lines give us an estimate of He/C and hence the carbon abundance. In principle one could estimate C/He of EHe stars in the temperature range 8500 K to 10000 K, from the equivalent widths of C I lines, if they have C/He $< 1\%$. We find that for stars in the temperature range 8500 K to 10000 K, it is not possible to estimate the C/He from the equivalent widths of C I lines if C/He $\geq 1\%$. The C/He determined for most of these

stars from carbon and helium lines lies in the range of 0.3% to 1.0%.

We have determined the parameters T_{eff} , $\log g$ and ξ of these stars. From our analysis of cool EHe stars, we find that these stars are similar to R CrB stars and hot EHe stars in their photospheric abundances. These stars when plotted in the $\log g - \log T_{eff}$ plane fall between the loci of constant $\log(L/M)$ of 3.7 and 4.5, similar to R CrB and hot EHe stars.

The “carbon problem” has been nagging the R CrB investigators for quite sometime. They find that the abundances derived from the C I line strengths are far below (by 0.62 dex) the input abundance used in the model atmospheres. In our cool EHe stars, we find that the “carbon problem” definitely exists, but it is not as severe as in the case of R CrB stars. FQ Aqr and LS IV $-14^\circ 109$ give carbon abundance of 9.2 and 9.3, respectively, which translates to a “carbon problem” of 0.25 to 0.3 dex. For BD $-1^\circ 3438$ and LS IV $-1^\circ 002$ we do not find any “carbon problem” because the equivalent widths of carbon lines (C I and C II) give the same abundance as the input used for the model atmosphere. We have shown that the magnitude of “carbon problem” reduces as we go from the cool end to hot end.

Iron content of a star is an indicator of its metallicity. There is a possibility that iron might have condensed on to dust grains, resulting in artificially reducing the iron abundance. Since α -nuclei (Mg, Si, S, Ca, etc.) also reflect the metallicity approximately, we use the abundance of sulphur, which is probably one of the least depleted as the metallicity indicator. The metallicities $[Z(S)]$ for FQ Aqr, LS IV $-14^\circ 109$, BD $-1^\circ 3438$ and LS IV $-1^\circ 002$ are -1.13 , 0.37 , -0.33 and -0.53 , respectively. For cool EHe stars the metallicity $[Z(S)]$ lies in the range -1.1 to 0.37 and for hot EHe stars it lies in the range -0.63 to 0.57 .

Cool EHe stars obey a linear relation between $[Si/Fe]$ and $[S/Fe]$, like majority class R CrB stars, minority class R CrB stars and EHe stars. These stars in $[Si/Fe] \approx [S/Fe]$ ratios, are like majority class R CrB stars.

If we compare the mean hydrogen abundance of stars of each group, R CrB, cool EHe and hot EHe stars, we find that hydrogen deficiency increases in the order of hot EHe, cool EHe and R CrB stars, i.e., the hydrogen deficiency increases with decreasing temperature. Since hydrogen is consumed but never synthesized in a star, the amount of hydrogen deficiency reflects its evolutionary status.

The average values of $[N/Fe]$ are 1.7 ± 0.3 , 1.3 ± 0.1 and 0.9 ± 0.3 for majority class

R CrB, cool EHe and hot EHe stars, respectively. As the temperature decreases from hot EHe to cool EHe to majority class R CrB stars, the nitrogen abundance relative to iron apparently increases. The abundance of nitrogen gives us a clue to the evolutionary status of these stars. Enrichment of nitrogen is a result of nuclear processing and mixing. The nuclear processed material is brought to the surface as a result of mixing (dredge-up). In the course of its evolution the star dredges-up more and more nuclear processed material (here nitrogen) to the surface at various stages of its evolution. From the trend observed in the nitrogen abundance relative to iron for these groups, the evolutionary sequence appears to be from hot EHe to cool EHe and then to majority class R CrB stars.

The abundances of s-process elements are not available for hot EHe stars. Out of the four cool EHe stars studied, FQ Aqr and LS IV -14° 109 show abundance of s-process elements relative to Fe, like solar. The abundances of s-process elements in the other two stars, BD -1° 3438 and LS IV -1° 002, are not well-determined due to the uncertainty in the stellar parameters derived. Relative to Fe, s-process elements are enriched compared to solar in the case of majority class R CrB stars. Looking at the abundances of s-process elements, we suggest that the cool EHe stars, FQ Aqr and LS IV -14° 109 might evolve to majority class R CrB stars. Since majority class R CrB stars show material exposed to s-processing they might be more evolved than cool EHe stars.

The main conclusion of our study is that there are similarities in the observational properties and continuity in the abundance pattern among the three groups of objects; RCr B, cool EHe and hot EHe stars, indicating a continuous evolutionary sequence. Based on the derived abundances in particular the hydrogen abundance, [N/Fe] ratios, abundances of s-process elements, and the location of these stars on $\log g$ - $\log T_{eff}$ diagram, we suggest that the evolution is in the direction hot EHe stars \rightarrow cool EHe stars \rightarrow majority class R CrB stars.

7.2 MV Sgr

The radial velocity measured by us from the photospheric absorption lines agree with the earlier measurements suggesting that the radial velocity of MV Sgr is nearly constant: if it pulsates, it does so with a small amplitude; if it is a spectroscopic binary, the velocity amplitude of the visible star is small.

The emission line spectrum shows MV Sgr supports a wind: the HeI lines show blue-

shifted absorption at an expansion velocity of about 80 km s^{-1} . The line profiles of other lines from strong Fe II lines to weaker forbidden lines are centred on the stellar velocity with a width that is an increasing function of excitation potential. We tentatively associate the emission lines with two flows, towards and away from the observer. We cannot exclude the possibility that the emitting gas is concentrated in a rotating (dust-free) torus; measurements of polarization will be helpful in refining the model.

A novel result of our study is the detection of the Li I resonance feature at 6707 \AA in emission. We infer an abundance ratio Li/Ca using the Li I 6707 \AA and the Ca I 6752 \AA intercombination line. If, as the Fe I and Fe II lines suggest, the excitation is quasi-thermal, we find a value of -4.2 for $\log N(\text{Li I})/N(\text{Ca I})$, and the similarity of ionization potentials suggests that this is also the elemental ratio $\log N(\text{Li})/N(\text{Ca})$. If the star's calcium abundance is solar, we find $\log \text{Li} = 2.1$ on the usual scale. Since all stars prior to the onset of He core burning destroy or dilute the Li in their outer envelopes to a level well below this abundance ($\log \text{Li} \sim -1$ to 1 , Brown et al. 1989), it appears that MV Sgr was able to resynthesize Li. Lithium production is observed and predicted to occur in the envelopes of intermediate mass stars at high luminosities on the asymptotic giant branch (cf. Sackmann and Boothroyd 1992; Smith et al. 1995). The raw material for Li production is the ^3He synthesized on the main sequence; since the initial step of ^3He production from hydrogen is controlled by a very slow weak reaction, the main sequence phase for low mass stars seems to be the sole practical site for ^3He synthesis. In principle, ^3He may be processed to ^7Li at other sites and other stages of evolution; for example, Podsiadlowski, Cannon and Rees (1995) suggest ^7Li production to occur in a Thorne-Zytkow object, a red giant with a neutron star as its core. We infer that MV Sgr has evolved from an intermediate mass AGB star and possibly the Li was produced in the final He thermal flash after the star had left the AGB to enter the white dwarf cooling track.

The abundance analysis by Jeffery et al. (1988) suggests that N is more abundant than C, a situation different from other hot hydrogen deficient stars. The super Li rich AGB stars observed by Smith and Lambert in LMC are of high luminosities ($M_{\text{bol}} \sim -6.5$) and show N to be more abundant than C. This has been interpreted as a consequence of C from the helium burning being further processed by CNO cycles to N (Sackmann and Boothroyd 1992). If such a star evolves to hotter regions and becomes hydrogen deficient it probably would show abundances similar to MV Sgr.

Lithium is not an unknown ingredient of R CrBs. Lambert and Rao (1994) report lithium to be present and with an abundance similar to that inferred for MV Sgr in 4 out of a sample of 18 stars. Lithium is also found in 1 out of 5 Hydrogen deficient cool carbon stars (Warner 1967). Of course, lithium will not be detectable in hot R CrBs unless these stars also possess cooler absorbing/emitting regions, as is the case for MV Sgr.

7.3 Future prospects

The present analysis does not allow us to either explain the cause of hydrogen deficiency, or provide a clear evolutionary link between R CrB stars and EHe stars. There are definite indications of an evolutionary link. Further studies of a larger sample are required to pinpoint the evolutionary status of these objects and order them sequentially. There are only six known cool EHe stars, which were the result of several surveys. These surveys have covered mainly the disc of the Galaxy. For a larger sample, it is necessary to conduct an extensive survey of other regions of the Galaxy to look for cool EHe stars.

An enhancement of s-process elements in a star is an indication that it has gone through the Asymptotic Giant Branch phase of evolution and has experienced the third dredge-up. The temperatures of our stars fall in the range 8000 K to 14000 K. The s-process elements in this temperature range will be mostly in second and third ionization states. The lines of s-process elements in these ionization states would be strong even for solar composition and would appear in ultraviolet wavelengths. Hence, an extensive analysis of high-resolution ultraviolet and optical spectra of a large sample of EHe stars, including the candidates used in the present study, would be highly desirable. Our analysis of EHe stars shows that it is possible to determine Sr, Y, Zr, and Ba abundances from the optical spectra of cool EHe stars, that is for $T_{eff} \leq 12000$ K. Our analysis eventually provides Sr – Ba abundances only for a few stars – a sample too small to clearly establish an evolutionary link and continuity in the abundances of s-process elements between R CrB and EHe stars. We have predicted the equivalent widths of some strong Y III (2327.3 and 2414.6 Å) and Zr III (1937.2, 1940.2, and 1941.1 Å) lines for EHe stars. The computed equivalent widths of these lines are quite large for solar abundances relative to Fe. An underabundance of Y and Zr is not shown by cool EHe and R CrB stars and an underabundance of these in hot EHe stars would be a surprising result. High resolution ($\lambda/\Delta\lambda \approx 30,000$) UV spectra for EHe stars using HST, could provide the Y and Zr abundances from the lines mentioned

above for EHe stars with effective temperatures $9000 \leq T_{eff} \leq 20000$ K. There are many Fe II and Fe III lines in the region, especially around the Zr III lines. These will provide a check on the optical Fe abundances. Our predicted equivalent widths of Y III and Zr III, and also the synthetic spectra show that these lines can be detected in the spectra of EHe stars unless the Y and Zr are greatly underabundant relative to the Fe abundance determined from optical spectra.

Of the many questions unanswered by our study of MV Sgr, we expect to answer a few by extending high resolution spectroscopy across the visible spectrum and beyond. High S/N spectra will surely reveal additional details about the line profiles. Spectra in the blue may show lines of heavy elements which should be enhanced if MV Sgr has evolved from an AGB star. The lighter elements, say Ge-Mo, should be severely enhanced if MV Sgr is a Thorne-Zytkow object (Biehle 1991, 1994; Cannon 1993).

Bibliography

- Appenzeller, L., Jankovics, I. & Ostreicher, R., 1984, A&A 141, 108.
- Asplund, M., Gustafsson, B., Lambert, D. L. & Kameswara Rao, N., 1997, A&A (Letters), 321, L17.
- Asplund, M., Gustafsson, B., Kiselman, D., Eriksson, K., 1997a, A&A, 318, 521.
- Asplund, M., Lambert, D. L., Kipper, T., Pollacco, D., Shetrone, M. D., 1999, A&A, 343, 507.
- Baschek, B., & Norris, J., 1975, ApJ, 199, 694.
- Bassalo, J. M., Cattani, M., Walder, V. S., 1980, Phys. Rev. A - Gen. Phys., 22, 1194.
- Becker, S. A., & Iben, I. Jr., 1979, ApJ, 232, 831.
- Becker, S. R., & Butler, K., 1988, A&A, 201, 232.
- Becker, S. R., & Butler, K., 1989, A&A 209, 244.
- Becker, S. R., & Butler, K., 1990, A&A, 235, 326.
- Benett, S. M., Griem, H. R., 1971, University of Maryland, Technical Report 71-128.
- Berman, L., 1935, ApJ, 81, 369.
- Biehle, G.T., 1991, ApJ, 380, 167.
- Biehle, G.T., 1994, ApJ, 420, 364.
- Bowen, G. H., & Willson, L. A., 1991, ApJ (Letters), 375, L53.
- Bowers, R. L., 1984. Astrophysics: I. Stars, Jones and Bartlett, Boston.

- Bragaglia, A., Greggio, L., Renzini, A., D'Odorico, S., 1990, *ApJ (Letters)*, 365, L13.
- Brown, J. A., Sneden, C., Lambert, D. L., Dutchover, E., Jr., 1989, *ApJSS*, 71, 293.
- Cameron, A. G. W., & Fowler, W. A., 1971, *ApJ*, 164, 111.
- Campbell, W. W., 1899, *ApJ*, 10, 241.
- Cannon, R. C., Eggleton, P. P., Żytkow, A. N., Podsiadlowski, P., 1992, *ApJ*, 386, 206.
- Canuto, W., & Mendoza, C., 1992, *Rev. Mexicana Astron. Astrofis.*, 23, 107.
- Conti, P. S., Leep, M. E., Perry, D. N., 1983, *ApJ*, 268, 228.
- Cottrell, P. L. & Lambert, D. L., 1982, *ApJ*, 261, 595.
- Crowther, P. A., Hillier, D. J., Smith, L. J., 1995a, *A&A*, 293, 172.
- Crowther, P. A., Hillier, D. J., Smith, L. J., 1995b, *A&A*, 293, 403.
- Crowther, P. A., Hillier, D. J., Schmutz, W., 1995c, *A&A*, 293, 427.
- Dahari, O., & Osterbrock, D. E., 1984, *ApJ*, 277, 648.
- Dimitrijevic, M. S., Sahal-Brechot, S., 1984, *JQSRT*, 31, 301.
- D'Odorico, S., Ghigo, M., Ponz, D., March 1987: An Atlas of Th-Ar Spectrum for the ESO Echelle Spectrograph in $\lambda\lambda$ 3400–9000 Å Region, ESO Scientific Report No. 6.
- Drilling, J. S., 1979, *ApJ*, 228, 491.
- Drilling, J. S., 1980, *ApJ (Letters)*, 242, L43.
- Drilling, J. S., 1983, *ApJ*, 270, 13.
- Drilling, J.S., Schönberner, D., Heber, U., Lynas-Gray, A. E., 1984, *ApJ*, 278, 224.
- Drilling, J. S., 1986, in: "Hydrogen-Deficient Stars and Related Objects", K. Hunger, D. Schönberner and N. K. Rao, (eds.). Dordrecht: Reidel, p. 9.
- Drilling J. S., and Hill, P. W., 1986, in: "Hydrogen-Deficient Stars and Related Objects", K. Hunger, D. Schönberner and N. K. Rao, (eds.). Dordrecht: Reidel, p. 499.
- Drilling J. S., 1987, in: " Second Conference on Faint Blue Stars ", IAU Colloquium No. 95, p. 489.

- Drilling J. S., and Bergeron, 1995, *PASP*, 107, 846.
- Drilling J. S., 1996, in: Hydrogen deficient stars, Jeffery C.S., Heber U. (eds.). ASP conf. series vol. 96, p. 461.
- Drilling, J. S., Jeffery, C. S., Heber, U., 1998, *A&A*, 329, 1019.
- Dufton, P. L., Hibbert, A., Kingston, A. E., Tully, J. A., 1983, *MNRAS*, 202, 145.
- Feast, M.W., & Glass, I., 1973, *MNRAS*, 161, 293.
- Fujimoto, M. Y., 1977, *PASJap*, 29, 331.
- Gallino, R., Busso, M., Picchio, G., Raiteri, C. M., 1989, in: "From Miras to Planetary Nebulae: Which Path for Stellar Evolution?", eds, M. O. Mennessier, A. Omont, Edition Frontières, p. 315.
- Giridhar, S., & Arellano Ferro, A., 1989, *JAA*, 10, 47.
- Giridhar, S., & Arellano Ferro, A., 1995, *Revi. Mex. Astr. Astrofisica*, 31, 23.
- Goeres, A., 1996, in: Hydrogen deficient stars, Jeffery C.S., Heber U. (eds.). ASP conf. series vol. 96, p. 69.
- Gonzalez, Guillermo; Lambert, David L.; Wallerstein, George; Rao, N. Kameswara; Smith, verne V.; McCarthy, James K., 1998, *ApJ Suppl.*, 114, 133.
- Green, R. F., Schmidt, M., Liebert, J., 1986, *ApJS*, 61, 305.
- Greenstein, J. L., 1940, *ApJ*, 91, 438.
- Grevesse, N., Noels, A., Sauval, A. J., 1996, in: Cosmic abundances, Holt S.S., Sonneborn G. (eds.). ASP conf. series vol. 99, p. 117.
- Griem, H. R., Baranger, M., Kolb, A. C., Oertel, G., 1962, *Phys. Rev.*, 125, 177.
- Gustafsson, B., Bell, R. A., Eriksson, K., Nordlund, Å., 1975, *A&A*, 42, 407.
- Gustafsson, B., Asplund, M., 1996, in: Hydrogen deficient stars, Jeffery C.S., Heber U. (eds.). ASP conf. series vol. 96, p. 27.
- Gustafsson, B., 1997, in: Fundamental Stellar Properties: The Interaction Between Observation And Theory, Bedding T.R., Booth A.J., Davis J. (eds.). IAU Symp. No. 189, p. 265.

- Hamann, W., Koesterke, L., Wessolowski, U., 1995, *A&A*, 299, 151.
- Heber, U., & Schönberner, D., 1981, *A&A*, 102, 73.
- Heber, U., 1983, *A&A*, 118, 39.
- Herbig, G. H., 1961, *ApJ*, 140, 1317.
- Herbig, G. H., 1975a, *ApJ*, 199, 702.
- Herbig, G. H., 1975b, *ApJ*, 196, 129.
- Herwig, F., Böcker, T., Driebe, T., 1999, to appear in *A&A* (Letters).
- Hibbert, A., 1988, *Physica Scripta*, 38, 37.
- Hibbert, A., Biemont, E., Godefroid, M., Vaeck, N., 1993, *A&AS*, 99, 179.
- Hill, P. W., 1961, *MNRAS*, 127, 113.
- Hill, P. W., 1965, *MNRAS*, 129, 137.
- Hillier, D. J., 1989, *ApJ*, 317, 392.
- Hoffleit, D., 1958, *AJ*, 63, 50.
- Hunger, K., 1975, *Problems in Stellar Atmospheres and Envelopes*, eds. B. Baschek, W. H. Kegel, and G. Traving (New York: Springer-Verlag), p. 57.
- Hunger, K., 1986, in: "Hydrogen-Deficient Stars and Related Objects", K. Hunger, D. Schönberner and N. K. Rao, (eds.), Dordrecht: Reidel, p. 261.
- Husfeld, D., Butler, K., Heber, U., Drilling, J. S., 1989, *A&A*, 222, 150.
- Iben, I. Jr., & Rood, R. L., 1970, *ApJ*, 161, 587.
- Iben, I. Jr., 1975, *ApJ*, 196, 525.
- Iben, I. Jr., & Renzini, A., 1983, *Ann. Rev. Astr. Astrophys.*, 21, 271.
- Iben, I. Jr., 1984, *ApJ*, 277, 333.
- Iben, I. Jr., & Tutukov, A. V., 1985, *ApJ Suppl.*, 58, 661.
- Iben, I. Jr., 1985, *Quart. J. R. astr. Soc.*, 26, 1.

- Iben, I. Jr., 1990, ApJ, 353, 215.
- Iben, I. Jr., 1991, ApJ Suppl., 76, 55.
- Iben, I. Jr., & McDonald, J., 1995, in: "White Dwarfs", eds. D. Koester & K. Warner (Berlin: Springer), 48.
- Jeffery, C. S., Heber, U., Hill, P. W., Pollacco, D., 1988, MNRAS, 231, 175.
- Jeffery, C. S., Heber U., 1992, A&A, 260, 133.
- Jeffery, C. S., 1994, Newsletter on "Analysis of Astronomical Spectra", No. 16, p.17.
- Jeffery, C. S., 1994, CCP7 Newslett., 21, 27.
- Jeffery C.S., 1996, in: Hydrogen deficient stars, Jeffery C.S., Heber U. (eds.). ASP conf. series vol. 96, p. 152.
- Jeffery, C. S., Heber, U., Hill, P. W., Dreizler, S., Drilling, J. S., Lawson, W. A., Leuenhagen, U., Werner, K., 1996, in: Hydrogen deficient stars, Jeffery C.S., Heber U. (eds.). ASP conf. series vol. 96, p. 471.
- Jeffery, C. S., 1998, MNRAS, 294, 391.
- Jeffery, C. S., Hamill, P. J., Harrison, P. M., Jeffers, S. V., 1998, A&A, 340, 476.
- Kelleher, D. E., 1981, JQSRT, 25, 191.
- Kilkenny, D., & Whittet, D. C. B., 1984, MNRAS, 208, 25.
- Kilkenny, D., Marang, F., Menzies, D. W., 1988, MNRAS, 233, 209.
- Kingsburgh, R. L., Barlow, M. J., Storey, P. J., 1995, A&A, 295, 75.
- Knapp, G. R., Phillips, T. G., Leighton, R. B., Lo, K. Y., Wannier, P. G., Wotten, H. A., Huggins, P. J., 1982, ApJ, 252, 616.
- Koesterke, L., and Hamann, W.-R., 1995, A&A, 299, 503.
- Krelowski, J. 1989, in Interstellar Dust, ed. L. J. Allamandola & A. G. G. M. Tielens(Dordrecht:Kluwer) p. 67.
- Kurucz, R. L.: 1970, ATLAS: A Computer Program For Calculating Model Stellar Atmospheres, SAO Special Report No. 309, Cambridge, Massachusetts 02138.

- Kurucz, R. L., Peytreman, E.: 1975, SAO - Special Report No. 362.
- Lambert, D. L., 1986, in: "Hydrogen-Deficient Stars and Related Objects", K. Hunger, D. Schönberner and N. K. Rao, (eds.). Dordrecht: Reidel, p. 127.
- Lambert, D. L., & Rao, N. K., 1994, JAA, 15, 47.
- Lambert, D. L., 1996, in: Hydrogen deficient stars, Jeffery C.S., Heber U. (eds.). ASP conf. series vol. 96, p. 443.
- Lambert, D. L., Rao, N. K., Gustafsson, B., Asplund, M., 1999, (preprint), submitted to A&A.
- Landolt, A.R. 1979, IAU Circ. No. 3419
- Lawson, W. A., Kilkenny, D., van Wyk, F., Marang, F., Pollard, K., Ryder, S. D., 1993, MNRAS, 265, 351.
- Lawson, W. A., Cottrell, P. L., 1997, MNRAS, 285, 266.
- Leuenhagen, U., Hamann, W. -R., 1994, A&A, 283, 567.
- Leuenhagen, U., Heber, U., Jeffery, C. S., 1994, A&A Suppl., 103, 445.
- Liebert, J., 1986, in: "Hydrogen-Deficient Stars and Related Objects", K. Hunger, D. Schönberner and N. K. Rao, (eds.). Dordrecht: Reidel, p. 367.
- Loreta, E., 1934, *Astronomische Nachrichten*, 254, 151.
- Ludendorff, H., 1906, *Astron. Nach.*, 173, 3.
- Luo D., Pradhan, A. K., 1989, *J. Phys. B.*, 22, 3377.
- MacConnell, D. J., Frye, R. L., Bidelman, W. P., 1970, *PASP*, 82, 730.
- MacConnell, D. J., Frye, R. L., Bidelman, W. P., 1972, *PASP*, 84, 388.
- Massey, P., Armandroff, T. E., 1991, in IAU Symp. 143, "Wolf-Rayet Stars and Interrelations with other Massive Stars in Galaxies", K. A. van der Hucht, and B. Hidayat, (eds.). Dordrecht: Kluwer, p. 575.
- McGraw, J. T., Liebert, J., Starrfield, S. G. & Green, R., 1979, in: *White Dwarfs and Variable Degenerate Stars*, IAU Coll. 53, p. 377.

- McWilliam, A., 1997, *Annual Reviews of Astronomy and Astrophysics*, 35, 503.
- Mendez, R. H., 1991, in *Evolution of Stars: The Photospheric Abundance Connection*, IAU Symp. 145, eds. Michaud & Tutukov, Dordrecht: Kluwer, 375.
- Mendoza, C. 1983, IAU Symp. No. 103, ed. D. R. Flower (Dordrecht: Reidel) p. 143.
- Moore, Ch. E.: 1970, *Selected Tables of Atomic Spectra*, Sect. 3 (C I - IV), NBS, Washington.
- Moore, Ch. E.: 1972, *A Multiplet Table of Astrophysical Interest*, NSRDS - NBS 40, Washington.
- O'Keefe, J. A., 1939, *ApJ*, 90, 294.
- Osterbrock, D.E. 1989, *Astrophysics of gaseous nebulae and active galactic nuclei*, University Science Books, Mill Valley, California.
- Paczynski, B., 1971, *Acta Astron.*, 21, 417.
- Pandey, G., Rao, N. K., Lambert, D. L., 1996, *MNRAS*, 282, 889.
- Peach, G., 1970, *MemRAS*, 73, 1.
- Pigott E., 1797, *Phil. Trans. Roy. Soc. Part I*, 133.
- Podsiadlowski, P., Cannon, R.C., Rees, M. J., 1995, *MNRAS*, 274, 485.
- Popper, D. M., 1942, *PASP*, 54, 160.
- Prabhu, T. P., Anupama, G. C., Giridhar, S., 1987, *BASI*, 15, 98.
- Rao, N. K., & Nandy, K., 1982, *JAA*, 3, 79.
- Rao, N. K., Houziaux, L., Giridhar, S. 1990, *JAA*, 11, 37.
- Rao N. K., & Lambert D. L., 1996, in: *Hydrogen deficient stars*, Jeffery C.S., Heber U. (eds.). ASP conf. series vol. 96, p. 152.
- Rao N. K., Lambert D. L., Adams, M. T., Doss, D. R., Gonzalez, G., Hatzes, A. P., James, R., Johns-Krull, C. M., Luck, R. E., Pandey, G., Reinsch, K., Tomkin, J., 1999, to appear in *MNRAS*.
- Reimers, D., 1975, *Mem. R. Soc. Sci. Liege*, 6^e, 8, 369.

- Sackmann, I. -J., & Boothroyd, A. I. 1992, ApJ, 392, L71.
- Sargent, W. L. W., and Searle, L., 1968, ApJ, 152, 443.
- Schönberner, D., and Wolf, R. E. A., 1974, A&A, 37, 87.
- Schönberner, D., 1975, A&A, 44, 383.
- Schönberner, D., 1978, Mitt. Astr. Ges., 43, 266.
- Schönberner, D., 1979, A&A, 79, 108.
- Schönberner, D., 1996, in: Hydrogen deficient stars, Jeffery C.S., Heber U. (eds.). ASP conf. series vol. 96, p. 433.
- Searle, L., 1961, ApJ, 133, 531.
- Seaton, M. J., 1979, MNRAS, 187, 735.
- Seaton, M. J., Yan, Y., Mihalas, D., Pradhan, A. K., 1994, MNRAS, 266, 805.
- Smith, L. F., 1973, in IAU Symp. 49, " Wolf-Rayet Stars and High Temperature Stars ", M. K. V. Bappu and J. Sahade, (eds.). Dordrecht: Reidel, p. 15.
- Smith, V. V., Plez, B., Lambert, D. L., Lubowich, D. A., 1995, ApJ, 441, 735.
- Stephenson, C. B., & Sanduleak, N., 1971, Publ. Warner and Swasey Obs. 1, 1.
- Thevenin, F, 1989, A&A Suppl., 77, 137.
- Thevenin, F, 1990, A&A Suppl., 82, 179.
- Tomkin, J., Edvardsson, B., Lambert, D. L., Gustafsson, B., 1997, A&A, 327, 587.
- Tull, R. G., McQueen, P. J., Sneden, C. and Lambert, D. L., 1995, PASP, 107, 251.
- Walborn, N. R., 1983, ApJ, 268, 195.
- Walker, H. J., 1985, A&A 152, 58.
- Walker, H. J., 1986, Proc. IAU Coll. No. 87, (Dordrecht: Reidel) p. 407.
- Wallerstein, G., Iben, I. Jr., Parker, P., Boesgaard, A. M., Hale, G. M.,
Champagne, A. E., Barnes, C. A., Käppeler, F., Smith, V. V., Hoffman, R. D.,

- Timmes, F. X., Sneden, C., Boyd, R. N., Meyer, B. S., Lambert, D. L., 1997, *Rev. Mod. Phys.*, 69 No. 4, 995.
- Warner, B., 1967, *MNRAS*, 137, 119.
- Wasemael, F., Green, R. F., and Liebert, J., 1985, *ApJS*, 58, 379.
- Weaver, T. A., Woosley, S. E., 1993, *Phys. Rep.*, 227, 65.
- Webbink, R. F., 1984, *ApJ*, 277, 355.
- Woitke, P., Goeres, A. & Sedelmyr, E., 1996, *A&A*, 311, 927.
- Wolf, C. J. E., and Rayet, G., 1867, *Comptes Rendus*, 65, 292.
- Wolf, R. E. A., 1973, *A&A*, 26, 127.
- Wiese, W. L., Smith, M. W., Glennon, 1966, *National Bureau of Standards (USA) Publs. Vols I-II*.
- Wiese, W. L., Smith, M. W., & Miles, B. M., 1969, "Atomic Transition Probabilities", NBS, Washington.
- Yan, Y., Taylor, K. T., Seaton, M. J., 1987, *J.Phys.B.*, 20, 6399.